THESIS

STUDIES OF SPACE-TIMES EMERGING FROM MATRIX MODELS

Kohta Hatakeyama

Graduate School of Science and Technology,
Educational Division

Department of Information Science and Technology

Shizuoka University

December 2019

THESIS

STUDIES OF SPACE-TIMES EMERGING FROM MATRIX MODELS
行列模型から創発する時空に関する研究

畠山　洸太

静岡大学
自然科学系教育部

情報科学専攻

2019年12月

Abstract

Superstring theory is a promising candidate for the unified theory including quantum gravity. However, it is only formulated perturbatively. In order to make physical predictions from superstring theory, its non-perturbative formulation is needed. Matrix models have been proposed as candidates for such a formulation. The feature of the matrix models is that space(-time) emerges dynamically from degrees of freedom of matrices. To establish the matrix models completely as non-perturbative formulations of superstring theory, one needs to elucidate a mechanism of emergence of space-times from the matrix models and properties of those emergent space-times.

In this thesis, we study the following three topics to gain insight into the above issues. The first one is concerning non-commutative spaces emerging from matrix models. We study quantum aspects of a scalar field theory on the fuzzy sphere. By performing Monte Carlo simulations, we show that theory is non-perturbatively renormalizable and that it behaves as a conformal field theory at short distances on the phase boundary. Second, we study the large-N volume independence, which states that large-N gauge theories are independent of the volume of the space-times on which they are defined. We show that it holds on group manifolds. Finally, we investigate properties of space-times emerging from the type IIB matrix model, which is one of the above mentioned matrix models proposed as non-perturbative formulations of superstring theory. We solve classical equations of motion and find that our solutions give rise to the (3+1)-dimensional expanding space with smooth structure and Dirac zero modes.

Contents

Chapter 1

Introduction

1.1 Background

Superstring theory is expected to be the unified theory including quantum gravity. However, superstring theory is only formulated perturbatively, which causes some issues. First, there are a lot of stable vacua which give various space-time dimensionalities, gauge groups, and matter contents. Second, it is known that the cosmic singularity at the beginning of the universe cannot be resolved within perturbative superstring theory [1–4]. Non-perturbative formulation is needed in order to solve these issues. In the latter half of 1990s, several matrix models were proposed as such a non-perturbative formulation of superstring theory. Those matrix models include the type IIB matrix model [5], the matrix theory or the BFSS matrix model [6], and the matrix string theory [7], which can be obtained formally by dimensional reduction of 10-dimensional $\mathcal{N} = 1$ super Yang-Mills theory to d dimensions with $d = 0, 1, 2$, respectively. In particular, the feature of the type IIB matrix model is that space-time does not exist a priori but emerges dynamically from degrees of freedom of matrices.

In order to establish the above matrix models completely as non-perturbative formulations of superstring theory, it is needed to elucidate mechanism of emergence of space-times, especially curved space-times [8], from matrix models and properties of those emergent space-times.

In this thesis, to gain insights into the above issues, we study the following three topics: renormalization in a scalar field theory on the fuzzy sphere, the large-N volume independence on group manifolds, and classical solutions in the Lorentzian type IIB matrix model. In the following, as background of the three topics, we review field theories on noncommutative spaces, the large-N volume independence, and the Lorentzian type IIB matrix model.

Field theories on non-commutative spaces

It is known that non-commutative spaces naturally appear in matrix models [9,10]. Hence, quantum properties of field theories on non-commutative spaces[1] are quite non-trivial as seen in below. The product for the fields is non-commutative and non-local, which is one of the most important features of the theories. In perturbative expansion, IR divergences originating from UV divergences are yielded due to this feature. This phenomenon is called the UV/IR mixing [12] and is known to be an obstacle to perturbative renormalization. In [13, 14], the UV/IR mixing in a scalar field theory on the fuzzy sphere[2] was examined perturbatively: the 1-loop self-energy differs from that in the ordinary theory on a sphere by finite and non-local terms even in the commutative limit. This effect is sometimes called the UV/IR anomaly [13].

The large-N volume independence

The large-N reduction or the large-N volume independence [34] is a mechanism of emergence of space-time. It states that large-N gauge theories are independent of the volume of the space-times on which they are defined. In a narrow sense, this tells us that large-N gauge theories are equivalent to the matrix models called the reduced models that are obtained by dimensionally reducing the original theories to 0 dimension. It was shown in [35,36] that the large-N reduction holds on group manifolds in the above narrow sense[3]. Those works are important from the viewpoint of elucidating how curved space-time emerges from matrix models because the large-N reduction have been considered almost in flat spaces[4].

The Lorentzian type IIB matrix model

It was shown in [56] by Monte Carlo simulation that the (3+1)-dimensional expanding universe appears in the Lorentzian type IIB matrix model[5]. The time scale that has been probed by simulation is typically of the order of the Planck scale. In order to see the uni-

[1] See, [11] for a review.

[2] The theory has been studied by Monte Carlo simulation in [15–22]. For related analytic studies of the model, see [23–31]. A similar analysis for a scalar field theory on the non-commutative torus was performed in [32, 33].

[3] In [37], another type of the large-N reduction on group manifolds was shown.

[4] For other developments in the large-N reduction, see [38–55].

[5] For developments in numerical simulations of the Lorentzian type IIB matrix model, see [57–62], and for numerical simulations of the Euclidean type IIB matrix model, see [63, 64]. For other studies to obtain cosmology from the type IIB matrix model, see, for example, [65–68].

verse at late time compared to the Planckian time, we need to take the matrix size N to be large. Furthermore, a recent study [61] showed that the (3+1)-dimensional space-time obtained by Monte Carlo simulation is singular one essentially consisting of the Pauli matrices. This singularity is attributed to the approximation made to avoid the sign problem in the Monte Carlo simulation. In another recent study [62], a numerical simulation of the bosonic type IIB matrix model was performed without such an approximation by using the complex Langevin method. It was observed that there appears a space-time that departs from the Pauli-matrix structure keeping the (3+1)-dimensional expanding behavior. From this result, the authors of [62] conjectured that the (3+1)-dimensional space-time with smooth structure is obtained in the large-N limit. As we mentioned in the above, the matrix size should be large to see the late-time behavior and the structure of the (3+1)-dimensional space-time. However, it is difficult to perform numerical simulations with large matrix size. Thus, we need to consider another way to see the (3+1)-dimensional space-time with large matrix size.

One expects to obtain the Standard Model particles from the type IIB matrix model if it is really a non-perturbative formulation of superstring theory. In [69–71], matrix configurations which can yield fermions in the Standard Model were given by hand[6]. We should see whether matrix configurations which give the Standard Model fermions are obtained dynamically.

1.2 Purposes and results

Field theories on non-commutative spaces are naturally realized by matrix models. Curved space-times should also be realized by matrix models because the models include quantum gravity. Thus, it is useful for establishing the type IIB matrix model as a non-perturbative formulation of superstring theory to study properties of the field theories and mechanism of emergence of curved space-times . Keeping this in mind, we study the three topics as we mentioned in the previous section. In this section, we explain purposes and results of the three topics.

[6]The fermions in the Standard Model are also obtained by considering the type IIB matrix model on the non-commutative torus, which includes a model with *unitary* matrices [72, 73] and a model with matrices of *infinite* matrix size [74]. Note that the supersymmetry is broken in the unitary matrix model and the matrix model with infinite matrix size is not suitable for the regularization of superstring theory.

Renormalization in a scalar field theory on the fuzzy sphere

We study a scalar field theory on the fuzzy sphere [20–22]. We define the correlation functions by using the Berezin symbol [75] constructed from the Bloch coherent state [76], and calculate them non-perturbatively by Monte Carlo simulations. We show that the 2-point and 4-point correlation functions are made independent of the matrix size, which is interpreted as a UV cutoff, by tuning a parameter in the theory and performing a wave function renormalization. Our results strongly suggest that the field theory on the fuzzy sphere is non-perturbatively renormalizable. Moreover, we identify the phase boundary by measuring the susceptibility that is an order parameter for the Z_2 symmetry and calculate the 2-point and 4-point correlation functions on the boundary. We find that the correlation functions at different points on the boundary agree so that the theories on the boundary are universal as in ordinary field theories. Furthermore, we observe that the 2-point correlation functions behave as those in a conformal field theory (CFT) at short distances but deviate from it at long distances. It is non-trivial that the behavior of the CFT is seen because field theories on non-commutative spaces are non-local ones.

The large-N volume independence on group manifolds

Next, we examine whether a phenomenon analogous to the large-N volume independence occurs on group manifolds. We find that it indeed does in the sense that a large-N gauge theory on a group manifold G is equivalent to the theory obtained by reducing it to a coset space G/H where H is a subgroup of G [77].

Classical solutions in the Lorentzian type IIB matrix model

Finally, we solve classical equations of motion of the Lorentzian type IIB matrix model [78]. As we mentioned in the previous section, we need to take the matrix size to be large to see the universe at late time compared to the Planckian time. On the other hand, at late time, a classical approximation is expected to be valid because the action becomes large due to the expansion of universe. We, therefore, solve classical equations[7]. Indeed, solving classical equations of motion is easier than performing numerical simulations. A systematic method of searching for classical solutions analytically was developed in [66][8]. However, one cannot obtain all classes of solutions with the method. Thus, we will develop a numerical method for obtaining wider classes of solutions. Solving classical equations of motion is non-trivial because there exists no time a priori in the type IIB matrix model,

[7] Our results on the Dirac zero modes also hold for the Euclidean model.

[8] See also, [67].

so we apply the gradient decent method to solve classical equations of the type IIB matrix model. We expect that there exist a specific classical solution which is smoothly connected to the dominant configuration obtained in numerical simulations and describes our real world. Here, we start with random initial configurations using the above method and obtain a lot of solutions. We consider the common features possessed by our solutions to reflect those of the specific solution.

In particular, we see whether the (3+1)-dimensional expanding universe with smooth structure is reproduced as classical solutions in the Lorentzian type IIB matrix model, and search for solutions which yield Dirac zero modes. For this purpose, we assume configurations with a quasi-direct-product structure of (3+1) dimensions and 6 extra dimensions, which is the most general structure preserving the (3+1)-dimensional Lorentz symmetry [79].

We obtain the following results. First, in a typical solution, we show that the (3+1)-dimensional space-time exhibits an expanding behavior with a smooth structure. Next, we examine spectra of a counterpart of the 6-dimensional Dirac operator[9] because zero eigenvectors in extra dimensions correspond to Dirac zero modes in (3+1) dimensions. To obtain Dirac zero modes, we introduce ansatz for matrix configurations, solve classical equations of motion, and calculate eigenvalues of the 6-dimensional Dirac operator. We find that the lowest eigenvalues decrease as the matrix size increases, and show that the ratio of the lowest eigenvalues to the second lowest ones converges to 0 in the $N \to \infty$ limit, which implies that we can obtain Dirac zero modes in the $N \to \infty$ limit. Moreover, we see that wave functions corresponding to zero modes are localized at a point, which is consistent with the picture of intersecting D-branes.

1.3 Organization

This thesis is organized as follows. In chapter 2, we review emergence of space-time from matrix models. In chapter 3, we perform renormalization in a scalar field theory on the fuzzy sphere, which is realized by a matrix model. In chapter 4, we show the large-N volume independence on a group manifold. In chapter 5, we solve classical equations of motion in the Lorentzian type IIB matrix model, and show that (3+1)-dimensional expanding space-time with smooth structure emerges and Dirac zero modes in extra 6 dimensions are obtained from classical solutions. Chapter 6 is devoted to conclusion and outlook. In appendix A, we briefly review the Bloch coherent state and the Berezin symbol. In

[9]Here, a counterpart of the 6-dimensional Dirac operator is obtained by dimensionally reducing the 6-dimensional Dirac operator to 0 dimension.

appendix B, we explain the UV/IR anomaly in a scalar field theory on the fuzzy sphere. In cppendix C, we give the $3j$ and the $6j$ symbols that are related to the Clebsch-Gordan coefficients. In Appendix D, we describe the method of numerical simulation used in our study. In appendix E, we show definition of the band size introduced in section 5.2. Details of some calculations are given in appendix F.

Chapter 2

Review of emergence of space-time from matrix models

In this chapter, we review emergence of space-time from matrix models. We explain non-commutative spaces, the large-N reduction, and the type IIB matrix model in sections 2.1, 2.2, and 2.3, respectively.

2.1 Non-commutative spaces

Here, we review non-commutative spaces. In particular, the UV/IR mixing that we explain in the following is an important property of non-commutative spaces.

2.1.1 Non-commutative plane

We consider the non-commutative plane, which is the simplest non-commutative space. The extension to the non-commutative $\mathbb{R}^d$ is easy.

The coordinates $\hat{x}_i$ $(i = 1, 2)$ on the non-commutative plane are non-commutative:

$$[\hat{x}_1, \hat{x}_2] = i\theta \ , \tag{2.1.1}$$

where θ is a real number and the $\theta \to 0$ limit corresponds to the continuum limit. Note that " $\hat{}$ " implies that coordinates are not ordinary numbers, but operators, or infinite-dimensional matrices. We define conjugate momenta as follows:

$$\hat{p}_1 = \theta^{-1}\hat{x}_2 \ , \quad \hat{p}_2 = -\theta^{-1}\hat{x}_1 \ . \tag{2.1.2}$$

They satisfy the commutation relation

$$[\hat{p}_1, \hat{p}_2] = i\theta^{-1} \ , \tag{2.1.3}$$

and $\hat{x}_i$ and $\hat{p}_j$ satisfy the following relation:

$$[\hat{x}_i, \hat{p}_j] = i\delta_{i,j} \ . \tag{2.1.4}$$

This looks the form of the canonical commutation relation for quantum mechanics of the single particle system in two dimensions. However, we consider the Hilbert space of 1-dimensional quantum mechanics because the momenta depend on the coordinates according to (2.1.2).

Operator acting on this Hilbert space, $\hat{f}$, are expanded in terms of $\hat{x}_i$:

$$\hat{f} = \int \frac{d^2k}{(2\pi)^2} f(k) e^{ik\cdot\hat{x}} \ . \tag{2.1.5}$$

For $\hat{f}$, one can define $f(x)$ that is a function on $\mathbb{R}^2$:

$$f(x) = \int \frac{d^2k}{(2\pi)^2} f(k) e^{ik\cdot x} \ . \tag{2.1.6}$$

The correspondence between $\hat{f}$ and $f(x)$ is given by

$$\hat{f} = \int \frac{d^2k}{(2\pi)^2} \int d^2x f(x) e^{-ik\cdot x} e^{ik\cdot\hat{x}} \ . \tag{2.1.7}$$

From (2.1.4) and (2.1.5), one can show

$$\left[\hat{p}_i, \hat{f}\right] = \int \frac{d^2k}{(2\pi)^2} \int d^2x \left[-i\partial_{x_i} f(x)\right] e^{-ik\cdot x} e^{ik\cdot\hat{x}} \ . \tag{2.1.8}$$

Thus, one finds the following relation on $\mathbb{R}^2$:

$$[\hat{p}_i, \ ] \longleftrightarrow -i\partial_{x_i} \ . \tag{2.1.9}$$

The product is evaluated as

$$\begin{aligned}
\hat{f}\hat{g} &= \int \frac{d^2k}{(2\pi)^2} \int \frac{d^2l}{(2\pi)^2} \int d^2x \int d^2y f(x) g(y) e^{-ik\cdot x} e^{-il\cdot y} e^{ik\cdot\hat{x}} e^{il\cdot\hat{x}} \\
&= \int \frac{d^2k}{(2\pi)^2} \int \frac{d^2l}{(2\pi)^2} \int d^2x \int d^2y f(x) g(y) e^{-ik\cdot x} e^{-il\cdot y} e^{-\frac{i\theta}{2}(k_1 l_2 - k_2 l_1)} e^{i(k+l)\cdot\hat{x}} \\
&= \int \frac{d^2k}{(2\pi)^2} \int \frac{d^2l}{(2\pi)^2} \int d^2x \int d^2y \left[e^{\frac{i\theta}{2}\left(\partial_{x_1}\partial_{y_2} - \partial_{x_2}\partial_{y_1}\right)} f(x) g(y)\right] e^{-ik\cdot x} e^{-il\cdot y} e^{i(k+l)\cdot\hat{x}} \\
&= \int \frac{d^2k}{(2\pi)^2} \int d^2x \left[e^{\frac{i\theta}{2}\left(\partial_{x_1}\partial_{y_2} - \partial_{x_2}\partial_{y_1}\right)} f(x) g(y)\right]\Big|_{y=x} e^{-ik\cdot x} e^{ik\cdot\hat{x}} \ ,
\end{aligned} \tag{2.1.10}$$

where the following formula is used

$$e^A e^B = e^{A+B} e^{[A,B]/2} \ , \tag{2.1.11}$$

which is the Baker-Campbell-Hausdorff formula for $[[A,B],A] = [[A,B],B]$. Thus, one obtains the correspondence:

$$\hat{f}\hat{g} \longleftrightarrow f(x) \star g(x) = e^{\frac{i\theta}{2}\left(\partial_{x_1}\partial_{y_2} - \partial_{x_2}\partial_{y_1}\right)}\Big|_{y=x} \ , \tag{2.1.12}$$

which implies that the product of operators corresponds to the star product, or the Moyal product. The star product satisfies the associativity:

$$[f(x) \star g(x)] \star h(x) = f(x) \star [g(x) \star h(x)] \tag{2.1.13}$$

because $f(x) \star g(x) \neq g(x) \star f(x)$ and the product of operators satisfies the associativity $\left(\hat{f}\hat{g}\right)\hat{h} = \hat{f}\left(\hat{g}\hat{h}\right)$. In addition, the commutation relation using the star product is

$$\frac{1}{i\theta}\left[f(x), g(x)\right]_\star = \partial_{x_1} f(x) \partial_{x_2} g(x) - \partial_{x_2} f(x) \partial_{x_1} g(x) + O(\theta) \ . \tag{2.1.14}$$

In order to calculate the trace of the operators, we use the following basis on the Hilbert space:

$$\hat{x}_1 \left|x_1\right\rangle = x_1 \left|x_1\right\rangle \ , \quad \hat{x}_2 \left|x_2\right\rangle = x_2 \left|x_2\right\rangle \ . \tag{2.1.15}$$

By analogy with quantum mechanics, one obtains

$$\int \frac{dx_1}{\sqrt{2\pi\theta}} \left|x_1\right\rangle\left\langle x_1\right| \ , \quad \int \frac{dx_2}{\sqrt{2\pi\theta}} \left|x_2\right\rangle\left\langle x_2\right| \ , \tag{2.1.16}$$

$$\left\langle x_1 \middle| x_2 \right\rangle = e^{i\theta^{-1} x_1 x_2} \ . \tag{2.1.17}$$

Then, the trace is

$$\begin{aligned}
\mathrm{Tr}\hat{f} &= \int \frac{d^2k}{(2\pi)^2} \int d^2x \int \frac{dx_1'}{\sqrt{2\pi\theta}} f(x) e^{-ik\cdot x} \left\langle x_1' \middle| e^{ik\cdot\hat{x}} \middle| x_1' \right\rangle \\
&= \int \frac{d^2k}{(2\pi)^2} \int d^2x \int \frac{dx_1'}{\sqrt{2\pi\theta}} \int \frac{dx_2'}{\sqrt{2\pi\theta}} f(x) e^{-ik\cdot x} e^{\frac{i\theta}{2} k_1 k_2} \left\langle x_1' \middle| e^{ik\cdot\hat{x}_1} e^{ik\cdot\hat{x}_2} \middle| x_2' \right\rangle \left\langle x_2' \middle| x_1' \right\rangle \\
&= \int \frac{d^2k}{(2\pi)^2} \int d^2x \int \frac{d^2x'}{2\pi\theta} f(x) e^{-ik\cdot x} e^{\frac{i\theta}{2} k_1 k_2} e^{i\left(k_1 x_1' + k_2 x_2'\right)} \\
&= \int \frac{d^2x}{2\pi\theta} f(x) \ .
\end{aligned} \tag{2.1.18}$$

Namely, one finds the correspondence between the trace and the integral on $\mathbb{R}^2$:

$$\mathrm{Tr} \longleftrightarrow \int \frac{d^2x}{2\pi\theta} \ . \tag{2.1.19}$$

The RHS of (2.1.19) can be interpreted as phase space divided by $2\pi\hbar$ by viewing θ in (2.1.1) as $\hbar$. From the cyclicity of the trace, the integral of the star product satisfies

$$\int d^2x f_1(x) \star f_2(x) \star \cdots \star f_n(x) = \int d^2x f_n(x) \star f_1(x) \star \cdots \star f_{n-1}(x) \ . \tag{2.1.20}$$

In particular,

$$\int d^2x f(x) \star g(x) = \int d^2x f(x) g(x) \ . \tag{2.1.21}$$

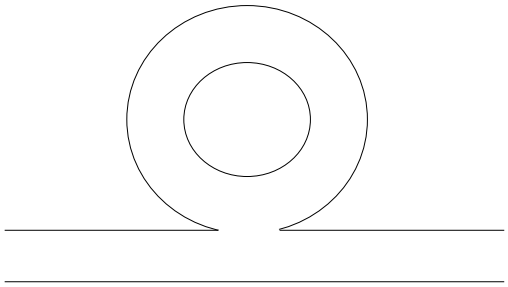

Figure 2.1: Planar diagram.

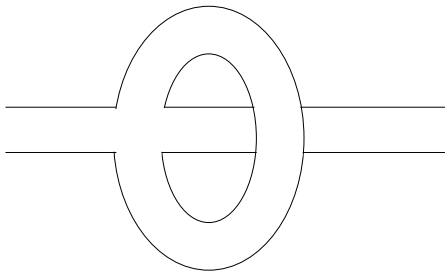

Figure 2.2: Non-planar diagram.

Let us consider a field theory on the non-commutative plane. We start with the matrix model:

$$S_{\rm MM} = 2\pi\theta {\rm Tr}\left(-\frac{1}{2}\left[\hat{p}_i, \Phi\right]^2 + \frac{\mu^2}{2}\Phi^2 + \frac{\lambda}{4}\Phi^4\right) \ . \tag{2.1.22}$$

By using the above properties, one can rewrite the action of the matrix model to that of a field theory on non-commutative plane:

$$S_{\rm NCP} = \int d^2x \left[\frac{1}{2}\left(\partial_{x_i}\phi(x)\right)^2 + \frac{\mu^2}{2}\phi(x)^2 + \frac{\lambda}{4}\phi(x)\star\phi(x)\star\phi(x)\star\phi(x)\right] \ . \tag{2.1.23}$$

The quadratic term in (2.1.23) agrees with that in the ordinary ϕ^4 theory, but the interaction term does not because of the star product.

In order to see the UV/IR mixing, we calculate the 1-loop correction to the propagator on the non-commutative plane. We consider (2.1.23) and rewrite it by Fourier modes:

$$S_{\rm NCP} = S_{\rm NCP,\,free} + S_{\rm NCP,\,int} \ , \tag{2.1.24}$$

$$S_{\rm NCP,\,free} = \int \frac{d^2p}{(2\pi)^2}\frac{d^2q}{(2\pi)^2}(2\pi)^2\delta^{(2)}(p+q)\frac{1}{2}\left(p^2+\mu^2\right)\phi(p)\phi(q) \ , \tag{2.1.25}$$

$$\begin{aligned} S_{\rm NCP,\,int} = {} & \frac{\lambda}{4}\int\frac{d^2p}{(2\pi)^2}\int\frac{d^2q}{(2\pi)^2}\int\frac{d^2r}{(2\pi)^2}\int\frac{d^2s}{(2\pi)^2}(2\pi)^2\delta^{(2)}(p+q+r+s) \\ & \times e^{-\frac{i\theta}{2}[p_1q_2-p_2q_1+(p_1+q_1)(r_2+s_2)-(p_2+q_2)(r_1+s_1)+r_1s_2-r_2s_1]}\phi(p)\phi(q)\phi(r)\phi(s) \ . \end{aligned} \tag{2.1.26}$$

The free propagator is the same as that in the ordinary field theory:

$$\langle\phi(p)\phi(q)\rangle = (2\pi)^2\delta^{(2)}(p+q)\frac{1}{p^2+\mu^2} \ . \tag{2.1.27}$$

There exist two diagrams for the 1-loop correction, one is the planar diagram (Fig. 2.1) and the other is the non-planar diagram (Fig. 2.2), and these diagrams are evaluated as

$$-2\lambda\int\frac{d^2q}{(2\pi)^2}\frac{1}{q^2+\mu^2} \ , \tag{2.1.28}$$

$$-\lambda \int \frac{d^2q}{(2\pi)^2} \frac{e^{-i\theta(p_1q_2-p_2q_1)}}{q^2+\mu^2} \ , \tag{2.1.29}$$

respectively. In (2.1.29), there is a phase factor $e^{-i\theta(p_1q_2-p_2q_1)}$, while there is no such factor in (2.1.28). In general, the planar diagram in field theories on non-commutative spaces agrees with that in corresponding theories on ordinary commutative spaces.

By using the Schwinger expression for the propagator

$$\frac{1}{q^2+\mu^2} = \int_0^\infty ds e^{-\left(q^2+\mu^2\right)s} \ , \tag{2.1.30}$$

we calculate (2.1.29):

$$(2.1.29) = -\lambda \int_0^\infty ds \int \frac{d^2q}{(2\pi)^2} e^{-\left(q^2+\mu^2\right)s+i\theta(p_1q_2-p_2q_1)} = -\frac{\lambda}{2\pi} \int_0^\infty ds \frac{1}{2s} e^{-\mu^2 s-\frac{\theta^2p^2}{4s}} \ . \tag{2.1.31}$$

In the case of commutative spaces ($\theta = 0$), this diverges logarithmically. We introduce a UV cutoff Λ and insert a factor $e^{-1/(4\Lambda^2 s)}$ in the integral (2.1.31):

$$(2.1.31) = -\frac{\lambda}{2\pi} \int_0^\infty ds \frac{1}{2s} e^{-\mu^2 s-\frac{1}{4s}(\theta^2p^2+1/\Lambda^2)} = -\frac{\lambda}{2\pi} K_0\left(\mu\sqrt{\theta^2p^2+\frac{1}{\Lambda^2}}\right) \ , \tag{2.1.32}$$

where $K_0(x)$ is the Bessel function of the second kind[10] and its asymptotic expansion is

$$K_0(x) = \sum_{a=0}^\infty \frac{1}{a!^2} \left(\frac{x}{2}\right)^{2a} \left(-\gamma + \sum_{b=1}^a \frac{1}{b} - \log\frac{x}{2}\right) \ . \tag{2.1.33}$$

Here, γ is the Euler's number[11]. (2.1.32) is expanded as

$$(2.1.32) = \frac{\lambda}{2\pi} \left[\gamma + \log\left(\frac{\mu}{2}\sqrt{\theta^2p^2+\frac{1}{\Lambda^2}}\right)\right] \left[1 + O\left(\mu\sqrt{\theta^2p^2+\frac{1}{\Lambda^2}}\right)\right] \tag{2.1.34}$$

For $\theta = 0$, (2.1.34) reproduces the UV logarithmic divergence. On the other hand, for $\theta \neq 0$, this is finite in the $\Lambda \to \infty$ limit with $p \neq 0$, while it diverges in the IR regime ($p \to 0$). The IR divergence originates from the UV divergence in commutative spaces. This is because the divergence is called the UV/IR mixing.

[10] The general form is $K_\nu(x) = \frac{1}{2}\left(\frac{\nu}{2}\right)^2 \int_0^\infty dt t^{-\nu-1} e^{-t-x^2/4t}$.

[11] $\gamma \equiv \lim_{n\to\infty} \left(\sum_{i=1}^n \frac{1}{i} - \log n\right) = 0.57721\ldots$.

2.1.2 Fuzzy sphere

Here, we introduce the fuzzy sphere, which is a typical example of compact non-commutative spaces. A scalar field theory on it is realized by a matrix model with a finite matrix size.

The coordinates $\hat{x}_i$ $(i = 1, 2, 3)$ on the fuzzy sphere satisfy the SU(2) algebra

$$[\hat{x}_i, \hat{x}_j] = i\rho\varepsilon_{ijk}\hat{x}_k \ . \tag{2.1.35}$$

They act on the Hilbert space with finite dimensions and take the following form

$$\hat{x}_i = \rho L_i \ , \tag{2.1.36}$$

where $(2j+1) \times (2j+1)$ matrices L_i are generators of SU(2) algebra with spin-j representations, which obey the commutation relation

$$[L_i, L_j] = i\epsilon_{ijk}L_k \ . \tag{2.1.37}$$

One can show the following relation:

$$\hat{x}_1^2 + \hat{x}_2^2 + \hat{x}_3^2 = \rho^2 j(j+1)\mathbf{1}_{2j+1} \ . \tag{2.1.38}$$

(2.1.38) is indeed the equation defining the sphere with radius

$$R = \rho\sqrt{j(j+1)} \ . \tag{2.1.39}$$

The continuum and commutative limit is give as

$$\rho \to 0 \ , \quad j \to \infty \ , \quad R = \rho\sqrt{j(j+1)} : \text{ fixed} \ . \tag{2.1.40}$$

We use standard basis on $(2j+1)$-dimensional Hilbert space:

$$|jr\rangle \quad (r = -j, -j+1, \ldots, j) \ . \tag{2.1.41}$$

L_i act on these basis as follows:

$$L_\pm |jr\rangle = \sqrt{(j \mp r)(j \pm r + 1)}\, |j\, r \pm 1\rangle \ , \quad L_3 |jr\rangle = r |jr\rangle \ , \tag{2.1.42}$$

where $L_\pm \equiv L_1 \pm iL_2$.

An arbitrary operator on this Hilbert space, $\hat{f}$, is expanded

$$\hat{f} = \sum_{r,r'} f_{r,r'} |jr\rangle \langle jr'| \ . \tag{2.1.43}$$

We define the fuzzy spherical harmonics as more useful basis:

$$\hat{Y}^{[j]}_{lm} = \sqrt{2j+1}\sum_{r,r'}(-1)^{-j+r'}C^{l\,m}_{j\,r\;j\,-r'}\,|jr\rangle\,\langle jr'|\ , \tag{2.1.44}$$

where $C^{l\,m}_{j\,r\;j\,-r'}$ are Clebsh-Gordan coefficients and $0 \le l \le 2j$, $-l \le m \le l$. Later, we can see that $2j$ is a UV cutoff. (2.1.44) corresponds to the composition of two spin-j, and the following commutation relations are satisfied:

$$\left[L_\pm, \hat{Y}^{[j]}_{lm}\right] = \sqrt{(l\mp m)(l\pm m+1)}\hat{Y}^{[j]}_{l\,m\pm1}\ , \quad \left[L_3, \hat{Y}^{[j]}_{lm}\right] = m\hat{Y}^{[j]}_{lm}\ . \tag{2.1.45}$$

The Hermitian conjugate is given as

$$\left(\hat{Y}^{[j]}_{lm}\right)^\dagger = (-1)^m\hat{Y}^{[j]}_{l\,-m}\ . \tag{2.1.46}$$

The orthonormal relation also holds

$$\frac{1}{2j+1}\mathrm{Tr}\left[\left(\hat{Y}^{[j]}_{lm}\right)^\dagger\hat{Y}^{[j]}_{l'm'}\right] = \delta_{l,l'}\delta_{m,m'}\ . \tag{2.1.47}$$

Moreover, the product of two fuzzy spherical harmonics is

$$\hat{Y}^{[j]}_{l_2m_2}\hat{Y}^{[j]}_{l_3m_3} = \sum_{l_1,m_1}\hat{C}^{l_1\,m_1}_{l_2\,m_2\;\;l_3\,m_3}\hat{Y}^{[j]}_{l_1m_1}\ , \tag{2.1.48}$$

where

$$\begin{aligned}\hat{C}^{l_1\,m_1}_{l_2\,m_2\;\;l_3\,m_3} &\equiv \frac{1}{2j+1}\mathrm{Tr}\left[\left(\hat{Y}^{[j]}_{l_1m_1}\right)^\dagger\hat{Y}^{[j]}_{l_2m_2}\hat{Y}^{[j]}_{l_3m_3}\right]\\ &= (-1)^{l_1+2j}\sqrt{(2j+1)(2l_2+1)(2l_3+1)}\;C^{l_1\,m_1}_{l_2\,m_2\;\;l_3\,m_3}\begin{Bmatrix} l_1 & l_2 & l_3\\ j & j & j\end{Bmatrix}\ ,\end{aligned} \tag{2.1.49}$$

and $\begin{Bmatrix} * & * & *\\ * & * & *\end{Bmatrix}$ is a $6j$ symbol.

On the other hand, the angular momentum operators

$$\mathcal{L}_\pm \equiv \mathcal{L}_1 \pm i\mathcal{L}_2 = e^{\pm i\varphi}\left(\pm\frac{\partial}{\partial\theta} + i\cot\theta\frac{\partial}{\partial\varphi}\right), \quad \mathcal{L}_3 = -i\frac{\partial}{\partial\varphi}\ , \tag{2.1.50}$$

act on the ordinal spherical harmonics $Y_{lm}(\Omega)$ as

$$\mathcal{L}_\pm Y_{lm}(\Omega) = \sqrt{(l\mp m)(l\pm m+1)}Y_{l\,m\pm1}(\Omega)\ , \quad \mathcal{L}_3Y_{lm}(\Omega) = mY_{lm}(\Omega)\ . \tag{2.1.51}$$

Here, $\Omega = (\theta,\varphi)$ is a coordinate on the sphere. The complex conjugate and the orthonormal relation of $Y_{lm}(\Omega)$ are

$$Y^*_{lm}(\Omega) = (-1)^mY_{l\,-m}(\Omega)\ , \tag{2.1.52}$$

$$\int \frac{d\Omega}{4\pi} Y^*_{lm}(\Omega) Y_{l'm'}(\Omega) = \delta_{l,l'}\delta_{m,m'} \ , \tag{2.1.53}$$

where $d\Omega \equiv \sin\theta d\theta d\varphi$ is the invariant measure on the sphere. (2.1.51)–(2.1.53) correspond to (2.1.45)–(2.1.47), respectively. Moreover, the product of two spherical harmonics is

$$Y_{l_2m_2}(\Omega) Y_{l_3m_3}(\Omega) = \sum_{l_1,m_1} \sqrt{\frac{(2l_2+1)(2l_3+1)}{2l_1+1}} C^{l_1\,0}_{l_2\,0\ l_3\,0} C^{l_1\,m_1}_{l_2\,m_2\ l_3\,m_3} Y_{l_1m_1}(\Omega) \ , \tag{2.1.54}$$

where

$$\sqrt{\frac{(2l_2+1)(2l_3+1)}{2l_1+1}} C^{l_1\,0}_{l_2\,0\ l_3\,0} C^{l_1\,m_1}_{l_2\,m_2\ l_3\,m_3} = \int \frac{d\Omega}{4\pi} Y^*_{l_1m_1}(\Omega) Y_{l_2m_2}(\Omega) Y_{l_3m_3}(\Omega) \ . \tag{2.1.55}$$

In the $j \to \infty$ limit, one can show

$$\hat{C}^{l_1\,m_1}_{l_2\,m_2\ l_3\,m_3} \to \sqrt{\frac{(2l_2+1)(2l_3+1)}{2l_1+1}} C^{l_1\,0}_{l_2\,0\ l_3\,0} C^{l_1\,m_1}_{l_2\,m_2\ l_3\,m_3} \tag{2.1.56}$$

for $l_1, l_2, l_3 \ll j$. Thus, (2.1.54) corresponds to (2.1.48). From the above, the fuzzy spherical harmonics corresponds to the spherical harmonics in the continuum limit:

$$\hat{Y}^{[j]}_{lm} \longleftrightarrow Y_{lm}(\Omega) \ , \tag{2.1.57}$$

$$[L_i, \ ] \longleftrightarrow \mathcal{L}_i \ , \tag{2.1.58}$$

$$\frac{1}{2j+1}\mathrm{Tr} \longleftrightarrow \int \frac{d\Omega}{4\pi} \ . \tag{2.1.59}$$

$\hat{f}$ is expanded as

$$\hat{f} = \sum_{l=0}^{2j} \sum_{m=-l}^{l} f_{lm} \hat{Y}^{[j]}_{lm} \tag{2.1.60}$$

with the fuzzy spherical harmonics $\hat{Y}^{[j]}_{lm}$. From this relation, a function on S^2 is defined by

$$f(\Omega) = \sum_{l=0}^{2j} \sum_{m=-l}^{l} f_{lm} Y_{lm}(\Omega) \ . \tag{2.1.61}$$

Thus, an operator on the Hilbert space is mapped to a function on the sphere. The upper limit of summation with respect to l, $2j$, corresponds to a UV cutoff. This regularization keeps a rotational symmetry.

2.2 Large-N reduction

Although the large-N reduction [34] was originally shown in the lattice gauge theory, we review the large-N reduction in ϕ^3 matrix field theory. We demonstrate the large-N reduction by using the momentum basis (section 2.2.1) as well as the coordinate basis (section 2.2.2).

2.2.1 Large-N reduction based on the momentum basis

Here, we consider the ϕ^3 matrix field theory:

$$S = \int d^D x \mathrm{Tr} \left\{ \frac{1}{2} \left[\partial_\mu \phi(x) \right]^2 + \frac{m^2}{2} \phi(x)^2 + \frac{\kappa}{3} \phi(x)^3 \right\} \ , \tag{2.2.1}$$

where $\phi(x)$ is an $N \times N$ Hermitian matrix-valued field. In order to obtain the reduced model, we apply the following rule

$$\phi(x) \to e^{iP_\mu x^\mu} \Phi e^{-iP_\mu x^\mu} \ , \quad \int d^D x \to \left(\frac{2\pi}{\Lambda} \right)^D = v \ , \tag{2.2.2}$$

where Φ is an $N \times N$ Hermitian matrix independent of the space and P_μ ($\mu = 1, \ldots, D$) are diagonal matrices:

$$P_\mu = \begin{pmatrix} p_\mu^{(1)} & & & \\ & p_\mu^{(2)} & & \\ & & \ddots & \\ & & & p_\mu^{(N)} \end{pmatrix} \ . \tag{2.2.3}$$

$p_\mu^{(i)}$ ($i = 1, \ldots, N$) represent N points distributing uniformly in D-dimensional cube with length Λ. Here, Λ corresponds to a UV cutoff of momenta and v corresponds to a volume for unit lattice, so that the second relation of (2.2.2) coincides with the prescription in the large- N reduction in the lattice theory where the volume V of space is replaced with the volume v of a unit lattice. Namely, the following relation holds:

$$V = Nv \ . \tag{2.2.4}$$

From (2.2.2), one can show

$$\partial_\mu \phi(x) \to e^{iP_\mu x^\mu} i \left[P_\mu, \Phi \right] e^{-iP_\mu x^\mu} \ . \tag{2.2.5}$$

Then, the reduced model takes the form:

$$\begin{aligned} S_{\mathrm{red}} &= v \mathrm{Tr} \left\{ -\frac{1}{2} \left[P_\mu, \Phi \right]^2 + \frac{m^2}{2} \Phi^2 + \frac{\kappa}{3} \Phi^3 \right\} \\ &= v \left\{ \frac{1}{2} \sum_{i,j} \left[\left(p^{(i)} - p^{(j)} \right)^2 + m^2 \right] |\Phi_{ij}|^2 + \frac{\kappa}{3} \sum_{i,j,k} \Phi_{ij} \Phi_{jk} \Phi_{ki} \right\} \ . \end{aligned} \tag{2.2.6}$$

From the action of the reduced model, the propagator and the vertex are read off as

$$\langle \Phi_{ij} \Phi_{kl} \rangle = \frac{1}{v} \frac{\delta_{il} \delta_{kj}}{\left(p^{(i)} - p^{(j)} \right)^2 + m^2} \ , \tag{2.2.7}$$

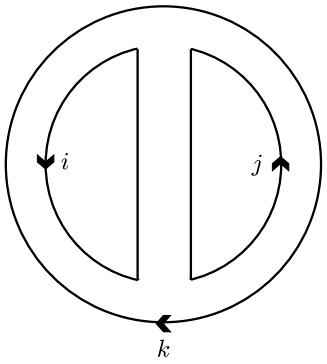

Figure 2.3: 2-loop planar diagram for the free energy.

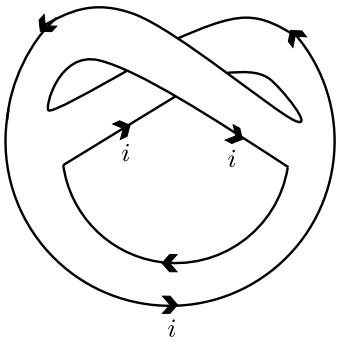

Figure 2.4: 2-loop non-planar diagram for the free energy.

and

$$v\kappa\delta_{jk}\delta_{lm}\delta_{ni} \ , \tag{2.2.8}$$

respectively. The preservation of momenta at the vertex is ensured by the product of matrices.

Let us calculate the free energy perturbatively. There are two 2-loop diagrams; one is a planar diagram (Fig. 2.3) and the other is a non-planar diagram (Fig. 2.4). The former is calculated as follows:

$$\text{Fig. } 2.3 = \frac{\kappa^2}{6} v^2 \frac{1}{v^3} \sum_{i,j,k} \frac{1}{\left(p^{(i)} - p^{(k)}\right)^2 + m^2} \frac{1}{\left(p^{(j)} - p^{(i)}\right)^2 + m^2} \frac{1}{\left(p^{(k)} - p^{(j)}\right)^2 + m^2} \ . \tag{2.2.9}$$

Here, we change variables

$$q_1 = p^{(i)} - p^{(k)} \ , \quad q_2 = p^{(k)} - p^{(j)} \ , \tag{2.2.10}$$

and use the relation valid in the large-N limit:

$$\frac{1}{v}\sum_i = N \int \frac{d^D q_1}{(2\pi)^D} \ , \quad \frac{1}{v}\sum_j = N \int \frac{d^D q_2}{(2\pi)^D} \ . \tag{2.2.11}$$

Then, the summation over the index k gives N, so that

$$(2.2.9) = v \frac{N^2 \lambda}{6} \int \frac{d^D q_1}{(2\pi)^D} \frac{d^D q_2}{(2\pi)^D} \frac{1}{q_1^2 + m^2} \frac{1}{q_2^2 + m^2} \frac{1}{\left(q_1 + q_2\right)^2 + m^2} \ , \tag{2.2.12}$$

where $\lambda \equiv \kappa^2 N$ is the 't Hooft coupling constant. On the other hand, the non-planar diagram is

$$\text{Fig. } 2.4 = v \frac{N^2 \lambda}{6} \frac{1}{m^6} \times \frac{1}{V^2} \ . \tag{2.2.13}$$

The 2-loop diagrams for the free energy in the original theory (2.2.1) are also Figs. 2.3 and 2.4. (2.2.12)/v is equivalent to Fig. 2.3 divided by V in the original theory, while (2.2.13) does not agree with Fig. 2.4 in the original theory. In the large-N limit (the 't Hooft limit or the planar limit), the non-planar diagram is suppressed by $1/N^2$ compared to the planar diagram. Generally, only the planar diagram contributes to the free energy in the large-N limit. In the reduced model, the limit

$$V = Nv \to \infty \tag{2.2.14}$$

is taken when summations over the index i are replaced with integrals over the momenta. (2.2.13) is suppressed by $1/V^2$ compared to (2.2.12).

Thus, one finds that the reduced model (2.2.6) reproduces the large-N limit of the original theory in the following limit:

$$N \to \infty \ , \quad \kappa \to 0 \ , \quad V = Nv \to \infty \ , \quad \lambda : \text{ fixed} \ . \tag{2.2.15}$$

The relation between F and $F_{\rm red}$ which are free energies in the original theory and the reduced model, respectively, is

$$\frac{F}{N^2 V} = \frac{F_{\rm red}}{N^2 v} \ . \tag{2.2.16}$$

For n-point correlation functions, the following relation holds:

$$\frac{1}{N^{n/2+1}} \left\langle \mathrm{Tr}\left(\phi(x_1)\phi(x_2)\cdots\phi(x_n)\right)\right\rangle = \frac{1}{N^{n/2+1}} \left\langle \mathrm{Tr}\left(\hat{\phi}(x_1)\hat{\phi}(x_2)\cdots\hat{\phi}(x_n)\right)\right\rangle_{\rm red} \ , \tag{2.2.17}$$

where

$$\hat{\phi}(x) = e^{iP_\mu x^\mu} \Phi e^{-iP_\mu x^\mu} \ , \tag{2.2.18}$$

and $\langle\cdots\rangle$ and $\langle\cdots\rangle_{\rm red}$ denote expectation values in the original theory and the reduced model, respectively.

2.2.2 Large-N reduction based on the coordinate basis

Here, we illustrate the large-N reduction by using the coordinate basis.

Again, we consider the ϕ^3 matrix field theory (2.2.1). The propagator is

$$\langle \phi_{ij}(x_1)\phi_{kl}(x_2)\rangle = D(x_1 - x_2)\delta_{il}\delta_{jk} \ , \tag{2.2.19}$$

where the explicit form of $D(x)$ is not necessary in the following. Let us again calculate the free energy at the 2-loop level. One can show

$$\text{Fig. 2.3} = \frac{N^2\lambda}{6} \int d^D x_1 d^D x_2 D(x_1 - x_2)^3 \ , \tag{2.2.20}$$

and Fig. $2.4 = (2.2.20)/N^2$, which implies that only the planar diagram contributes in the large-N limit.

The rule to obtain the reduced model is the same as (2.2.2). Here, we represent the rule using the coordinate basis:

$$\phi(x) \to e^{i\hat{P}_\mu x^\mu}\hat{\Phi}e^{-i\hat{P}_\mu x^\mu} \ , \quad \int d^D x \to v \ , \tag{2.2.21}$$

where $\hat{\Phi}$ is a Hermitian operator acting on the function space on $\mathbb{R}^D$. momentum operators $\hat{P}_\mu$ act on the coordinate basis $|x\rangle$ $(x \in \mathbb{R}^D)$ as follows:

$$\hat{P}_\mu |x\rangle = i\partial_\mu |x\rangle \ , \quad \langle x| \hat{P}_\mu = -i\partial_\mu \langle x| \ . \tag{2.2.22}$$

One obtains the reduced model by applying the rule (2.2.21) to (2.2.1):

$$S_{\rm red} = v{\rm Tr}\left(-\frac{1}{2}\left[\hat{P}_\mu, \hat{\Phi}\right]^2 + \frac{m^2}{2}\hat{\Phi}^2 + \frac{\kappa}{3}\hat{\Phi}^3\right) \ . \tag{2.2.23}$$

We introduce the bi-local field representation:

$$\phi(x, x') \equiv \left\langle x\middle|\hat{\Phi}\middle|x'\right\rangle \ . \tag{2.2.24}$$

From the Hermiticity of $\hat{\Phi}$, $\phi^*(x, x') = \phi(x', x)$ is satisfied. (2.2.23) is rewritten by using the bi-local representation:

$$\begin{aligned} S_{\rm red} = v\int d^D x d^D x' \left[-\frac{1}{2}\phi(x, x')\left(\partial_\mu + \partial'_\mu\right)^2 \phi(x', x) + \frac{m^2}{2}\phi(x, x')\phi(x', x)\right] \\ + v\int d^D x d^D x' d^D x'' \frac{\kappa}{3}\phi(x, x')\phi(x', x'')\phi(x'', x) \ . \end{aligned} \tag{2.2.25}$$

By changing variables

$$X^\mu = x^\mu \ , \quad \xi^\mu = x^\mu - x'^\mu \ , \tag{2.2.26}$$

it is useful to regard $\phi(x, x')$ as the function of X and ξ, and then one finds the relation

$$\left(\partial_\mu + \partial'_\mu\right)\phi(x, x') = \frac{\partial}{\partial X^\mu}\phi(x, x') \ . \tag{2.2.27}$$

The propagator of the reduced model is given as

$$\langle \phi(x_1, x'_1)\phi(x'_2, x_2)\rangle = \frac{1}{v}D(x_1 - x_2)\delta^{(D)}\left((x_1 - x'_1) - (x_2 - x'_2)\right) \ , \tag{2.2.28}$$

which implies relative coordinates are preserved in the propagation.

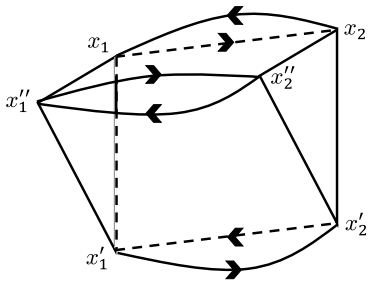

Figure 2.5: 2-loop planar diagram in the bi-local representation for the free energy.

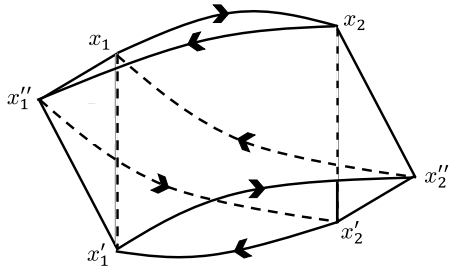

Figure 2.6: 2-loop non-planar diagram in the bi-local representation for the free energy.

Here, let us calculate the free energy at the 2-loop level in the reduced model. Figs. 2.5 and 2.6 are the planar diagram[12] and the non-planar diagram, respectively. The planar diagram is calculated as

$$\begin{aligned}\text{Fig. 2.5} = \frac{\kappa^2}{6v}\int d^Dx_1 d^Dx_1' d^Dx_1'' d^Dx_2 d^Dx_2' d^Dx_2'' D(x_1-x_2)\delta^{(D)}\left((x_1-x_1')-(x_2-x_2')\right) \\ \times D(x_1'-x_2')\delta^{(D)}\left((x_1'-x_1'')-(x_2'-x_2'')\right)D(x_1''-x_2'')\delta^{(D)}\left((x_1''-x_1)-(x_2''-x_2)\right) \\ = \frac{\kappa^2}{6v}\delta^{(D)}(0)V^2\int d^Dx_1 d^Dx_2 D(x_1-x_2)^3\ , \qquad (2.2.29)\end{aligned}$$

where V^2 comes from degrees of freedom of x_1' and x_1''. Since

$$\delta^{(D)}(0) = \frac{1}{v}\ , \quad V = Nv \qquad (2.2.30)$$

one finds the following relation:

$$\frac{(2.2.20)}{N^2V} = \frac{(2.2.29)}{N^2v} \qquad (2.2.31)$$

in the $N\to\infty$, $v\to 0$, $V\to\infty$ limit as before. On the other hand, the non-planar diagram is

$$\begin{aligned}\text{Fig. 2.6} = \frac{\kappa^2}{6v}\int d^Dx_1 d^Dx_1' d^Dx_1'' d^Dx_2 d^Dx_2' d^Dx_2'' D(x_1-x_2)\delta^{(D)}\left((x_1-x_1')-(x_2-x_2')\right) \\ \times D(x_1'-x_2'')\delta^{(D)}\left((x_1'-x_1'')-(x_2''-x_2)\right)D(x_1''-x_2')\delta^{(D)}\left((x_1''-x_1)-(x_2'-x_2'')\right) \\ = \frac{\kappa^2}{6v}\delta^{(D)}(0)\int d^Dx_1 d^Dx_1' d^Dx_2 d^Dx_2'' D(x_1-x_2)D(x_1'-x_2'')D(x_1-x_2'')\ , \qquad (2.2.32)\end{aligned}$$

which is suppressed by $1/V^2$ compared to (2.2.29) in the $V\to\infty$ limit as before. Thus, one finds again (2.2.16). One can show again (2.2.17) in the same way.

[12]Although this diagram is no longer drawn in the plane, it is called the *planar* diagram.

2.3 Type IIB matrix model

The action of the type IIB matrix model is formally given by the form of a dimensional reduction of 10-dimensional $\mathcal{N} = 1$ supersymmetric SU(N) Yang-Mills theory to 0 dimension. It takes the following form:

$$S_{\rm IIB} = S_{\rm b} + S_{\rm f} \ , \tag{2.3.1}$$

$$S_{\rm b} = -\frac{1}{4g^2}{\rm Tr}\left(\left[A^M, A^N\right]\left[A_M, A_N\right]\right) \ , \tag{2.3.2}$$

$$S_{\rm f} = -\frac{1}{2g^2}{\rm Tr}\left(\bar{\Psi}\Gamma^M\left[A_M, \Psi\right]\right) \ , \tag{2.3.3}$$

where A^M $(M = 0, \ldots, 9)$ and Ψ are $N \times N$ traceless Hermitian matrices and Γ^M are 10-dimensional Gamma matrices. The model has SO(9,1) symmetry. A^M and Ψ are transformed as the Lorentz vector and the Majorana-Weyl spinor, respectively, under the SO(9,1) transformation. The model possesses SU(N) symmetry:

$$A'_M = \mathcal{U}A_M\mathcal{U}^\dagger \ , \quad \Psi' = \mathcal{U}\Psi\mathcal{U}^\dagger \ , \tag{2.3.4}$$

where $\mathcal{U} \in {\rm SU}(N)$. The model is also invariant under the following transformations:

$$\delta^{(1)}A_M = i\bar{\epsilon}_1\Gamma_M\Psi \ , \quad \delta^{(1)}\Psi = \frac{i}{2}\Gamma^{MN}\left[A_M, A_N\right]\epsilon_1 \ , \tag{2.3.5}$$

$$\delta^{(2)}A_M = 0 \ , \quad \delta^{(2)}\Psi = \epsilon_2\mathbf{1}_{N\times N} \ , \tag{2.3.6}$$

$$\delta_{\rm T}A_M = c_M\mathbf{1}_{N\times N} \ , \quad \delta_{\rm T}\Psi = 0 \ , \tag{2.3.7}$$

$$\delta_G A_M = i\left[\Lambda, A_M\right] \ , \quad \delta_G\Psi = i\left[\Lambda, \Psi\right] \ . \tag{2.3.8}$$

Here, ϵ_1 and ϵ_2 are 10-dimensional Majorana-Weyl spinors and Grassmann-odd parameters, c_M are 10-dimensional vectors and Grassmann-even parameters, $\mathbf{1}_{N\times N}$ is the $N\times N$ identity matrix, and Λ is an $N \times N$ Hermitian matrix. Let generators of (2.3.5) – (2.3.7) be $Q^{(1)}$, $Q^{(2)}$, and P_M, respectively, and $\tilde{Q}^{(i)}$ $(i = 1, 2)$ are defined by

$$\tilde{Q}^{(1)} = Q^{(1)} + Q^{(2)} \ , \quad \tilde{Q}^{(2)} = i\left(Q^{(1)} - Q^{(2)}\right) \ . \tag{2.3.9}$$

One can show that the following relation holds

$$\left[\bar{\epsilon}_1\tilde{Q}^{(i)}, \bar{\epsilon}_2\tilde{Q}^{(j)}\right] = -2\delta^{ij}\bar{\epsilon}_1\Gamma^M\epsilon_2 P_M \tag{2.3.10}$$

up to terms proportional to equations of motion of Ψ $\Gamma^M\left[A_M, \Psi\right] = 0$ and the gauge transformation (2.3.8). This is the algebra of $\mathcal{N} = 2$ supersymmetry in 10 dimensions with P_M identified with momenta. In this case, (2.3.7) represents the translation, and

eigenvalues of A_M are interpreted as coordinates. $\mathcal{N} = 2$ supersymmetry is maximal symmetry in 10 dimensions, so that the theory must include the graviton if the theory is unitary and includes massless fields. Thus, the existence of this symmetry strongly suggests that the type IIB matrix model includes gravity.

In the following, we show that the action is derived from the Green-Schwarz action of the Nambu-Goto type for the type IIB superstring theory:

$$S_{\rm NG} = -T \int d^2\sigma \left[\sqrt{-\frac{1}{2}\Sigma^{MN}\Sigma_{MN}} + i\epsilon^{ab}\partial_a X^M \left(\bar{\theta}^1 \Gamma_M \partial_b \theta^1 + \bar{\theta}^2 \Gamma_M \partial_b \theta^2 \right) + \epsilon^{ab} \bar{\theta}^1 \Gamma_M \partial_a \theta^1 \bar{\theta}^2 \Gamma_M \partial_b \theta^2 \right] . \tag{2.3.11}$$

Here, T is a tension of a string, σ^a $(a = 1, 2)$ are coordinates of the world-sheet, θ^1 and θ^2 are 10-dimensional Majorana-Weyl spinors and have the same chirality in 10 dimensions because we consider the type IIB superstring theory. Σ^{MN} are defined by

$$\Sigma^{MN} = \epsilon^{ab} \Pi_a^M \Pi_b^N , \tag{2.3.12}$$

$$\Pi_a^M = \partial_a X^M - i\bar{\theta}^1 \Gamma^M \partial_a \theta^1 + i\bar{\theta}^2 \Gamma^M \partial_a \theta^2 . \tag{2.3.13}$$

By removing θ^1 and θ^2 and setting M to be $0, 1, \ldots, 25$, (2.3.11) reduces to the Numbu-Goto action for the bosonic string.

(2.3.11) has 10-dimensional $\mathcal{N} = 2$ supersymmetry:

$$\delta_{\rm SUSY}\theta^i = \epsilon^i , \quad \delta_{\rm SUSY} X^M = i\bar{\epsilon}^1 \Gamma^M \theta^1 - \bar{\epsilon}^2 \Gamma^M \theta^2 , \tag{2.3.14}$$

and κ-symmetry:

$$\delta_\kappa \theta^i = \alpha^i , \quad \delta_\kappa X^M = i\bar{\theta}^1 \Gamma^M \alpha^1 - \bar{\theta}^2 \Gamma^M \alpha^2 . \tag{2.3.15}$$

Here,

$$\alpha^1 = \left(1 + \tilde{\Gamma} \kappa^1 \right) , \tag{2.3.16}$$

$$\alpha^2 = \left(1 - \tilde{\Gamma} \kappa^2 \right) , \tag{2.3.17}$$

$$\tilde{\Gamma} = \Sigma_{MN} \Gamma^{MN} \Big/ 2\sqrt{-\frac{1}{2}\Sigma^{KL}\Sigma_{KL}} , \tag{2.3.18}$$

and κ^1 and κ^2 are local Grassmann-odd parameters that are Majorana-Wely fermions. One can show $\tilde{\Gamma}^2 = 1$, and finds from (2.3.16) and (2.3.17) that each α^i has half degrees of freedom of local Majorana-Weyl fermion.

We fix the κ-symmetry by taking a gauge-fixing condition:

$$\theta^1 = \theta^2 = \Psi , \tag{2.3.19}$$

which preserves the 10-dimensional Lorentz symmetry since θ^i have the same chirality.

This gauge fixing leads (2.3.11) to

$$\tilde{S}_{\rm NG} = -T \int d^2\sigma \left[\sqrt{-\frac{1}{2}\sigma^{MN}\sigma_{MN}} + 2i\epsilon^{ab}\partial_a X^M \bar{\Psi}\Gamma_M \partial_b \Psi \right] , \tag{2.3.20}$$

where

$$\sigma^{MN} = \epsilon^{ab}\partial_a X^M \partial_b X^N . \tag{2.3.21}$$

One can show that (2.3.20) still has $\mathcal{N} = 2$ supersymmetry. The supersymmetric transformation is obtained by combining with (2.3.14) and (2.3.15) such that the gauge-fixing condition (2.3.19) is kept. Namely, we define the following transformation δ

$$\delta\theta^i = (\delta_{\rm SUSY} + \delta_\kappa)\,\theta^i , \quad \delta X^M = (\delta_{\rm SUSY} + \delta_\kappa)\, X^M , \tag{2.3.22}$$

and take κ^i

$$\kappa^1 = \frac{-\epsilon^1 + \epsilon^2}{2} , \quad \kappa^2 = \frac{\epsilon^1 - \epsilon^2}{2} \tag{2.3.23}$$

so that $\delta\theta^1 = \delta\theta^2$. Here, we define ξ and ζ by

$$\xi = \frac{\epsilon^1 + \epsilon^2}{2} , \quad \zeta = \frac{\epsilon^1 - \epsilon^2}{2} , \tag{2.3.24}$$

and then (2.3.22) implies

$$\delta^{(1)} X^M = 4i\bar{\zeta}\Gamma^M\Psi , \quad \delta^{(1)}\Psi = -\sigma_{MN}\Gamma^{MN}\zeta \Big/ 2\sqrt{-\frac{1}{2}\sigma^{KL}\sigma_{KL}} , \tag{2.3.25}$$

$$\delta^{(2)} X^M = 0 , \quad \delta^{(2)}\Psi = \xi . \tag{2.3.26}$$

In order to rewrite $\tilde{S}_{\rm NG}$ to the Schild action, we introduce the Poisson bracket

$$\{X, Y\}_{\rm PB} = \frac{1}{\sqrt{g}}\epsilon^{ab}\partial_a X \partial_b Y , \tag{2.3.27}$$

where $g = \det g_{ab}$ and g_{ab} is the world-sheet metric. The Schild action is

$$S_{\rm Sch} = \int d^2\sigma\sqrt{g}\left[\alpha\left(\frac{1}{4}\left\{X^M, X^N\right\}^2_{\rm PB} - \frac{i}{2}\bar{\Psi}\Gamma^M\left\{X_M, \Psi\right\}_{\rm PB}\right) + \beta\right] . \tag{2.3.28}$$

From the equation of motion of $\sqrt{g}$, one finds

$$\sqrt{g} = \frac{1}{2}\sqrt{\frac{\alpha}{\beta}}\sqrt{(\epsilon^{ab}\partial_a X^M \partial_b X^N)^2} . \tag{2.3.29}$$

By substituting (2.3.29), one obtains

$$S_{\rm Sch} = \int d^2\sigma \left[-\frac{i}{2}\alpha\epsilon^{ab}\partial_a X_M \bar{\Psi}\Gamma^M\partial_b\Psi + \sqrt{\alpha\beta}\sqrt{(\epsilon^{ab}\partial_a X^M\partial_b X^N)^2}\right] , \tag{2.3.30}$$

which agrees with $\tilde{S}_{\rm NG}$ up to normalization of Ψ. In (2.3.28), symmetries of (2.3.25) and (2.3.26) are realized by

$$\delta^{(1)}X^M = i\bar{\zeta}\Gamma^M\Psi \ , \quad \delta^{(1)}\Psi = -\frac{1}{2}\left\{X_M, X_N\right\}_{\rm PB}\Gamma^{MN}\zeta \ , \tag{2.3.31}$$

and

$$\delta^{(2)}X^M = 0 \ , \quad \delta^{(2)}\Psi = \xi \ , \tag{2.3.32}$$

respectively.

The path integral for (2.3.28) is defined by

$$\mathcal{Z} = \int \mathcal{D}\sqrt{g}\mathcal{D}X\mathcal{D}\Psi e^{-S_{\rm Sch}} \ . \tag{2.3.33}$$

(2.3.28) has the diffeomorphic invariance on the world-sheet:

$$\delta_{\rm diff}X^M = \epsilon^a\partial_a X^M \ , \tag{2.3.34}$$

$$\delta_{\rm diff}\Psi = \epsilon^a\partial_a\Psi \ , \tag{2.3.35}$$

$$\delta_{\rm diff}\sqrt{g} = \partial_a\left(\epsilon^a\sqrt{g}\right) \ . \tag{2.3.36}$$

In (2.3.33), we assume that the path-integral measure also has this invariance. By fixing $\sqrt{g}$, this invariance is partially gauge-fixed. From (2.3.36), ϵ^a are restricted as

$$\partial_a\left(\epsilon^a\sqrt{g}\right) = 0 \ . \tag{2.3.37}$$

The diffeomorphism with this restriction is the area preserving diffeomorphism. (2.3.37) is solved

$$\epsilon^a = \frac{1}{\sqrt{g}}\epsilon^{ab}\partial_b\rho(\sigma) \ , \tag{2.3.38}$$

where $\rho(\sigma)$ is an arbitrary function of σ^a, and (2.3.34) and (2.3.35) become

$$\delta_{\rm apd}X^M = \left\{X^M, \rho\right\}_{\rm PB} \ , \tag{2.3.39}$$

$$\delta_{\rm apd}\Psi = \left\{\Psi, \rho\right\}_{\rm PB} \ , \tag{2.3.40}$$

which implies that the area preserving diffeomorphism is given by the Poisson bracket. The algebra satisfied by the Poisson bracket is w_∞-algebra.

Here, we regularize w_∞-algebra by using SU(n) algebra. Then, the Poisson bracket and the integral on the world-sheet are replaced by the commutator and the trace with respect to $n \times n$ matrices, respectively:

$$\{\ ,\ \}_{\rm PB} \longrightarrow -i\left[\ ,\ \right] \ , \quad \int\frac{d^2\sigma}{2\pi}\sqrt{g} \longrightarrow {\rm Tr} \ . \tag{2.3.41}$$

Fields on the world-sheet X^M, Ψ, and ρ become $n \times n$ Hermitian matrices. Properties of the Poisson bracket

$$\int d^2\sigma\sqrt{g}\,\{X,Y\}_{\rm PB} = 0\ , \quad \int d^2\sigma\sqrt{g}X\,\{Y,Z\}_{\rm PB} = \int d^2\sigma\sqrt{g}Z\,\{X,Y\}_{\rm PB} \tag{2.3.42}$$

become properties of the trace

$$\mathrm{Tr}([X,Y]) = 0\ , \quad \mathrm{Tr}(X\,[Y,Z]) = \mathrm{Tr}(Z\,[X,Y])\ . \tag{2.3.43}$$

By applying regularization (2.3.41) to (2.3.28), one obtains

$$S = 2\pi\alpha\mathrm{Tr}\left(-\frac{1}{4}\,[A_M,A_N]^2 - \frac{1}{2}\bar{\Psi}\Gamma^M\,[A_M,\Psi]\right) + 2\pi\beta\mathrm{Tr}\mathbf{1}\ , \tag{2.3.44}$$

where $n\times n$ Hermitian matrices A_M correspond to fields on the world-sheet X_M. The path integral (2.3.33) becomes

$$Z = \sum_{n=0}^{\infty}\int dAd\Psi e^{-S}\ , \tag{2.3.45}$$

where

$$\begin{aligned} dA &= \prod_M \left[\prod_i d\,(A_M)_{ii}\right]\left[\prod_{i>j} d\mathrm{Re}\,(A_M)_{ij}\,d\mathrm{Im}\,(A_M)_{ij}\right]\ , \\ d\Psi &= \prod_\alpha \left[\prod_i d\,(\Psi_\alpha)_{ii}\right]\left[\prod_{i>j} d\mathrm{Re}\,(\Psi_\alpha)_{ij}\,d\mathrm{Im}\,(\Psi_\alpha)_{ij}\right]\ . \end{aligned} \tag{2.3.46}$$

The summation over n comes from $\int \mathcal{D}g$, which remains even after the gauge fixing $\sqrt{g} =$ const.. In this way, one obtains a matrix model.

By applying the regularization (2.3.41) to (2.3.39) and (2.3.40), one obtains

$$\delta A^M = i\left[\rho, A^M\right]\ , \quad \delta\Psi = i\,[\rho,\Psi]\ , \tag{2.3.47}$$

where ρ is an arbitrary $n\times n$ Hermitian matrix. (2.3.47) agrees with (2.3.8) if n is replaced with N. (2.3.31) and (2.3.32) become

$$\delta^{(1)}A^M = i\bar{\zeta}\Gamma^M\Psi, \quad \delta^{(1)}\Psi = \frac{i}{2}\,[A_M,A_N]\,\Gamma^{MN}\zeta\ , \tag{2.3.48}$$

and

$$\delta^{(2)}A^M = 0, \quad \delta^{(2)}\Psi = \xi\ , \tag{2.3.49}$$

respectively. If n is replaced with N, (2.3.48) and (2.3.49) agree with (2.3.5) and (2.3.6), respectively. (2.3.44) and (2.3.45) are invariant under (2.3.47), (2.3.48) and (2.3.49), and the matrix model has this symmetry.

Let us see the relation between the type IIB matrix model and the theory defined by (2.3.44) and (2.3.45). The summation over the matrix size n exists in (2.3.45) and the term proportional to Tr$\mathbf{1}$ exists in (2.3.44), while those do not in the type IIB matrix model. The measure in both of matrix models is the same as (2.3.46). Let us consider $n \times n$ diagonal block in A_M and Ψ on the type IIB matrix model. By integrating out the other parts of matrices, one obtains the effective action with respect to $n \times n$ matrices, which contains the original action and βTr$\mathbf{1}$ as the leading correction, where β is interpreted as the chemical potential. Therefore, (2.3.44) is considered as the effective theory of the type IIB matrix model.

The type IIB matrix model is regarded as the regularization of the type IIB superstring. This model naturally includes the many-body system of string, so that it is non-perturbative formulation of superstring theory.

Chapter 3

Renormalization in a scalar field theory on the fuzzy sphere

In this chapter, we study renormalization of a scalar field theory on the fuzzy sphere by Monte Carlo simulations. We define the correlation functions by using the Berezin symbol [75]. First, we show that the 2-point and 4-point correlation functions are made independent of the matrix size by tuning a parameter in the theory. This implies that the theory is non-perturbatively renormalizable. Next, we identify the phase boundary by measuring the susceptibility that is an order parameter for the Z_2 symmetry and calculate the 2-point and 4-point correlation functions on the boundary. We find that the theory behaves as a conformal field theory at short distances on the phase boundary.

3.1 Review of scalar field theory on the fuzzy sphere

Here, we examine a following matrix model:

$$S_{\text{fuzzy}} = \frac{1}{N}\text{Tr}\left(-\frac{1}{2}[L_i,\Phi]^2 + \frac{\mu^2}{2}\Phi^2 + \frac{\lambda}{4}\Phi^4\right) , \tag{3.1.1}$$

where Φ is an $N \times N$ Hermitian matrix and $N = 2j+1$. The theory possesses the Z_2 symmetry: $\Phi \to -\Phi$. The path integral measure is given by $d\Phi e^{-S}$, where

$$d\Phi = \prod_{i=1}^{N} d\Phi_{ii} \prod_{1\le j<k\le N} d\text{Re}\Phi_{jk} d\text{Im}\Phi_{jk} . \tag{3.1.2}$$

The theory (3.1.1) reduces to the following continuum theory on a sphere with the radius R at the tree level in the $N \to \infty$ limit, which corresponds to the so-called commutative limit:

$$S_{\text{comm}} = \frac{R^2}{4\pi}\int d\Omega \left(-\frac{1}{2R^2}(\mathcal{L}_i\phi)^2 + \frac{m^2}{2}\phi^2 + \frac{g}{4}\phi^4\right) . \tag{3.1.3}$$

The correspondence of the parameters in (3.1.1) and (3.1.3) is given by

$$\mu^2 = R^2 m^2 , \quad \lambda = R^2 g . \tag{3.1.4}$$

By expanding Φ in terms of $\hat{Y}^{[j]}_{lm}$, one can rewrite (3.1.1) as

$$S_{\text{fuzzy}} = S_{\text{fuzzy, free}} + S_{\text{fuzzy, int}} \ , \tag{3.1.5}$$

$$S_{\text{fuzzy, free}} = \sum_{l,m} \frac{(-1)^m}{2} \left[l(l+1) + \mu^2 \right] \phi_{lm} \phi_{l\,-m} \ , \tag{3.1.6}$$

$$S_{\text{fuzzy, int}} = \sum_{l_1,\ldots,l_5} \sum_{m_1,\ldots,m_5} \frac{\lambda(-1)^{m_5}}{4} \hat{C}^{l_5\, m_5}_{l_1\, m_1\ l_2\, m_2} \hat{C}^{l_5\, -m_5}_{l_3\, m_3\ l_4\, m_4} \phi_{l_1 m_1} \phi_{l_2 m_2} \phi_{l_3 m_3} \phi_{l_4 m_4} \ . \tag{3.1.7}$$

On the other hand, by expanding $\phi(\Omega)$ in terms of $Y_{lm}(\Omega)$, one can rewrite (3.1.3) as

$$S_{\text{comm}} = S_{\text{comm, free}} + S_{\text{comm, int}} \ , \tag{3.1.8}$$

$$S_{\text{comm, free}} = \sum_{l,m} \frac{(-1)^m}{2} \left[l(l+1) + R^2 m^2 \right] \phi_{lm} \phi_{l\,-m} \ , \tag{3.1.9}$$

$$\begin{aligned} S_{\text{comm, int}} = & \sum_{l_1,\ldots,l_5} \sum_{m_1,\ldots,m_5} \frac{R^2 g(-1)^{m_5}}{4} \sqrt{\frac{(2l_1+1)(2l_2+1)(2l_3+1)(2l_4+1)}{2l_5+1}} \\ & \times C^{l_5\, m_5}_{l_1\, m_1\ l_2\, m_2} C^{l_5\, -m_5}_{l_3\, m_3\ l_4\, m_4} C^{l_5\, 0}_{l_1\, m_1\ l_2\, m_2} C^{l_5\, 0}_{l_3\, m_3\ l_4\, m_4} \phi_{l_1 m_1} \phi_{l_2 m_2} \phi_{l_3 m_3} \phi_{l_4 m_4} \ . \end{aligned} \tag{3.1.10}$$

From (2.1.56), the above theories agree on the $j \to \infty$ limit. Indeed, this statement is correct only at the tree level by paying attention to (2.1.56) with $l_1, l_2, l_3 \ll j$, but they differ with the quantum correction, which is the UV/IR anomaly [13, 14] and argued in Appendix B.

To define correlation functions, we introduce the Berezin symbol [75] that is constructed from the Bloch coherent state [76] because this definition is useful for numerical simulation. We parametrize the sphere in terms of the standard polar coordinates $\Omega = (\theta, \varphi)$. The Bloch coherent state $|\Omega\rangle$ is localized around the point (θ, φ) with the width $R/\sqrt{N}$. The Berezin symbol for an $N \times N$ matrix Φ is given by $\langle \Omega | \Phi | \Omega \rangle$, and identified with the field $\phi(\Omega)$ in the correspondence at the tree level between (3.1.1) and (3.1.3). The Bloch coherent state and the Berezin symbol are reviewed in appendix.

3.2 Correlation functions

3.2.1 Definition

By denoting the Berezin symbol (see, Appendix A) briefly as

$$\varphi(\Omega) = \langle \Omega | \Phi | \Omega \rangle \ , \tag{3.2.1}$$

we define the n-point correlation function in the theory (3.1.1) as

$$\langle \varphi(\Omega_1) \varphi(\Omega_2) \cdots \varphi(\Omega_n) \rangle = \frac{\int d\Phi \ \varphi(\Omega_1) \varphi(\Omega_2) \cdots \varphi(\Omega_n) \ e^{-S_{\text{fuzzy}}}}{\int d\Phi \ e^{-S_{\text{fuzzy}}}} \ . \tag{3.2.2}$$

The correlation function (3.2.2) is a counterpart of $\langle\phi(\Omega_1)\phi(\Omega_2)\cdots\phi(\Omega_n)\rangle$ in the theory (3.1.3).

We assume that the matrix Φ in (3.1.1) is renormalized as

$$\Phi = \sqrt{Z}\Phi_{\rm r} \ , \tag{3.2.3}$$

where $\Phi_{\rm r}$ is the renormalized matrix. Then, we define the renormalized Berezin symbol $\varphi_{\rm r}(\Omega)$ by

$$\varphi(\Omega) = \sqrt{Z}\varphi_{\rm r}(\Omega) \ , \tag{3.2.4}$$

and the renormalized n-point correlation function $\langle\varphi_{\rm r}(\Omega_1)\varphi_{\rm r}(\Omega_2)\cdots\varphi_{\rm r}(\Omega_n)\rangle$ by

$$\langle\varphi(\Omega_1)\varphi(\Omega_2)\cdots\varphi(\Omega_n)\rangle = Z^{\frac{n}{2}}\,\langle\varphi_{\rm r}(\Omega_1)\varphi_{\rm r}(\Omega_2)\cdots\varphi_{\rm r}(\Omega_n)\rangle \ . \tag{3.2.5}$$

In the following, we calculate the following correlation functions:

$$\begin{aligned}
&\text{1-point function: } \langle\varphi(\Omega_1)\rangle \ , \\
&\text{2-point function: } \langle\varphi(\Omega_p)\varphi(\Omega_q)\rangle \ (1 \le p < q \le 4) \ , \\
&\text{4-point function: } \langle\varphi(\Omega_1)\varphi(\Omega_2)\varphi(\Omega_3)\varphi(\Omega_4)\rangle \ .
\end{aligned} \tag{3.2.6}$$

We verified that the 1-point functions vanish in the parameter region we examined in this section. Thus, the 2-point correlation functions are themselves the connected ones, while the connected 4-point correlation functions are given by

$$\begin{aligned}
\langle\varphi(\Omega_1)\varphi(\Omega_2)\varphi(\Omega_3)\varphi(\Omega_4)\rangle_{\rm c} =& \langle\varphi(\Omega_1)\varphi(\Omega_2)\varphi(\Omega_3)\varphi(\Omega_4)\rangle - \langle\varphi(\Omega_1)\varphi(\Omega_2)\rangle\langle\varphi(\Omega_3)\varphi(\Omega_4)\rangle \\
&- \langle\varphi(\Omega_1)\varphi(\Omega_3)\rangle\langle\varphi(\Omega_2)\varphi(\Omega_4)\rangle - \langle\varphi(\Omega_1)\varphi(\Omega_4)\rangle\langle\varphi(\Omega_2)\varphi(\Omega_3)\rangle \ ,
\end{aligned} \tag{3.2.7}$$

where c stands for the connected part. The renormalized correlation functions are defined as

$$\langle\varphi(\Omega_1)\rangle = \sqrt{Z}\,\langle\varphi_{\rm r}(\Omega_1)\rangle \ , \tag{3.2.8}$$

$$\langle\varphi(\Omega_p)\varphi(\Omega_q)\rangle = Z\,\langle\varphi_{\rm r}(\Omega_p)\varphi_{\rm r}(\Omega_q)\rangle \ , \tag{3.2.9}$$

$$\langle\varphi(\Omega_1)\varphi(\Omega_2)\varphi(\Omega_3)\varphi(\Omega_4)\rangle_{\rm c} = Z^2\,\langle\varphi_{\rm r}(\Omega_1)\varphi_{\rm r}(\Omega_2)\varphi_{\rm r}(\Omega_3)\varphi_{\rm r}(\Omega_4)\rangle_{\rm c} \ . \tag{3.2.10}$$

We pick up four points $\Omega_p = (\theta_p, \varphi_p)$ on the sphere as follows (see Fig. 3.1):

$$\Omega_1 = \left(\frac{\pi}{2} + \Delta\theta,\ 0\right) \ , \quad \Omega_2 = \left(\frac{\pi}{2},\ 0\right) \ , \quad \Omega_3 = \left(\frac{\pi}{2},\ \hat{\varphi}\right) \ , \quad \Omega_4 = \left(\frac{\pi}{2},\ -\hat{\varphi}\right) \ , \tag{3.2.11}$$

where $\hat{\varphi} = \pi/12$ and $\Delta\theta = m/10$ with $m \in \mathbb{Z}$ taken from 1 to 15.

We apply the hybrid Monte Carlo method to our simulation of the theory.

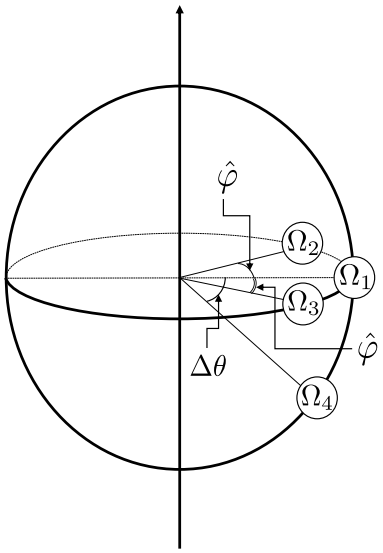

Figure 3.1: Four points on the sphere chosen for the correlation functions.

3.2.2 Renormalization

Tuning λ with fixing μ^2

Here, we renormalize the theory by tuning λ. We fix μ^2 to -6.0.

We simulate at $N = 32$ for various values of λ. In Fig.3.2, we plot

$$\langle\varphi(\Omega_1)\varphi(\Omega_2)\rangle = Z\,\langle\varphi_{\rm r}(\Omega_1)\varphi_{\rm r}(\Omega_2)\rangle \tag{3.2.12}$$

against $\Delta\theta$ at $N = 40$ and $\lambda = 1.0$ and at $N = 32$ and typical values of λ, $1.0, 1.234, 2.0$. We find that the data for $N = 32$ and $\lambda = 1.234$ agree with the ones for $N = 40$ and $\lambda = 1.0$ if the formers are multiplied by a constant $\zeta_{32\to40} = Z(40)/Z(32) = 1.129(8)$ and that this is not the case for the data for $N = 32$ and $\lambda = 1.0, 2.0$. In Fig.3.3, we plot $\langle\varphi(\Omega_1)\varphi(\Omega_2)\rangle$ at $N = 40$ and $\lambda = 1.0$ and $\zeta_{32\to40}\,\langle\varphi(\Omega_1)\varphi(\Omega_2)\rangle$ at $N = 32$ and $\lambda = 1.234$ against $\Delta\theta$. As in the previous section, we see that the data for $N = 32$ agree nicely with the ones for $N = 40$. This implies that the renormalized 2-point functions at $N = 32$ and $N = 40$ agree.

Furthermore, in Fig.3.4, we plot $\langle\varphi(\Omega_1)\varphi(\Omega_2)\varphi(\Omega_3)\varphi(\Omega_4)\rangle_{\rm c}\,c$ at $N = 40$ and $\lambda = 1.0$ and $\zeta^2_{32\to40}\,\langle\varphi(\Omega_1)\varphi(\Omega_2)\varphi(\Omega_3)\varphi(\Omega_4)\rangle_{\rm c}$ at $N = 32$ and $\lambda = 1.234$ against $\Delta\theta$. We again see a nice agreement between the data for $N = 32$ and the ones for $N = 40$, which means that the renormalized connected 4-point functions at $N = 32$ agree with those at $N = 40$.

The above results strongly suggest that the theory is non-perturbatively renormalized also by tuning λ in the sense that the renormalized correlation functions are independent of N.

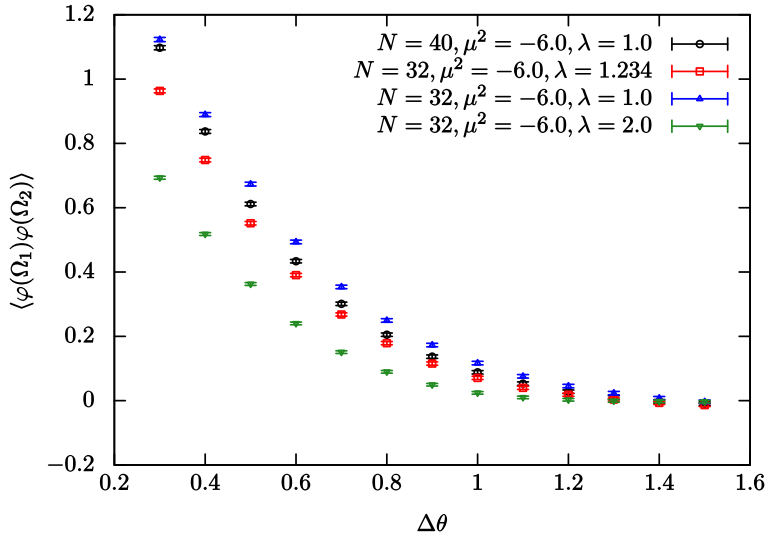

Figure 3.2: $\langle\varphi(\Omega_1)\varphi(\Omega_2)\rangle$ at $\mu^2 = -6.0$ is plotted against $\Delta\theta$. Circles represent the data for $N = 40$ and $\lambda = 1.0$, while squares, triangles and inverted triangles represent the data for $N = 32$ and $\lambda = 1.234, 1.0, 2.0$, respectively.

The results in the previous and present sections imply that the theory is renormalized by tuning a parameter, namely, it is universal up to a parameter fine-tuning.

Tuning μ^2 with fixing λ

Here, we renormalize the theory by tuning μ^2. We fix λ to 1.0.

First, we simulate at $N = 40$ and $\mu^2 = -6.0$. Then, we simulate at $N = 32$ for various values of μ^2. In Fig.3.5, we plot

$$\langle\varphi(\Omega_1)\varphi(\Omega_2)\rangle = Z\,\langle\varphi_{\rm r}(\Omega_1)\varphi_{\rm r}(\Omega_2)\rangle \tag{3.2.13}$$

against $\Delta\theta$ at $N = 40$ and $\mu^2 = -6.0$ and at $N = 32$ and typical values of μ^2, $-6.0, -3.34, -1.0$. We find that the data for $N = 32$ and $\mu^2 = -3.34$ agree with the ones for $N = 40$ and $\mu^2 = -6.0$ if the formers are multiplied by a constant and that this is not the case for the data for $N = 32$ and $\mu^2 = -6.0, -1.0$. We determined the above constant as $\zeta'_{32\to 40} = Z(40)/Z(32) = 1.263(8)$ by using the least-squares method. In Fig.3.6, we plot $\langle\varphi(\Omega_1)\varphi(\Omega_2)\rangle$ at $N = 40$ and $\mu^2 = -6.0$ and $\zeta'_{32\to 40}\,\langle\varphi(\Omega_1)\varphi(\Omega_2)\rangle$ at $N = 32$ and $\mu^2 = -3.34$ against $\Delta\theta$. We indeed see that the data for $N = 32$ agree nicely with the ones for $N = 40$. This implies that the renormalized 2-point functions at $N = 32$ and $N = 40$ agree.

Furthermore, in Fig.3.7, we plot $\langle\varphi(\Omega_1)\varphi(\Omega_2)\varphi(\Omega_3)\varphi(\Omega_4)\rangle_{\rm c}$ at $N = 40$ and $\mu^2 = -6.0$ and $\zeta'^2_{32\to 40}\,\langle\varphi(\Omega_1)\varphi(\Omega_2)\varphi(\Omega_3)\varphi(\Omega_4)\rangle_{\rm c}$ at $N = 32$ and $\mu^2 = -3.34$ against $\Delta\theta$. We again

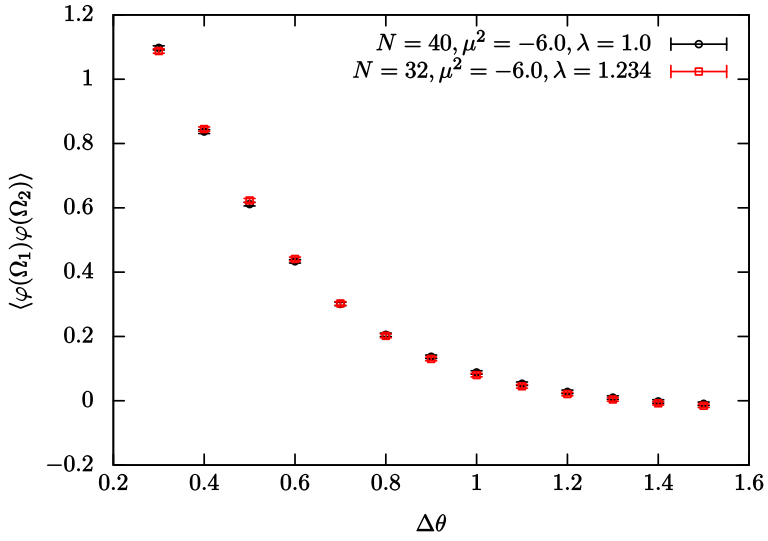

Figure 3.3: $\langle\varphi(\Omega_1)\varphi(\Omega_2)\rangle$ at $N = 40$, $\mu^2 = -6.0$ and $\lambda = 1.0$ is plotted against $\Delta\theta$ (circles). $\zeta_{32\to40}\,\langle\varphi(\Omega_1)\varphi(\Omega_2)\rangle$ with $\zeta_{32\to40} = 1.129(8)$ at $N = 32$, $\mu^2 = -6.0$ and $\lambda = 1.234$ is also plotted against $\Delta\theta$ (squares).

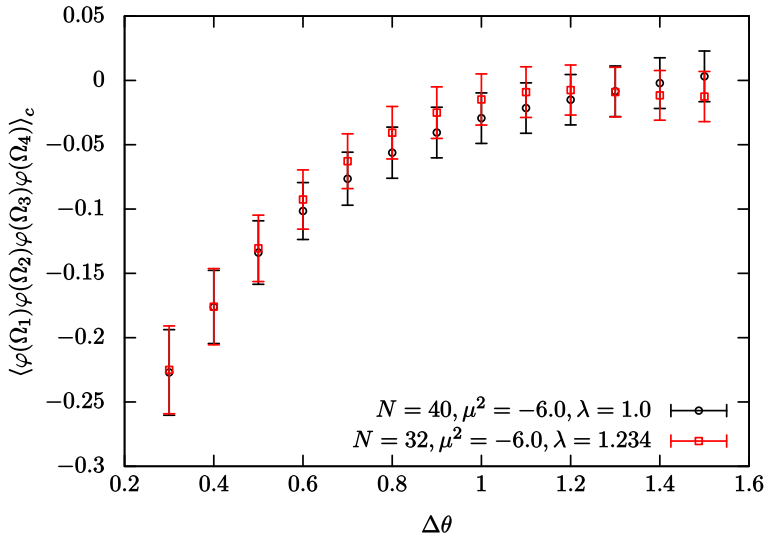

Figure 3.4: $\langle\varphi(\Omega_1)\varphi(\Omega_2)\varphi(\Omega_3)\varphi(\Omega_4)\rangle_{\rm c}$ at $N = 40$, $\mu^2 = -6.0$ and $\lambda = 1.0$ is plotted against $\Delta\theta$, where circles represent the data. $\zeta^2_{32\to40}\,\langle\varphi(\Omega_1)\varphi(\Omega_2)\varphi(\Omega_3)\varphi(\Omega_4)\rangle_{\rm c}$ with $\zeta^2_{32\to40} = 1.275$ at $N = 32$, $\mu^2 = -6.0$ and $\lambda = 1.234$ is also plotted against $\Delta\theta$, where squares represent the data.

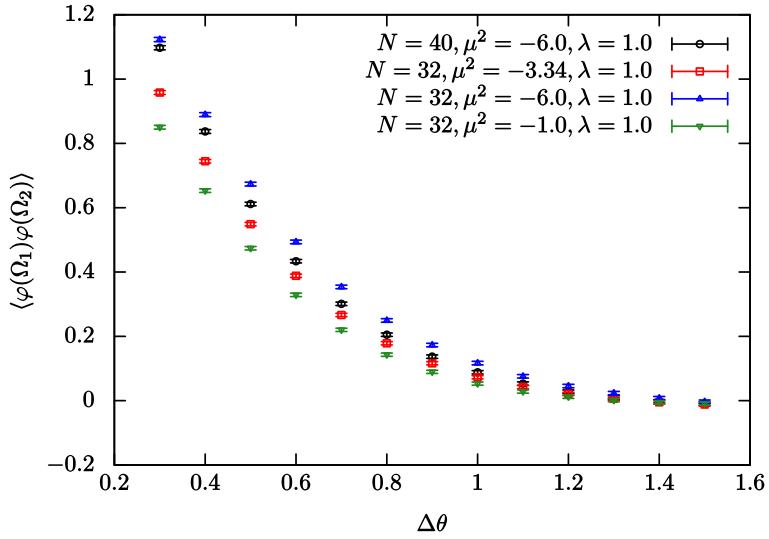

Figure 3.5: $\langle\varphi(\Omega_1)\varphi(\Omega_2)\rangle$ at $\lambda = 1.0$ is plotted against $\Delta\theta$. Circles represent the data for $N = 40$ and $\mu^2 = -6.0$, while squares, triangles and inverted triangles represent the data for $N = 32$ and $\mu^2 = -3.34, -6.0, -1.0$, respectively.

see a nice agreement between the data for $N = 32$ and the ones for $N = 40$, which means that the renormalized connected 4-point functions at $N = 32$ agree with those at $N = 40$. We do not see the above agreement of the correlation functions for $m = 1, 2$ in (3.2.11). We consider this to be attributed to the UV cutoff.

The above results strongly suggest that the correlation functions are made independent of N up to a wave function renormalization by tuning μ^2 and that the theory is non-perturbatively renormalizable in the ordinary sense.

3.3 Critical behavior of correlation functions

Here, we examine the 2-point and 4-point correlation functions on the phase boundary. We fix N to 24 in this section.

We introduce the stereographic projection (Fig. 3.8) defined by

$$z = R \tan \frac{\theta}{2} e^{i\varphi} \ , \tag{3.3.1}$$

which maps a sphere with the radius R to the complex plane. Here, we fix R to 1 without loss of generality. We calculate the 2-point correlation function

$$\langle\varphi(z_m)\varphi(1)\rangle \tag{3.3.2}$$

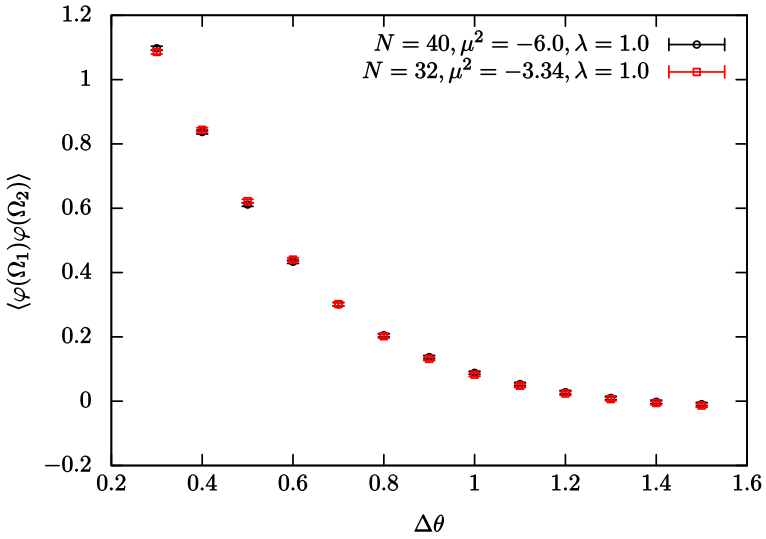

Figure 3.6: $\langle\varphi(\Omega_1)\varphi(\Omega_2)\rangle$ at $N = 40$, $\mu^2 = -6.0$ and $\lambda = 1.0$ is plotted against $\Delta\theta$ (circles). $\zeta'_{32\to40}\langle\varphi(\Omega_1)\varphi(\Omega_2)\rangle$ with $\zeta'_{32\to40} = 1.263(8)$ at $N = 32$, $\mu^2 = -3.34$ and $\lambda = 1.0$ is also plotted against $\Delta\theta$ (squares).

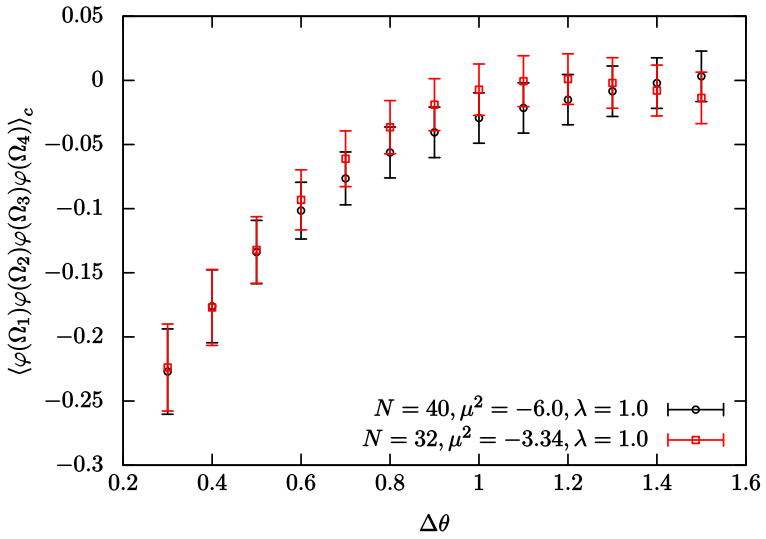

Figure 3.7: $\langle\varphi(\Omega_1)\varphi(\Omega_2)\varphi(\Omega_3)\varphi(\Omega_4)\rangle_{\rm c}$ at $N = 40$, $\mu^2 = -6.0$ and $\lambda = 1.0$ is plotted against $\Delta\theta$ (circles). $\zeta'^2_{32\to40}\langle\varphi(\Omega_1)\varphi(\Omega_2)\varphi(\Omega_3)\varphi(\Omega_4)\rangle_{\rm c}$ with $\zeta'^2_{32\to40} = 1.595$ at $N = 32$, $\mu^2 = -3.34$ and $\lambda = 1.0$ is also plotted against $\Delta\theta$ (squares).

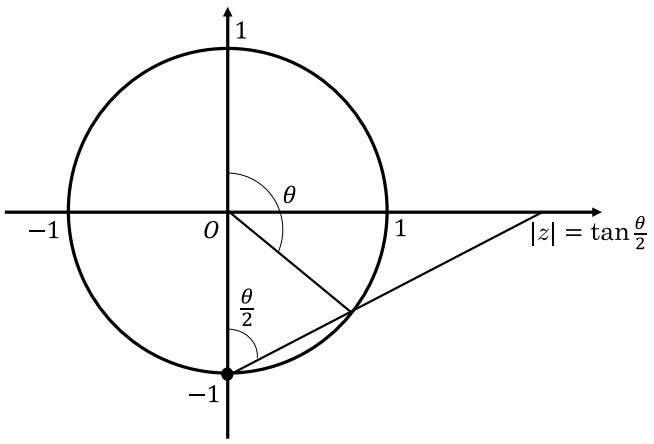

Figure 3.8: The stereographic projection: a point on the sphere with angle θ is projected onto the z-plane on the equator from the south pole.

and the connected 4-point correlation function

$$\langle\varphi(z_m)\varphi(1)\varphi(e^{i\frac{\pi}{3}})\varphi(e^{i\frac{5\pi}{3}})\rangle_{\rm c}\ , \tag{3.3.3}$$

where

$$z_m = \tan\left[\frac{1}{2}\left(\frac{\pi}{2}+\frac{m}{10}\right)\right] \tag{3.3.4}$$

with m taken from 1 to 15. See Fig. 3.1 with $\hat{\varphi}=\pi/3$.

The renormalized 2-point correlation function $\langle\varphi_{\rm r}(z_m)\varphi_{\rm r}(1)\rangle$ and the renormalized connected 4-point correlation function $\langle\varphi_{\rm r}(z_m)\varphi_{\rm r}(1)\varphi_{\rm r}(e^{i\frac{\pi}{3}})\varphi_{\rm r}(e^{i\frac{5\pi}{3}})\rangle_{\rm c}$ are defined by

$$\langle\varphi(z_m)\varphi(1)\rangle = Z\langle\varphi_{\rm r}(z_m)\varphi_{\rm r}(1)\rangle\ , \tag{3.3.5}$$

$$\langle\varphi(z_m)\varphi(1)\varphi(e^{i\frac{\pi}{3}})\varphi(e^{i\frac{5\pi}{3}})\rangle_{\rm c} = Z^2\langle\varphi_{\rm r}(z_m)\varphi_{\rm r}(1)\varphi_{\rm r}(e^{i\frac{\pi}{3}})\varphi_{\rm r}(e^{i\frac{5\pi}{3}})\rangle_{\rm c}\ . \tag{3.3.6}$$

Here, in order to see a connection to a CFT we use the log-log plot. We plot $\log\langle\varphi(z_m)\varphi(1)\rangle$ and $\log\langle\varphi(z_m)\varphi(1)\varphi(e^{i\frac{\pi}{3}})\varphi(e^{i\frac{5\pi}{3}})\rangle_{\rm c}$ against $\log|z-1|$ for $(\mu^2,\lambda)=(-10.801,0.5),(-12.810,0.6)$, $(-14.925,0.7)$ in Figs.3.9 and 3.10, respectively.

We also define the susceptibility χ that is an order parameter for the Z_2 symmetry by

$$\chi = \left\langle\left(\frac{1}{N}{\rm Tr}\Phi\right)^2\right\rangle - \left\langle\frac{1}{N}\left|{\rm Tr}\Phi\right|\right\rangle^2\ . \tag{3.3.7}$$

In Fig.3.11, we plot χ against $-\mu^2$ for each value of λ, $0.5, 0.6, 0.7$. The critical values of $-\mu^2$, $-\mu^2_{\rm crit}$, that give the peaks of χ correspond to the phase transition points where the symmetry breaking of the Z_2 symmetry occurs: the Z_2 symmetry is broken for $-\mu^2 > -\mu^2_{\rm crit}$, while it is unbroken for $-\mu^2 < -\mu^2_{\rm crit}$. We find the peaks of χ for

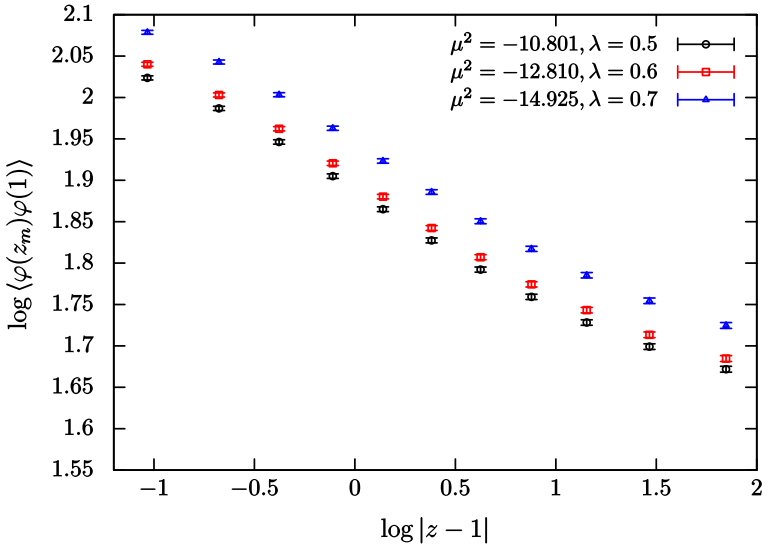

Figure 3.9: $\log\langle\varphi(z_m)\varphi(1)\rangle$ at $N = 24$ is plotted against $\log|z-1|$. The data for $(\mu^2, \lambda) = (-10.801, 0.5), (-12.810, 0.6), (-14.925, 0.7)$ are represented by the circles, the squares and the triangles, respectively.

$\lambda = 0.5, 0.6, 0.7$ exist around $\mu^2 = -10.8, -12.8, -14.8$, respectively. We tune the values of μ^2 around the above values such that the 2-point and 4-point correlation functions for different λ's agree up to a wave function renormalization. We shift the data of the 2-point correlation functions for $(\mu^2, \lambda) = (-12.810, 0.6), (-14.925, 0.7)$ simultaneously in the vertical direction by $\alpha_{0.6\to0.5} = \log[Z(\lambda = 0.5)/Z(\lambda = 0.6)] = -0.015(1)$ and $\alpha_{0.7\to0.5} = -0.056(1)$, respectively, and plot the shifted data in Fig.3.12. We also shift the data of the 4-point correlation functions for $(\mu^2, \lambda) = (-12.810, 0.6), (-14.925, 0.7)$ simultaneously by $2\alpha_{0.6\to0.5}$ and $2\alpha_{0.7\to0.5}$, respectively, and plot the shifted data in Fig.3.13. We see a good agreement of both the shifted 2-point and 4-point correlation functions. These shifts correspond to a wave function renormalization. Furthermore, we see that the above tuned values of μ^2 are consistent with the critical values of μ^2 read off from Fig.3.11. Thus, the agreement of the correlation functions implies that the theories are universal on the phase boundary as in ordinary field theories. We do not see the above agreement of the correlation functions not only in the UV region with $m = 1, 2$, but also in the IR region with $m = 14, 15$. We consider the disagreement in the latter region to be caused by an IR cutoff which is introduced when the theory on the fuzzy sphere is mapped to a theory on the plane with infinite volume.

Finally, we examine a connection of the present theory to a CFT. In Fig.3.12, we fit seven data points $(m = 4, \ldots, 10)$ of $\log\langle\varphi(z_m)\varphi(1)\rangle$ at $(\mu^2, \lambda) = (-10.801, 0.5)$ to $-u\log|z-1| + v$ and obtain $u = 0.149(2)$ and $v = 1.887(1)$. This implies that the 2-point

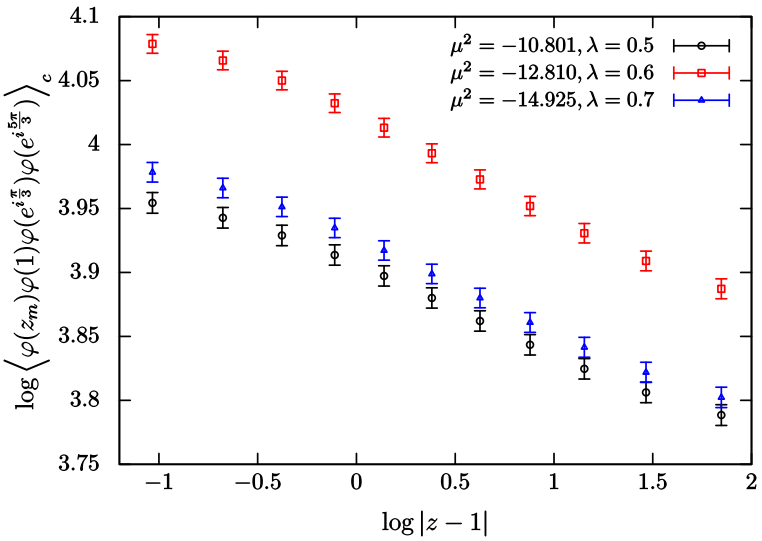

Figure 3.10: $\log\langle\varphi(z_m)\varphi(1)\varphi(e^{i\frac{\pi}{3}})\varphi(e^{i\frac{5\pi}{3}})\rangle_{\rm c}$ at $N = 24$ is plotted against $\log|z-1|$. The data for $(\mu^2, \lambda) = (-10.801, 0.5), (-12.810, 0.6), (-14.925, 0.7)$ are represented by the circles, the squares and the triangles, respectively.

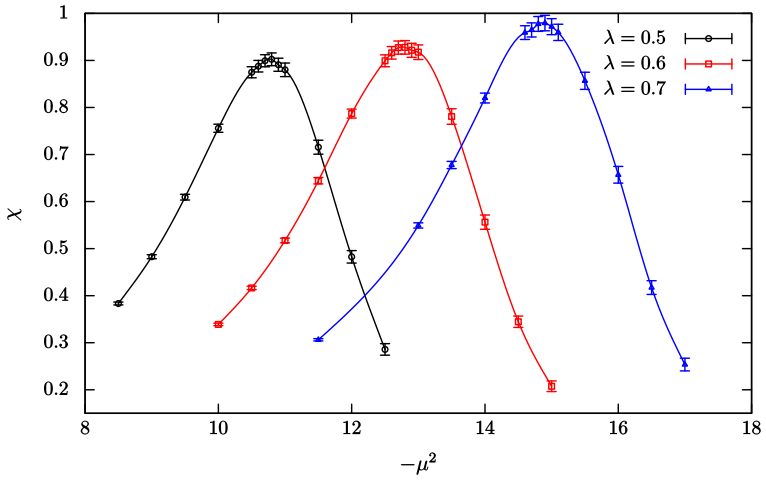

Figure 3.11: The susceptibility χ at $N = 24$ is plotted against $-\mu^2$. The data for $\lambda = 0.5, 0.6, 0.7$ are represented by the circles, the squares, and the triangles, respectively. The peaks of χ for $\lambda = 0.5, 0.6, 0.7$ exist around $\mu^2 = -10.8, -12.8, -14.8$, respectively.

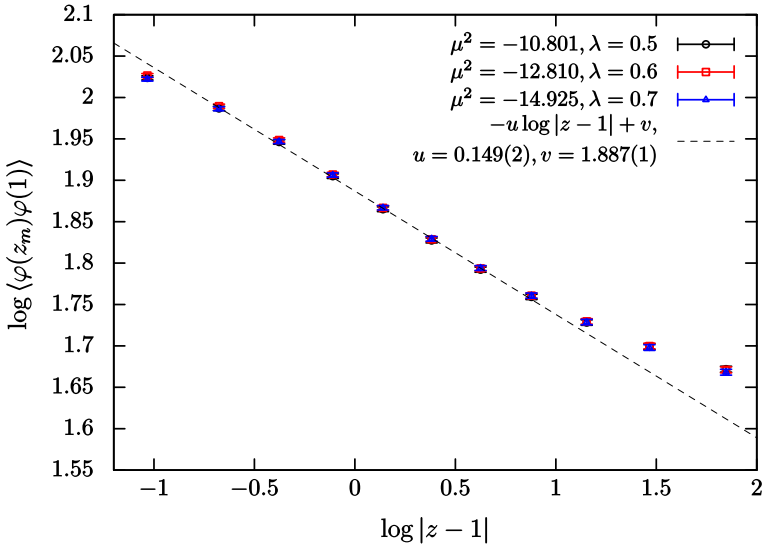

Figure 3.12: $\log\langle\varphi(z_m)\varphi(1)\rangle$ at $N = 24$ is plotted against $\log|z-1|$. The data for $(\mu^2, \lambda) = (-10.801, 0.5)$ are the same as in Fig. 3.9. The data for $(\mu^2, \lambda) = (-12.810, 0.6), (-14.925, 0.7)$ are simultaneously shifted by $\alpha_{0.6\to0.5} = -0.015(1)$ and $\alpha_{0.7\to0.5} = -0.056(1)$, respectively, in the vertical direction. The data for $(\mu^2, \lambda) = (-10.801, 0.5), (-12.810, 0.6), (-14.925, 0.7)$ are represented by the circles, the squares and the triangles, respectively. The dashed line is a fit of seven data points (from the second point to the eighth point) of $\log\langle\varphi(z_m)\varphi(1)\rangle$ at $(\mu^2, \lambda) = (-10.801, 0.5)$ to $-u\log|z-1|+v$ with $u = 0.149(2)$ and $v = 1.887(1)$.

correlation function behaves as

$$\langle\varphi(z)\varphi(1)\rangle = \frac{e^v}{|z-1|^u} \tag{3.3.8}$$

for $m = 4, \ldots, 10$. In CFTs, the 2-point correlation function behaves as

$$\langle\mathcal{O}(z)\mathcal{O}(z')\rangle \sim \frac{1}{|z-z'|^{2\Delta}} \ , \tag{3.3.9}$$

where the Δ is the scaling dimension of the operator $\mathcal{O}(z)$. Thus, the theory on the phase boundary behaves as a CFT in the UV region. In the IR region with $11 \leq m \leq 13$, our 2-point correlation function deviates universally from that in the CFT. In addition, in a further UV region with $m = 3$, it also deviates universally. These deviations are considered as an effect of the UV/IR mixing. It is non-trivial that we observe the behavior of the CFT because field theories on non-commutative spaces are non-local ones.

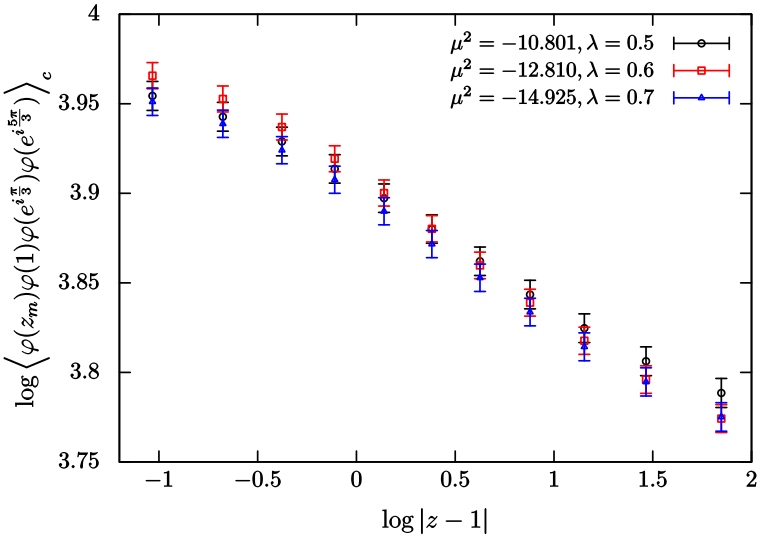

Figure 3.13: $\log\langle\varphi(z_m)\varphi(1)\varphi(e^{i\frac{\pi}{3}})\varphi(e^{i\frac{5\pi}{3}})\rangle_c$ at $N = 24$ is plotted against $\log|z-1|$. The data for $(\mu^2, \lambda) = (-10.801, 0.5)$ are the same as in Fig. 3.10, while the data for $(\mu^2, \lambda) = (-12.810, 0.6), (-14.925, 0.7)$ are simultaneously shifted by $2\alpha_{0.6\to0.5}$ and $2\alpha_{0.7\to0.5}$, respectively, in the vertical direction. The data for $(\mu^2, \lambda) = (-10.801, 0.5)$, $(-12.810, 0.6), (-14.925, 0.7)$ are represented by the circles, the squares and the triangles, respectively.

Chapter 4

Large-N volume independence on group manifolds

In this chapter, we examine whether phenomenon analogous to the large-N volume independence occurs on group manifolds. We find that it indeed does in the sense that a large-N gauge theory on a group manifold G is equivalent to the theory obtained by reducing it to a coset space G/H where H is a subgroup of G.

4.1 Large-N volume independence on torus

In this section, as a warm-up, we examine the large-N volume independence on a D-dimensional torus $T^D \simeq \mathrm{U}(1)^D$. We denote coordinates of T^D by x^μ ($\mu = 1, \ldots, D$), assuming, for simplicity, the periodicity $x^\mu \sim x^\mu + L$. Using a positive integer K, we define a 'reduced torus' $T^D/(Z_K)^D$ whose coordinates are denoted by σ^μ. The periodicity for σ^μ is

$$\sigma^\mu \sim \sigma^\mu + l \ , \tag{4.1.1}$$

where $l = L/K$. We have a relation

$$x^\mu = l u^\mu + \sigma^\mu \tag{4.1.2}$$

with u^μ integers.

To illustrate the large-N volume independence, we consider a scalar matrix field theory on T^D:

$$S = \int d^D x \ \mathrm{Tr} \left(\frac{1}{2} \partial_\mu \phi(x) \partial_\mu \phi(x) + \frac{m^2}{2} \phi(x)^2 + \frac{\kappa}{3} \phi(x)^3 \right) \ , \tag{4.1.3}$$

where $\phi(x)$ is a Hermitian matrix-valued field with the matrix size N.

We apply a following reduction rule to the above theory (4.1.3):

$$\phi(x) \to e^{i P_\mu x^\mu} \phi(\sigma) e^{-i P_\mu x^\mu} \quad \text{with} \quad P_\mu = \begin{pmatrix} \frac{2\pi n_\mu^{(1)}}{L} & & \\ & \frac{2\pi n_\mu^{(2)}}{L} & \\ & & \ddots \end{pmatrix} \ , \quad \int d^D x \to \frac{v}{v'} \int d^D \sigma \ . \tag{4.1.4}$$

Here the relation between x^μ and σ^μ is given by (4.1.2), and P_μ are constant diagonal matrices whose eigenvalues $2\pi n_\mu^{(i)}/L$ $(i = 1, \ldots, N)$ correspond to the momenta on T^D distributed uniformly in the momentum space. v and v' are given by

$$v = L^D/N \ , \quad v' = (2\pi/\Lambda)^D \ , \tag{4.1.5}$$

where Λ is a UV cutoff on $T^D/(Z_K)^D$. (4.1.5) implies that T^D is divided into N cells with the volume of a unit cell given by v and that $T^D/(Z_K)^D$ is divided into l^D/v' cells with the volume of a unit cell given by v'. Then, we obtain the action of a reduced model defined on $T^D/(Z_K)^D$:

$$S_{\rm red} = \frac{v}{v'} \int d^D\sigma \ {\rm Tr} \left(\frac{1}{2} \left(\partial_{\sigma^\mu} \phi(\sigma) + i \left[P_\mu, \phi(\sigma) \right] \right)^2 + \frac{m^2}{2} \phi(\sigma)^2 + \frac{\kappa}{3} \phi(\sigma)^3 \right) \ . \tag{4.1.6}$$

Note that vl^D/v' can be viewed as an effective volume in the reduced model.

We consider the 2-loop contribution to the free energy. There are two diagrams. One is planar (Fig.2.3) and the other non-planar (Fig.2.4). First, we calculate them in the original theory (4.1.3). The planar diagram is calculated as

$$\frac{\lambda N^2}{6} \int d^D x d^D x' D(x - x')^3 \ , \tag{4.1.7}$$

where $\lambda = \kappa^2 N$ is the 't Hooft coupling and $D(x - x')$ is the free propagator of the theory (4.1.3) with $N = 1$:

$$D(x - x') = \frac{1}{L^D} \sum_n \frac{e^{i \frac{2\pi n_\mu}{L} \left(x_\mu - x'_\mu \right)}}{\left(\frac{2\pi n_\mu}{L} \right)^2 + m^2} \ . \tag{4.1.8}$$

The non-planar diagram is given by (4.1.7)$/N^2$ so that it is suppressed by $1/N^2$ compared to the planar diagram in the $N \to \infty$ limit.

Next, we calculate them in the reduced model using a bi-local field representation for matrices [35,36]. We take a coordinate basis $|x\rangle$ in the vector space on which $\phi(\sigma)$ and P_μ act and define a bi-local field

$$\phi(\sigma, x, x') = \langle x | \phi(\sigma) | x' \rangle \ . \tag{4.1.9}$$

The reduced model (4.1.6) is rewritten as

$$\begin{aligned} S_{\rm red} = & \frac{v}{v'} \int d^D\sigma d^D x d^D x' \frac{1}{2} \phi(\sigma, x', x) \left[- \left(\partial_{\sigma^\mu} + \partial_\mu + \partial'_\mu \right)^2 + m^2 \right] \phi(\sigma, x, x') \\ & + \frac{\kappa v}{3v'} \int d^D\sigma d^D x d^D x' d^D x'' \phi(\sigma, x, x') \phi(\sigma, x', x'') \phi(\sigma, x'', x) \ . \end{aligned} \tag{4.1.10}$$

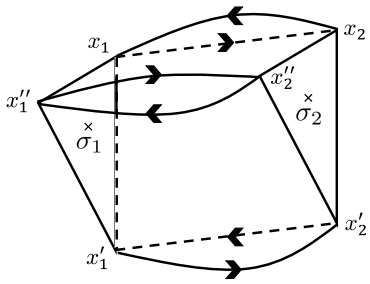

Figure 4.1: 2-loop planar diagram in the bi-local representation for the free energy.

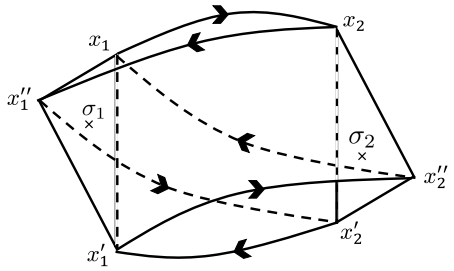

Figure 4.2: 2-loop non-planar diagram in the bi-local representation for the free energy.

We make a change of variables, $\bar{x}^\mu = x^\mu,\ \tilde{x}^\mu = x^\mu - x'^\mu,\ \bar{\sigma}^\mu = \sigma^\mu - x^\mu$, which gives

$$\frac{\partial}{\partial \sigma^\mu} + \frac{\partial}{\partial x^\mu} + \frac{\partial}{\partial x'^\mu} = \frac{\partial}{\partial \bar{x}^\mu} \ . \tag{4.1.11}$$

Thus, from (4.1.11) we obtain the propagator

$$\langle \phi(\sigma_1, x_1, x_1')\phi(\sigma_2, x_2', x_2)\rangle = \frac{v'}{v} D(x_1 - x_2)\delta_L^{(D)}((x_1 - x_1') - (x_2 - x_2'))\delta_l^{(D)}((\sigma_1 - \sigma_2) - (x_1 - x_2)) \ , \tag{4.1.12}$$

where $\delta_L^{(D)}$ and $\delta_l^{(D)}$ are periodic delta functions with the period L and l, respectively.

The planar diagram (Fig.4.1) in the reduced model is calculated as

$$\begin{aligned}
&3 \cdot \frac{1}{2}\left(\frac{\kappa v}{3v'}\right)^2 \int d^D\sigma_1 d^D\sigma_2 d^D x_1 d^D x_1' d^D x_1'' d^D x_2 d^D x_2' d^D x_2'' \\
&\quad \times \frac{v'}{v} D(x_1 - x_2)\delta_L^{(D)}((x_1 - x_1') - (x_2 - x_2'))\delta_l^{(D)}((\sigma_1 - \sigma_2) - (x_1 - x_2)) \\
&\quad \times \frac{v'}{v} D(x_1' - x_2')\delta_L^{(D)}((x_1' - x_1'') - (x_2' - x_2''))\delta_l^{(D)}((\sigma_1 - \sigma_2) - (x_1' - x_2')) \\
&\quad \times \frac{v'}{v} D(x_1'' - x_2'')\delta_L^{(D)}((x_1'' - x_1) - (x_2'' - x_2))\delta_l^{(D)}((\sigma_1 - \sigma_2) - (x_1'' - x_2'')) \\
&= \frac{\kappa^2 v'}{6v}\delta_L^{(D)}(0) L^{2D} \int d^D\sigma_1 d^D\sigma_2 d^D x_1 d^D x_2 D(x_1 - x_2)^3 \delta_l^{(D)}((\sigma_1 - \sigma_2) - (x_1 - x_2))^3 \\
&= \frac{\kappa^2 v'}{6v^2} L^{3D} \int d^D\sigma_1 d^D\sigma_2 d^D\tilde{x} D(\tilde{x})^3 \delta_l^{(D)}((\sigma_1 - \sigma_2) - \tilde{x})^3 \\
&= \frac{\kappa^2 L^{3D} v'}{6v^2}\delta_l^{(D)}(0)^2 \int d^D\sigma_1 d^D\sigma_2 \sum_u D(lu + \sigma_1 - \sigma_2)^3 \\
&= \frac{\kappa^2 L^{3D}}{6v^2 v'} \int d^D\tilde{x} d^D\sigma_2 D(\tilde{x} - \sigma_2)^3 \\
&= \frac{\kappa^2 L^{3D} l^D}{6v^2 v'} \int d^D\tilde{x} D(\tilde{x})^3
\end{aligned}$$

$$= \frac{\kappa^2 l^D}{6v^2 v'}(Nv)^3 \int d^D\tilde{x} D(\tilde{x})^3$$
$$= \frac{vl^D}{v'}\frac{\lambda N^2}{6}\frac{1}{L^D}\int d^D x d^D x' D(x-x')^3 \ , \tag{4.1.13}$$

where we have used $\delta_L(0) = 1/v$ and $\delta_l(0) = 1/v'$.

The non-planar diagram (Fig.4.2) in the reduced model is calculated as

$$\begin{aligned}
&3 \cdot \frac{1}{2}\left(\frac{\kappa v}{3v'}\right)^2 \int d^D\sigma_1 d^D\sigma_2 d^D x_1 d^D x_1' d^D x_1'' d^D x_2 d^D x_2' d^D x_2'' \\
&\quad \times \frac{v'}{v} D(x_1 - x_2)\delta_L^{(D)}((x_1 - x_1') - (x_2 - x_2'))\delta_l^{(D)}((\sigma_1 - \sigma_2) - (x_1 - x_2)) \\
&\quad \times \frac{v'}{v} D(x_1' - x_2'')\delta_L^{(D)}((x_1' - x_1'') - (x_2'' - x_2))\delta_l^{(D)}((\sigma_1 - \sigma_2) - (x_1' - x_2'')) \\
&\quad \times \frac{v'}{v} D(x_1'' - x_2')\delta_L^{(D)}((x_1'' - x_1) - (x_2' - x_2''))\delta_l^{(D)}((\sigma_1 - \sigma_2) - (x_1'' - x_2')) \\
&= \frac{\kappa^2 v'}{6v}\delta_L^{(D)}(0)\int d^D\sigma_1 d^D\sigma_2 d^D x_1 d^D x_1' d^D x_2 d^D x_2'' D(x_1 - x_2)D(x_1' - x_2'')D(x_1 - x_2'') \\
&\quad \times \delta_l^{(D)}((\sigma_1 - \sigma_2) - (x_1 - x_2))\delta_l^{(D)}((\sigma_1 - \sigma_2) - (x_1' - x_2''))\delta_l^{(D)}((\sigma_1 - \sigma_2) - (x_1 - x_2'')) \\
&= \frac{\kappa^2 v'}{6v^2} L^D \int d^D\sigma_1 d^D\sigma_2 \sum_{u,u',u''} D(lu + \sigma_1 - \sigma_2)D(lu' + \sigma_1 - \sigma_2)D(lu'' + \sigma_1 - \sigma_2) \\
&= \left\{ \frac{vl^D}{v'}\frac{\lambda N^2}{6}\frac{l^D}{L^{2D}}\int d^D\sigma_1 d^D\sigma_2 \sum_{u,u',u''} D(lu + \sigma_1 - \sigma_2)D(lu' + \sigma_1 - \sigma_2)D(lu'' + \sigma_1 - \sigma_2) \right\} \\
&\quad \times \left(\frac{v'}{l^D}\right)^2 \ .
\end{aligned} \tag{4.1.14}$$

We see again that the non-planar diagram is suppressed compared to the planar diagram in the $v' \to 0$ limit, because the quantity in the curly bracket in (4.1.14) has the same order of magnitude as (4.1.13).

The non-planar diagram is suppressed compared to the planar diagram in both the original and reduced models. By comparing the planar contribution (4.1.7) and (4.1.13), we find a relation between the free energy F in the original model and the one $F_{\rm red}$ in the reduced model in the $N \to \infty$ limit:

$$\frac{F}{N^2 V} = \frac{F_{\rm red}}{N^2 v V'/v'} \ , \tag{4.1.15}$$

where $V = L^D$ and $V' = l^D$ are the volumes of T^D and $T^D/(Z_K)^D$, respectively, and the LHS and RHS correspond to the planar contribution to the free energy per unit volume divided by N^2 in the original and reduced models, respectively. In a similar manner, by referring the argument in [41], one can show that the relation (4.1.15) holds to all orders

in perturbative expansion. It is also easy to show a correspondence between correlation functions in the $N \to \infty$ limit [41]:

$$\frac{1}{N^{n/2+1}} \langle \mathrm{Tr}(\phi(x_1)\phi(x_2)\cdots\phi(x_n)) \rangle = \frac{1}{N^{n/2+1}} \left\langle \mathrm{Tr}\left(\hat{\phi}(x_1)\hat{\phi}(x_2)\cdots\hat{\phi}(x_n)\right) \right\rangle_{\mathrm{red}} , \quad (4.1.16)$$

where $\langle \cdots \rangle$ and $\langle \cdots \rangle_{\mathrm{red}}$ stand for the expectation value in the original and reduced models, respectively, and $\hat{\phi}(x) = e^{iP_\mu x^\mu}\phi(\sigma)e^{-iP_\mu x^\mu}$ with (4.1.2). Thus, we find that the large-N volume independence holds on a torus in the sense that a theory on T^D is equivalent to a certain theory on $T^D/(Z_K)^D$ in the large-N limit.

Finally, we consider Yang-Mills theory on T^D:

$$S = \frac{1}{4\kappa^2} \int d^D x \ \mathrm{Tr}(F_{\mu\nu}F_{\mu\nu}) , \quad (4.1.17)$$

where $F_{\mu\nu} = \partial_\mu A_\nu - \partial_\nu A_\mu + i[A_\mu, A_\nu]$. By applying the reduction rule (4.1.4) to (4.1.17), we obtain

$$S_{\mathrm{red}} = \frac{v}{v'}\frac{1}{4\kappa^2} \int d^D \sigma \ \mathrm{Tr}\left(\tilde{F}_{\mu\nu}\tilde{F}_{\mu\nu}\right) , \quad (4.1.18)$$

where $\tilde{F}_{\mu\nu} = \partial_{\sigma^\mu}\tilde{A}_\nu - \partial_{\sigma^\nu}\tilde{A}_\mu + i\left[\tilde{A}_\mu, \tilde{A}_\nu\right]$ with $\tilde{A}_\mu(\sigma) = P_\mu + A_\mu(\sigma)$. Namely, the reduced model agrees with the one that is obtained by dimensionally reducing the original model to $T^D/(Z_K)^D$. If the background $\tilde{A}_\mu = P_\mu$ is stable in the reduced model (4.1.18), the reduced model is equivalent to the original model (4.1.17) in the $N \to \infty$ with $\kappa^2 N$ fixed in the sense that (4.1.15) holds and a following relation for Wilson loops also holds:

$$\left\langle \frac{1}{N} P \exp\left(i \int_0^1 d\zeta \frac{dx^\mu(\zeta)}{d\zeta} A_\mu(x(\zeta)) \right) \right\rangle = \left\langle \frac{1}{N} P \exp\left(i \int_0^1 d\zeta \frac{dx^\mu(\zeta)}{d\zeta} \tilde{A}_\mu(\sigma(\zeta)) \right) \right\rangle_{\mathrm{red}} , \quad (4.1.19)$$

where $x^\mu(\zeta)$ and $\sigma^\mu(\zeta)$ are related as (4.1.2). Namely, the large-N volume independence holds literally. Note that the stability depends on the dynamics of the model[13].

4.2 Group manifolds and coset spaces

In this section, we review some basic facts about group manifolds and coset spaces. For more details, see, for instance, [35,36,80]. Let G be a compact simply connected Lie group[14] and H be a Lie subgroup of G. D and d denote the dimensions of G and H, respectively. Then, the dimension of G/H is $D-d$. x^M $(M = 1, \ldots, D)$, y^m $(m = D-d+1, \ldots, D)$, and σ^μ $(\mu = 1, \ldots, D-d)$ denote the coordinates of G, H and G/H, respectively, while

[13] Instability corresponds to SSB of the so-called $U(1)^D$ symmetry or the center invariance.

[14] If G is not simply connected, the reduced model is not obtained in a globally consistent way.

$A, B = 1, \ldots, D$, $a, b = D-d+1, \ldots, D$, and $\alpha, \beta = 1, \ldots, D-d$ are the corresponding local Lorentz indices.

Let t_A be a basis for the Lie algebra of G in which t_a are a basis for the Lie algebra of H. t_A satisfy commutation relations

$$[t_A, t_B] = i f_{ABC} t_C \tag{4.2.1}$$

with f_{ABC} completely anti-symmetric and $f_{ab\alpha} = 0$. $g(x) \in G$ is factorized locally as

$$g(x) = L(\sigma) h(y) \ , \tag{4.2.2}$$

where $h(y) \in H$. The isometry of G is the $G \times G$ symmetry, where one corresponds to the left translation and the other the right translation. Only the left translation survives as the isometry of G/H.

A $D \times D$ matrix $\mathrm{Ad}(g)$ for $g \in G$ is defined by

$$g\, t_A\, g^{-1} = t_B\, \mathrm{Ad}(g)_{BA} \ . \tag{4.2.3}$$

It is easy to show that

$$\mathrm{Ad}(g)_{AB} \mathrm{Ad}(g)_{AC} = \delta_{BC} \ . \tag{4.2.4}$$

Note that if h is an element of H,

$$\mathrm{Ad}(h)_{\alpha a} = \mathrm{Ad}(h)_{a\alpha} = 0 \ , \tag{4.2.5}$$

which implies that

$$\mathrm{Ad}(h)_{\alpha\beta} \mathrm{Ad}(h)_{\alpha\gamma} = \delta_{\beta\gamma}, \ \mathrm{Ad}(h)_{ab} \mathrm{Ad}(h)_{ac} = \delta_{bc} \ . \tag{4.2.6}$$

The right invariant 1-form E_M^A and the left invariant 1-form S_M^A are defined by

$$\partial_M g(x) g^{-1}(x) = -i E_M^A(x)\, t_A \ , \quad g^{-1}(x) \partial_M g(x) = i S_M^A(x)\, t_A \ . \tag{4.2.7}$$

They satisfy the Maurer-Cartan equations:

$$\partial_M E_N^A - \partial_N E_M^A - f_{ABC} E_M^B E_N^C = 0 \ , \quad \partial_M S_N^A - \partial_N S_M^A - f_{ABC} S_M^B S_N^C = 0 \ . \tag{4.2.8}$$

Defining e_μ^A, $\tilde{e}_m^a$, s_μ^A and $\tilde{s}_m^a$ by

$$\begin{aligned} \partial_\mu L(\sigma) L^{-1}(\sigma) = -i e_\mu^A(\sigma)\, t_A \ , \quad \partial_m h(y) h^{-1}(y) = -i \tilde{e}_m^a(y)\, t_a \ , \\ L^{-1}(\sigma) \partial_\mu L(\sigma) = i s_\mu^A(\sigma) t_A \ , \quad h^{-1}(y) \partial_m h(y) = i \tilde{s}_m^a(y) t_a \ , \end{aligned} \tag{4.2.9}$$

we obtain the relations:

$$E^\alpha_\mu(x) = e^\alpha_\mu(\sigma)\ , \quad E^a_\mu(x) = e^a_\mu(\sigma)\ , \quad E^\alpha_m(x) = \mathrm{Ad}(L)_{\alpha b}(\sigma)\tilde{e}^b_m(y)\ , \quad E^a_m(x) = \mathrm{Ad}(L)_{ab}(\sigma)\tilde{e}^b_m(y)\ ,$$
$$S^\alpha_\mu(x) = \mathrm{Ad}(h^{-1})_{\alpha\beta}(y)s^\beta_\mu(\sigma)\ , \quad S^a_\mu(x) = \mathrm{Ad}(h^{-1})_{ab}(y)s^b_\mu(\sigma)\ , \quad S^\alpha_m(x) = 0\ , \quad S^a_m(x) = \tilde{s}^a_m(y)\ . \tag{4.2.10}$$

A metric of G,

$$G_{MN} = E^A_M E^A_N = S^A_M S^A_N\ , \tag{4.2.11}$$

is right and left invariant. By using (4.2.10), we obtain

$$ds^2_G = s^\beta_\mu s^\beta_\nu d\sigma^\mu d\sigma^\nu + \left[\mathrm{Ad}(h^{-1})_{ba}\tilde{s}^b_m dy^m + s^a_\mu d\sigma^\mu\right]^2\ , \tag{4.2.12}$$

where the invariant metric of G/H, $g_{\mu\nu}$, is given by

$$g_{\mu\nu} = s^\alpha_\mu s^\alpha_\nu \tag{4.2.13}$$

The Haar measure of G is given by

$$dg = d^D x\sqrt{G(x)}\ , \tag{4.2.14}$$

where $G(x)$ is $\det G_{MN}(x)$. It is factorized as

$$dg = d^{D-d}\sigma d^d y\sqrt{g(\sigma)}\det\tilde{s}^a_m(y)\ . \tag{4.2.15}$$

We denote the invariant measure of G/H, $d^{D-d}\sigma\sqrt{g}$, by dL.

We define the right invariant Killing vectors $\mathcal{L}_A$ and the left invariant Killing vectors $\mathcal{R}_A$ by

$$\mathcal{L}_A = -iE^M_A\frac{\partial}{\partial x^M}\ , \quad \mathcal{R}_A = -iS^M_A\frac{\partial}{\partial x^M}\ , \tag{4.2.16}$$

where E^M_A and S^M_A are the inverses of E^A_M and S^A_M, respectively. $\mathcal{L}_A$ and $\mathcal{R}_A$ generate the left translation and right translation, respectively, and obey the following commutation relations:

$$[\mathcal{L}_A, \mathcal{L}_B] = if_{ABC}\mathcal{L}_C, \quad [\mathcal{R}_A, \mathcal{R}_B] = if_{ABC}\mathcal{R}_C, \quad [\mathcal{L}_A, \mathcal{R}_B] = 0\ . \tag{4.2.17}$$

By using (4.2.10), we obtain

$$\mathcal{L}_\alpha = is^\mu_\beta\mathrm{Ad}(L)_{\beta\alpha}\frac{\partial}{\partial\sigma^\mu} - i\tilde{e}^m_b\left[\mathrm{Ad}(L)_{b\alpha} - s^b_\rho s^\rho_\beta\mathrm{Ad}(L)_{\beta\alpha}\right]\frac{\partial}{\partial y^m}\ ,$$
$$\mathcal{L}_a = is^\mu_\beta\mathrm{Ad}(L)_{\beta a}\frac{\partial}{\partial\sigma^\mu} - i\tilde{e}^m_b\left[\mathrm{Ad}(L)_{ba} - s^b_\rho s^\rho_\beta\mathrm{Ad}(L)_{\beta a}\right]\frac{\partial}{\partial y^m}\ ,$$
$$\mathcal{R}_\alpha = -i\mathrm{Ad}(h^{-1})_{\alpha\beta}s^\mu_\beta\frac{\partial}{\partial\sigma^\mu} + i\mathrm{Ad}(h^{-1})_{bc}\mathrm{Ad}(h^{-1})_{\alpha\beta}\,\tilde{s}^m_b s^c_\nu s^\nu_\beta\frac{\partial}{\partial y^m}\ ,$$

$$\mathcal{R}_a = -i\tilde{s}_a^m \frac{\partial}{\partial y^m} \ , \tag{4.2.18}$$

where s_α^μ, $\tilde{s}_a^m$ and $\tilde{e}_a^m$ are the inverses of s_μ^α, $\tilde{s}_m^a$ and $\tilde{e}_m^a$, respectively.

$$\mathcal{L}'_A = is_\beta^\mu \mathrm{Ad}(L)_{\beta A} \frac{\partial}{\partial \sigma^\mu} \tag{4.2.19}$$

are the Killing vectors on G/H and are indeed independent of y.

Let us consider a scalar matrix field theory on G given by[15]

$$\begin{aligned} S &= \int d^D x \sqrt{G(x)}\ \mathrm{Tr}\left[\frac{1}{2}G^{MN}\partial_M\phi(x)\partial_N\phi(x) + \frac{m^2}{2}\phi(x)^2 + \frac{\kappa}{3}\phi(x)^3\right] \\ &= \int d^{D-d}\sigma d^d y \sqrt{g(\sigma)}\det \tilde{s}_m^a(y) \mathrm{Tr}\left[-\frac{1}{2}\left(\mathcal{L}_A\phi(x)\right)^2 + \frac{m^2}{2}\phi(x)^2 + \frac{\kappa}{3}\phi(x)^3\right] \ , \end{aligned} \tag{4.2.20}$$

where $\phi(x)$ is an $N \times N$ hermitian matrix. This theory has the $G \times G$ symmetry. Namely, (4.2.20) is invariant under $\delta\phi = \epsilon\mathcal{L}_A\phi$ or $\delta\phi = \epsilon\mathcal{R}_A\phi$. We impose a constraint $\mathcal{R}_a\phi(x) = 0$, which implies from (4.2.18) that ϕ is independent of y. Then, the theory (4.2.20) is reduced to the theory on G/H as

$$\begin{aligned} S &= \int d^{D-d}\sigma d^d y \sqrt{g}\det \tilde{s}_m^a \mathrm{Tr}\left[-\frac{1}{2}\left(\mathcal{L}'_A\phi\right)^2 + \frac{m^2}{2}\phi^2 + \frac{\kappa}{3}\phi^3\right] \\ &= V_H \int d^{D-d}\sigma\sqrt{g}\ \mathrm{Tr}\left(\frac{1}{2}g^{\mu\nu}\partial_\mu\phi\partial_\nu\phi + \frac{m^2}{2}\phi^2 + \frac{\kappa}{3}\phi^3\right) \ , \end{aligned} \tag{4.2.21}$$

where V_H is the volume of H. The theory (4.2.21) has the left G symmetry. Note that this is a consistent truncation in the sense that every solution to the equation of motion in (4.2.21) is also a solution to the equation of motion in (4.2.20).

As an example, we consider $\mathrm{SU}(2) \simeq S^3$ and $\mathrm{SU}(2)/\mathrm{U}(1) \simeq S^2$. We have

$$g = e^{-i\varphi\sigma_3/2}e^{-i\theta\sigma_2/2}e^{-i\psi\sigma_3/2} \ , \quad L = e^{-i\varphi\sigma_3/2}e^{-i\theta\sigma_2/2} \ , \quad h = e^{-i\psi\sigma_3/2} \ , \tag{4.2.22}$$

where θ, φ and ψ are the Euler angles, and σ_i $(i = 1, 2, 3)$ are the Pauli matrices. Here $\mu = (\theta, \varphi)$, $m = \psi$, $\alpha = (1, 2)$, and $a = 3$. $\mathcal{L}_A$ are given by

$$\begin{aligned} \mathcal{L}_1 &= -i\left(-\sin\varphi\frac{\partial}{\partial\theta} - \cot\theta\cos\varphi\frac{\partial}{\partial\varphi} + \frac{\cos\varphi}{\sin\theta}\frac{\partial}{\partial\psi}\right) \ , \\ \mathcal{L}_2 &= -i\left(-\cos\varphi\frac{\partial}{\partial\theta} - \cot\theta\sin\varphi\frac{\partial}{\partial\varphi} + \frac{\sin\varphi}{\sin\theta}\frac{\partial}{\partial\psi}\right) \ , \\ \mathcal{L}_3 &= -i\frac{\partial}{\partial\varphi} \ . \end{aligned} \tag{4.2.23}$$

[15]The invariant 1-forms, the Killing vectors, the integral measures and the delta functions are all well-defined globally. Hence, all expressions on group manifolds and their coset spaces make sense globally, although they look dependent on coordinate patches.

$\mathcal{R}_A$ are given by

$$\begin{aligned}
\mathcal{R}_1 &= -i\left(-\sin\psi\frac{\partial}{\partial\theta}+\frac{\cos\psi}{\sin\theta}\frac{\partial}{\partial\varphi}-\cot\theta\cos\psi\frac{\partial}{\partial\psi}\right) ,\\
\mathcal{R}_2 &= -i\left(-\cos\psi\frac{\partial}{\partial\theta}-\frac{\sin\psi}{\sin\theta}\frac{\partial}{\partial\varphi}+\cot\theta\sin\psi\frac{\partial}{\partial\psi}\right) ,\\
\mathcal{R}_3 &= i\frac{\partial}{\partial\psi} .
\end{aligned} \tag{4.2.24}$$

The right and left invariant metric of SU(2) is given by

$$ds^2 = d\theta^2+\sin^2\theta d\varphi^2+(d\psi+\cos\theta d\varphi)^2 . \tag{4.2.25}$$

The first and second terms in the RHS give the metric of SU(2)/U(1). The Haar measure takes the form $dg=\sin\theta d\theta d\varphi d\psi$.

4.3 Bi-local representation for the reduced model on G/H

We consider a coordinate basis $|g\rangle$ for G as in the case of torus. We define the generators of the left translation $\hat{L}_A$[16] by

$$e^{i\epsilon\hat{L}_A}|g\rangle = |e^{i\epsilon t_A}g\rangle . \tag{4.3.1}$$

It is easy to show that

$$\hat{L}_A|g\rangle = -\mathcal{L}_A|g\rangle , \quad \langle g|\hat{L}_A = \mathcal{L}_A\langle g| . \tag{4.3.2}$$

We denote the volumes of G and G/H by V and V', respectively. To obtain a reduced model of (4.2.20) defined on G/H, we apply the following rule

$$\phi(g)\to\phi(L) , \quad \mathcal{L}_A\to\left[\hat{L}_A,\ \right] , \quad \int dg\to\frac{v}{v'}\int dL=\frac{v}{v'}\int d^{D-d}\sigma\sqrt{g} . \tag{4.3.3}$$

The first rule is realized by imposing $\mathcal{R}_a\phi=0$. Thus, by introducing the bi-local representation for $\phi(L)$

$$\phi(L,g,g') = \langle g|\phi(L)|g'\rangle , \tag{4.3.4}$$

we obtain a bi-local representation of the reduced model:

$$S_{\rm red} = \frac{v}{v'}\int dLdgdg'\frac{1}{2}\phi(L,g',g)\left[\left(\mathcal{L'}_A^L+\mathcal{L}_A^g+\mathcal{L}_A^{g'}\right)^2+m^2\right]\phi(L,g,g')$$

[16] $\hat{L}_A$ are the generators in the regular representation [35, 36].

$$+\frac{\kappa v}{3v'}\int dLdgdg'dg''\phi(L,g,g')\phi(L,g',g'')\phi(L,g'',g)\ . \tag{4.3.5}$$

As in the case of a torus, we make a change of variables

$$w=g\ ,\quad \xi=g'^{-1}g\ ,\quad \rho=g^{-1}L \tag{4.3.6}$$

and obtain a relation

$$\left(\mathcal{L}'^{L}_{A}+\mathcal{L}^{g}_{A}+\mathcal{L}^{g'}_{A}\right)\phi(L,g,g')=\mathcal{L}^{w}_{A}\phi(L,g,g')\ . \tag{4.3.7}$$

Thus, the propagator is read off as

$$\langle\phi(L_1,g_1,g_1')\phi(L_2,g_2',g_2)\rangle=\frac{v'}{v}\Delta\left(g_1g_2^{-1}\right)\delta\left(g_1'^{-1}g_1,g_2'^{-1}g_2\right)\delta_{G/H}\left(g_1^{-1}L_1,g_2^{-1}L_2\right)\ , \tag{4.3.8}$$

where $\Delta(g_1g_2^{-1})$ is the propagator of the original model (4.2.20) with $N=1$, $\delta(g_1,g_2)$ is the right and left invariant delta function on G, and $\delta_{G/H}(L_1,L_2)$ is the left invariant delta function on G/H.

We consider the 2-loop contribution to the free energy in the original and reduced models. The planar diagram (Fig.4.1) in the original theory is calculated as

$$\frac{\lambda N^2}{6}\int dg_1dg_2\Delta(g_1g_2^{-1})^3\ . \tag{4.3.9}$$

The non-planar diagram (Fig.4.2) is calculated as $(4.3.9)/N^2$. The planar diagram (Fig.4.1) in the reduced model is calculated as

$$\begin{aligned}3\cdot\frac{1}{2}\left(\frac{\kappa v}{3v'}\right)^2\left(\frac{v'}{v}\right)^3\int dL_1dL_2dg_1dg_1'dg_1''dg_2dg_2'dg_2''\\ \times\Delta\left(g_1g_2^{-1}\right)\delta\left(g_1'^{-1}g_1,g_2'^{-1}g_2\right)\delta_{G/H}\left(g_1^{-1}L_1,g_2^{-1}L_2\right)\\ \times\Delta\left(g_1'g_2'^{-1}\right)\delta\left(g_1''^{-1}g_1',g_2''^{-1}g_2'\right)\delta_{G/H}\left(g_1'^{-1}L_1,g_2'^{-1}L_2\right)\\ \times\Delta\left(g_1''g_2''^{-1}\right)\delta\left(g_1{}^{-1}g_1'',g_2{}^{-1}g_2''\right)\delta_{G/H}\left(g_1''^{-1}L_1,g_2''^{-1}L_2\right)\ .\end{aligned} \tag{4.3.10}$$

A change of variables $g_2'=g_2g_1^{-1}g_1'$ and $g_2''=g_2g_1^{-1}g_1''$ leads to

$$\begin{aligned}\frac{\kappa^2v'}{6v}\delta(0)\int dL_1dL_2dg_1dg_1'dg_1''dg_2\Delta\left(g_1g_2^{-1}\right)^3\delta_{G/H}\left(g_1^{-1}L_1,g_2^{-1}L_2\right)\\ \times\delta_{G/H}\left(g_1'^{-1}L_1,g_1'^{-1}g_1g_2^{-1}L_2\right)\delta_{G/H}\left(g_1''^{-1}L_1,g_1''^{-1}g_1g_2^{-1}L_2\right)\ .\end{aligned} \tag{4.3.11}$$

Making a further change of variables $g_1'^{-1}g_1\to g_1'^{-1}$ and $g_1''^{-1}g_1\to g_1''^{-1}$, we obtain

$$\frac{\kappa^2v'}{6v}\delta(0)\int dL_1dL_2dg_1dg_1'dg_1''dg_2\Delta\left(g_1g_2^{-1}\right)^3\delta_{G/H}\left(g_1^{-1}L_1,g_2^{-1}L_2\right)$$

$$
\begin{aligned}
&\times \delta_{G/H}\left(g_1'^{-1}g_1^{-1}L_1, g_1'^{-1}g_2^{-1}L_2\right)\delta_{G/H}\left(g_1''^{-1}g_1^{-1}L_1, g_1''^{-1}g_2^{-1}L_2\right)\\
&= \frac{\kappa^2 v'}{6v}\delta(0)\int dL_1 dL_2 dg_1 dg_1' dg_1'' dg_2 \Delta\left(g_1 g_2^{-1}\right)^3 \delta_{G/H}\left(g_1^{-1}L_1, g_2^{-1}L_2\right)^3\\
&= \frac{\kappa^2 v'}{6v}\delta(0)V^2\delta_{G/H}(0)^2 V'\int dg_1 dg_2 \Delta\left(g_1 g_2^{-1}\right)^3\\
&= \frac{vV'}{v'}\frac{\lambda N^2}{6V}\int dg_1 dg_2 \Delta\left(g_1 g_2^{-1}\right)^3 \ . \qquad (4.3.12)
\end{aligned}
$$

In the above calculation $\delta(0) = 1/v,\ \delta_{G/H}(0) = 1/v',\ V = Nv$ and $\lambda = \kappa^2 N$ have been used. The non-planar diagram (Fig.4.2) in the reduced model is calculated as

$$
\begin{aligned}
&3\cdot\frac{1}{2}\left(\frac{\kappa v}{3v'}\right)^2\left(\frac{v'}{v}\right)^3\int dL_1 dL_2 dg_1 dg_1' dg_1'' dg_2 dg_2' dg_2''\\
&\quad\times\Delta\left(g_1 g_2^{-1}\right)\delta\left(g_1'^{-1}g_1, g_2'^{-1}g_2\right)\delta_{G/H}\left(g_1^{-1}L_1, g_2^{-1}L_2\right)\\
&\quad\times\Delta\left(g_1' g_2''^{-1}\right)\delta\left(g_1''^{-1}g_1', g_2{}^{-1}g_2''\right)\delta_{G/H}\left(g_1'^{-1}L_1, g_2''^{-1}L_2\right)\\
&\quad\times\Delta\left(g_1'' g_2'^{-1}\right)\delta\left(g_1{}^{-1}g_1'', g_2''^{-1}g_2'\right)\delta_{G/H}\left(g_1''^{-1}L_1, g_2'^{-1}L_2\right) \ . \qquad (4.3.13)
\end{aligned}
$$

A change of variables $g_1'' = g_1' g_2''^{-1} g_2$ and $g_2' = g_2 g_1{}^{-1} g_1'$ gives rise to

$$
\begin{aligned}
&\frac{\kappa^2 v'}{6v}\int dL_1 dL_2 dg_1 dg_1' dg_2 dg_2''\ \Delta\left(g_1 g_2{}^{-1}\right)\Delta\left(g_1' g_2''^{-1}\right)\Delta\left(g_1' g_2''^{-1} g_2 g_1'^{-1} g_1 g_2{}^{-1}\right)\\
&\quad\times\delta\left(g_1^{-1}g_1' g_2''^{-1}g_2, g_2''^{-1}g_2 g_1^{-1}g_1'\right)\delta_{G/H}\left(g_1^{-1}L_1, g_2{}^{-1}L_2\right)\\
&\quad\times\delta_{G/H}\left(g_1'^{-1}L_1, g_2''^{-1}L_2\right)\delta_{G/H}\left(g_2^{-1}g_2'' g_1'^{-1}L_1, g_1'^{-1}g_1 g_2^{-1}L_2\right) \ . \qquad (4.3.14)
\end{aligned}
$$

A further change of variables $g_1 g_2^{-1} = \tilde{g}_2^{-1}$ and $g_1' g_2''^{-1} = \tilde{g}_1'$ leads to

$$
\begin{aligned}
&\frac{\kappa^2 v'}{6v}\int dL_1 dL_2 dg_1 d\tilde{g}_1' d\tilde{g}_2 dg_2''\Delta\left(\tilde{g}_2^{-1}\right)\Delta\left(\tilde{g}_1'\right)\Delta\left(\tilde{g}_1'\tilde{g}_2 g_1 g_2''^{-1}\tilde{g}_1'^{-1}\tilde{g}_2^{-1}\right)\delta\left(g_1^{-1}\tilde{g}_1'\tilde{g}_2 g_1, g_2''^{-1}\tilde{g}_2\tilde{g}_1' g_2''\right)\\
&\quad\times\delta_{G/H}\left(L_1, \tilde{g}_2^{-1}L_2\right)\delta_{G/H}\left(L_1, \tilde{g}_1'L_2\right)\delta_{G/H}\left(L_1, \tilde{g}_1'\tilde{g}_2 g_1 g_2''^{-1}\tilde{g}_1'^{-1}\tilde{g}_2^{-1}L_2\right)\\
&= \frac{\kappa^2 v'}{6v}\int dL_1 dL_2 dg_1 d\tilde{g}_1' d\tilde{g}_2 dg_2''\Delta\left(\tilde{g}_2^{-1}\right)\Delta\left(\tilde{g}_1'\right)\Delta\left(g_1 g_2''^{-1}\right)\delta\left(\tilde{g}_1'\tilde{g}_2 g_1, g_1 g_2''^{-1}\tilde{g}_2\tilde{g}_1' g_2''\right)\\
&\quad\times\delta_{G/H}\left(L_1, \tilde{g}_2^{-1}L_2\right)\delta_{G/H}\left(L_1, \tilde{g}_1'L_2\right)\delta_{G/H}\left(L_1, g_1 g_2''^{-1}L_2\right) \ . \qquad (4.3.15)
\end{aligned}
$$

By making a change of variables $g_1 g_2''^{-1} = \tilde{g}$, we obtain

$$
\begin{aligned}
&\frac{\kappa^2 v'}{6v}V\int dL_1 dL_2 d\tilde{g}_1' d\tilde{g}_2 d\tilde{g}\Delta\left(\tilde{g}_2^{-1}\right)\Delta\left(\tilde{g}_1'\right)\Delta\left(\tilde{g}\right)\\
&\quad\times\delta\left(\tilde{g}_1'\tilde{g}_2\tilde{g}, \tilde{g}\tilde{g}_2\tilde{g}_1'\right)\delta_{G/H}\left(L_1, \tilde{g}_2^{-1}L_2\right)\delta_{G/H}\left(L_1, \tilde{g}_1'L_2\right)\delta_{G/H}\left(L_1, \tilde{g}L_2\right) \ . \qquad (4.3.16)
\end{aligned}
$$

Since $\delta\left(\tilde{g}_1'\tilde{g}_2\tilde{g}, \tilde{g}\tilde{g}_2\tilde{g}_1'\right) \leq \delta(0) = 1/v$,

Absolute value of (4.3.16)

$$\begin{aligned}
&\leq \frac{\kappa^2 v'}{6v}\delta(0)V \int dL_1 dL_2 dh dh' dh'' \left|\Delta\left(L_2^{-1}L_1 h\right)\Delta\left(L_2^{-1}L_1 h'\right)\Delta\left(L_2^{-1}L_1 h''\right)\right| \\
&= \left\{\frac{vV'}{v'}\frac{\lambda N^2}{6V}\frac{V'}{V}\int dL_1 dL_2 dh dh' dh'' \left|\Delta\left(L_2^{-1}L_1 h\right)\Delta\left(L_2^{-1}L_1 h'\right)\Delta\left(L_2^{-1}L_1 h''\right)\right|\right\} \times \left(\frac{v'}{V'}\right)^2 .
\end{aligned} \tag{4.3.17}$$

We see that the above quantity is analogous to the one (4.1.14) and suppressed by $(v'/V')^2$ in the $v' \to 0$ limit compared to (4.3.12). Thus, the non-planar diagram is suppressed compared to the planar diagram in both the original and reduced model. By comparing (4.3.9) and (4.3.12), we again obtain the relation (4.1.15). As in the case of torus, one can show that (4.1.15) holds to all orders in perturbative expansion.

Defining $\hat{\phi}(g)$ by

$$\hat{\phi}(g) = e^{iL_A\theta_A}\phi(L)e^{-iL_A\theta_A} , \tag{4.3.18}$$

where $g = e^{i\theta_A t_A}$, we see that the relation (4.1.16) also holds in this case. Thus, we find that the large-N equivalence in dimensional reduction holds on group manifolds.

Finally, we consider U(N) Yang-Mills theory on G:

$$S = \frac{1}{4\kappa^2}\int d^D x\sqrt{G}G^{AC}G^{BD}\mathrm{Tr}(F_{AB}F_{CD}) , \tag{4.3.19}$$

where $F_{AB} = \partial_A A_B - \partial_B A_A + i[A_A, A_B]$. We expand the gauge field A_A in terms of the right invariant 1-form as

$$A_M = E_M^A X_A . \tag{4.3.20}$$

By using (4.2.8), we rewrite (4.3.19) as

$$S = -\frac{1}{4\kappa^2}\int d^D x\sqrt{G}\ \mathrm{Tr}\left(\mathcal{L}_A X_B - \mathcal{L}_B X_A - if_{ABC}X_C + [X_A, X_B]\right)^2 . \tag{4.3.21}$$

By imposing $\mathcal{R}_a X_A = 0$ on (4.3.19), we obtain Yang-Mills theory on G/H. The reduced model on G/H is given by

$$S_{\mathrm{red}} = -\frac{v}{v'}\frac{1}{4\kappa^2}\int d^{D-d}\sigma\sqrt{g}\ \mathrm{Tr}\left(\mathcal{L}_A\tilde{X}_B - \mathcal{L}_B\tilde{X}_A - if_{ABC}X_C + \left[\tilde{X}_A, \tilde{X}_B\right]\right)^2 , \tag{4.3.22}$$

where $\tilde{X}_A(\sigma) = L_A + X_A(\sigma)$. If G is simple, the gauge theory is massive due to the $f_{ABC}X_C$ term so that the there is no moduli for the background $\tilde{X}_A = L_A$. Thus, since the background $\tilde{X}_A = L_A$ is stable, the large-N volume independence on group manifolds holds. Namely, the reduced model is equivalent to the original model (4.3.21) in the $N \to \infty$ with

$\kappa^2 N$ fixed in the sense that (4.1.15) holds and a following relation for Wilson loops [81] holds:

$$\left\langle \frac{1}{N} P \exp\left(i \int_0^1 d\zeta \frac{dx^M(\zeta)}{d\zeta} E_M^A(x(\zeta)) X_A(x(\zeta)) \right) \right\rangle$$
$$= \left\langle \frac{1}{N} P \exp\left(i \int_0^1 d\zeta \frac{dx^M(\zeta)}{d\zeta} E_M^A(x(\zeta)) \tilde{X}_A(\sigma(\zeta)) \right) \right\rangle_{\text{red}} , \tag{4.3.23}$$

where $x^M(\zeta)$ and $\sigma^\mu(\zeta)$ are related through $g(x) = L(\sigma)h(y)$.

Chapter 5

Study of classical solutions in the Lorentzian type IIB matrix model

In this chapter, we develop a numerical method for obtaining wider classes of solutions. We apply the gradient decent method to solve classical equations of the type IIB matrix model because there exists no time a priori in the type IIB matrix model.

In particular, we see whether the (3+1)-dimensional expanding universe with smooth structure is reproduced as classical solutions in the Lorentzian type IIB matrix model, and search for solutions which yield Dirac zero modes.

5.1 Classical solutions of the type IIB matrix model

Here, we consider the Lorentzian type IIB matrix model. To make it well-defined, we need constraints corresponding to IR cutoffs [56]:

$$\frac{1}{N}\mathrm{Tr}(A_0)^2 = \kappa \ , \quad \frac{1}{N}\mathrm{Tr}(A_I)^2 = 1 \quad (I = 1, \ldots, 9) \ . \tag{5.1.1}$$

We would like to investigate the space-time structure in (3+1) dimensions and spectra of the 6-dimensional Dirac operator in the extra dimensions at late time compared to the Planckian time in this model. At late time, it is difficult to perform numerical simulations because the matrix size must be large, while we expect the classical approximation to be valid due to the expansion of universe. We, therefore, solve classical equations of motion of this model. While solving them is non-trivial, it is indeed easier to solve classical equations than to perform numerical simulations. We consider bosonic equations of motion of the type IIB matrix model with 'mass' term:

$$\big[A^M, [A_M, A_0]\big] - \xi A_0 = 0 \ , \quad \big[A^M, [A_M, A_I]\big] - \zeta A_I = 0 \ , \tag{5.1.2}$$

where ξ and ζ are Lagrange multipliers, and the second terms of the left hand side of the two equations in (5.1.2) come from constraints (5.1.1). Here, note that classical solutions

turn out to be always simultaneously diagonalizable if $\xi = \zeta = 0$, which is proved in footnote 17[17].

We search for solutions which are compatible with SO(3,1) symmetry because the universe is SO(3,1) symmetric at the time scale where the spacial expansion can be ignored. Thus, we assume configurations with a quasi-direct-product structure in the (3+1) dimensions and extra dimensions [79]:

$$A_\mu = X_\mu \otimes M \quad (\mu = 0, 1, 2, 3) \ , \quad A_a = \mathbf{1}_{N_X} \otimes Y_a \quad (a = 4, \ldots, 9) \ , \tag{5.1.3}$$

where the size of X_μ and the identity matrix $\mathbf{1}_{N_X}$ is N_X, that of M and Y_a is N_Y, and $N = N_X N_Y$. This structure is compatible with SO(3,1) symmetry:

$$\mathcal{U} A_\mu \mathcal{U}^\dagger = O_\mu{}^\nu A_\nu \ , \quad \mathcal{U} A_a \mathcal{U}^\dagger = A_a \tag{5.1.4}$$

with $\mathcal{U} = U \otimes \mathbf{1}_{N_Y} \in \mathrm{SU}(N)$ and $U X_\mu U^\dagger = O_\mu{}^\nu X_\nu$, where $O_\mu{}^\nu \in \mathrm{SO}(3,1)$ and $U \in \mathrm{SU}(N_X)$. Indeed, left hand sides of two equations in (5.1.4) are $\mathrm{SU}(N)$ transformations of (2.3.4). Moreover, it is the most general form preserving the SO(3,1) symmetry, and represents a direct-product space-time if $M = \mathbf{1}_{N_Y}$.

5.1.1 Algorithm searching for classical solutions in numerical calculation

There exist no time a priori in the type IIB matrix model, so we cannot use the algorithm to solve differential equations. Instead, we apply the gradient descent algorithm to search for classical solutions in our numerical calculation. In the following, we explain the algorithm. We define V as

$$V = \mathrm{Tr}\left(\left[A^M, [A_M, A_0]\right] - \xi A_0\right)^2 + \mathrm{Tr}\left(\left[A^M, [A_M, A_I]\right] - \zeta A_I\right)^2 \ , \tag{5.1.5}$$

and numerically search for A_M which make V equal to 0. We begin with random configurations of X_μ, Y_a, and M where their elements obey Gaussian distribution and satisfy the constraints (5.1.1). The solutions depend on the initial random configurations and initial ξ and ζ. We update X_μ, Y_a, and M following the relations:

$$\delta X_\mu = -\epsilon \frac{\partial V}{\partial X_\mu^\dagger} \ , \quad \delta Y_a = -\epsilon \frac{\partial V}{\partial Y_a^\dagger} \ , \quad \delta M = -\epsilon \frac{\partial V}{\partial M^\dagger} \ , \tag{5.1.6}$$

[17] From the first equation in (5.1.2) with $\xi = 0$, we obtain $\mathrm{Tr}\left(A_0 \left[A^I, [A_I, A_0]\right]\right) = 0$, which implies $[A_0, A_I] = 0$. Similarly, we obtain the following relation from the second equation in (5.1.2) with $\zeta = 0$: $[A_I, A_J] = 0$.

where we take ϵ to be small enough, which guarantees $\delta V \leq 0$. Then, we rescale A_M as $A_M \to sA_M$ such that the second equation in (5.1.1) is kept satisfied, and further rescale ξ and ζ as $\xi \to s^2\xi$ and $\zeta \to s^2\zeta$ such that V is scaled as $V \to s^6 V$. We can obtain configurations with $V \simeq 0$ by repeating this procedure[18]. In practice, we continue updating configurations until $V \sim O(10^{-4})$.

5.1.2 Typical solution

We solve (5.1.2) with $\xi = \zeta > 0$, which preserves SO(9,1) symmetry. Here, our ansatz (5.1.3) reduces the constraints (5.1.1) to the following ones[19]:

$$\frac{1}{N_X}\mathrm{Tr}\,(X_0)^2 = \kappa \ , \quad \frac{1}{N_Y}\mathrm{Tr}M^2 = 1 \ , \tag{5.1.7}$$

$$\frac{1}{N_X}\sum_{i=1}^{3}\mathrm{Tr}\,(X_i)^2 + \frac{1}{N_Y}\sum_{a=4}^{9}\mathrm{Tr}\,(Y_a)^2 = 1 \ . \tag{5.1.8}$$

In almost all of our solutions, the following equations are satisfied:

$$\frac{N_Y - n^{[0]}}{N_Y}M^3 = M \ , \tag{5.1.9}$$

$$[M, Y_a] = 0 \ , \tag{5.1.10}$$

$$[X^\nu, [X_\nu, X_0]] - \xi X_0 = 0 \ , \tag{5.1.11}$$

$$[X^\nu, [X_\nu, X_i]] - \zeta X_i = 0 \quad (i = 1, 2, 3) \ , \tag{5.1.12}$$

$$\big[Y^b, [Y_b, Y_a]\big] - \zeta Y_a = 0 \ , \tag{5.1.13}$$

where $n^{[\lambda]}$ denote numbers of eigenvalues $\lambda(= -1, 0, 1)$ of M. Indeed, these equations are sufficient conditions for (5.1.2). (5.1.9) implies that eigenvalues of M are $\pm\sqrt{N_Y/(N_Y - n^{[0]})}$ and 0. One can see from (5.1.10) that Y_a have the following block-diagonal structure in a basis which diagonalizes M:

$$M = \sqrt{\frac{N_Y}{N_Y - n^{[0]}}}\begin{pmatrix} -\mathbf{1}_{n^{[-1]}} & & \\ & \mathbf{0}_{n^{[0]}} & \\ & & \mathbf{1}_{n^{[1]}} \end{pmatrix} \longleftrightarrow Y_a = \begin{pmatrix} Y_a^{[-1]} & & \\ & Y_a^{[0]} & \\ & & Y_a^{[1]} \end{pmatrix} \ , \tag{5.1.14}$$

where $N_Y = n^{[-1]} + n^{[0]} + n^{[1]}$. It turns out that ξ and ζ converge to the range

$$0.1 \lesssim \xi = \zeta \lesssim 0.5 \tag{5.1.15}$$

[18] While it is possible that we reach a local minimum with $V \neq 0$, this dose not happen in our cases.

[19] Here, we fix the ratio of X_μ to M.

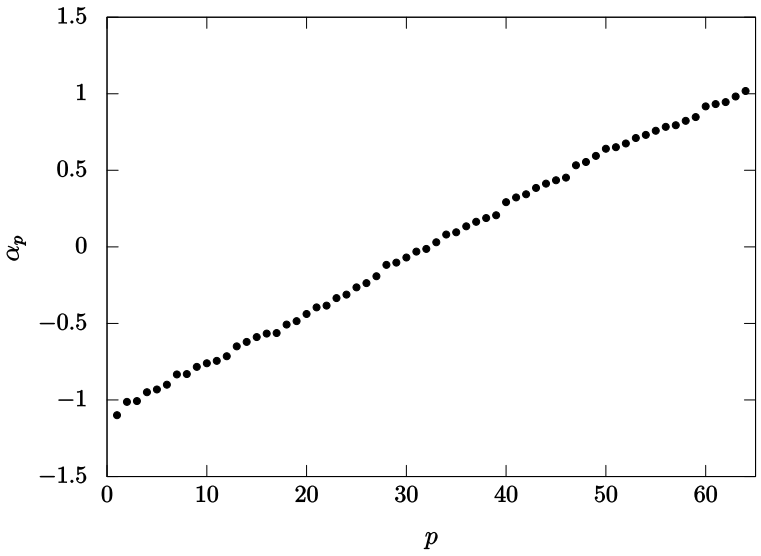

Figure 5.1: The 64 eigenvalues α_p ($p = 1, \ldots, N_X$) of X_0 in ascending order are plotted against the indices p in the typical solution for $N_X = 64$.

when we obtain the solution satisfying (5.1.9) – (5.1.13). In most of the cases in which ξ and ζ do not converge to the above range, we obtain the solutions not satisfying (5.1.9) – (5.1.13) or V decreases slowly or even never goes down so that solutions are quite hard to be obtained.

5.2 Space-time structure in the (3+1) dimensions

Using the method which we explained in the previous section, we solve the classical equations of motion. Staring with different initial conditions, we obtain many solutions satisfying (5.1.9) – (5.1.13) for the matrix sizes $N_X = N_Y = 32, 48, 64$[20]. We obtain twelve classical solutions for each N_X, which have some common features. In this paper, we denote a set of such solutions by $\mathcal{S}$. In the following sections except the last part of section 5.2.5, we focus on a typical classical solution with $N_X = N_Y = 64$ belonging to $\mathcal{S}$ in order to show the common features.

5.2.1 Band-diagonal structure

The structure of the (3+1)-dimensional space-time is represented by the matrices X_μ. Using the SU(N) symmetry (2.3.4) with $\mathcal{U} = U \otimes \mathbf{1}_{N_Y}, U \in \mathrm{SU}(N_X)$, we can choose a basis

[20]Note that we also find classical solutions which do not satisfy (5.1.9) – (5.1.13).

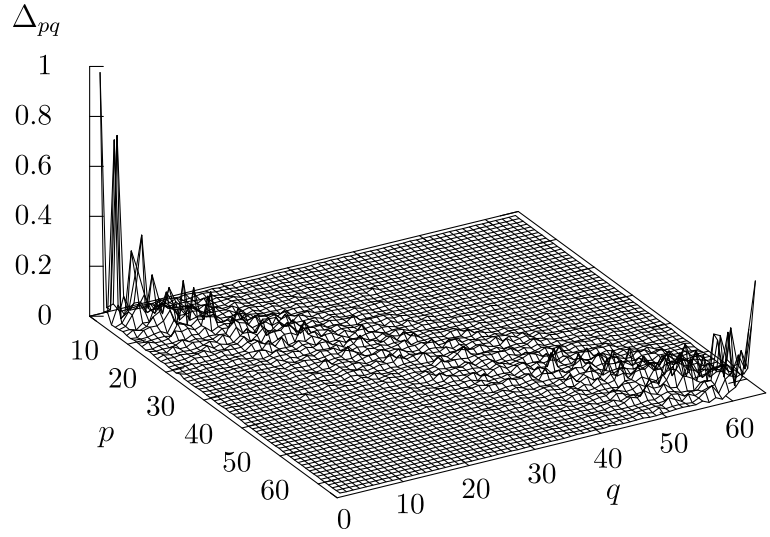

Figure 5.2: We plot Δ_{pq} in the typical solution for $N_X = 64$. The height of each grid point (p, q) represents the value of Δ_{pq}.

in which X_0 is diagonal such that its eigenvalues are arranged in ascending order. In Fig. 5.1, we show the 64 eigenvalues α_p $(p = 1, 2, \ldots, N_X)$ of X_0 for the solution. We expect to define a continuous time in the $N_X \to \infty$ limit because almost all of α_p are uniformly distributed.

Moreover, we define the following quantity

$$\Delta_{pq} = \sum_{i=1}^{3} \left| [X_i]_{pq} \right|^2 \ , \tag{5.2.1}$$

which tells us how the elements of X_i are distributed in this basis, and plot Δ_{pq} for the solution in Fig. 5.2. We see that the spatial components X_i are band-diagonal, which means that $|[X_i]_{pq}|$ are large for $|p-q| \leq n-1$, while very small for $|p-q| \geq n$. Here, n is an integer which represents the size of the band. The band-diagonal structure guarantees locality of time, which enables us to derive time evolution as in the next section.

The almost uniform distribution of α_p and the band-diagonal structure are common for the solutions in $\mathcal{S}$, and also possessed by the dominant configurations of X_i in the numerical simulation. Note that the band-diagonal structure can be interpreted as deviation from a diagonal matrix due to $\xi, \zeta \neq 0$ (See footnote 17.).

5.2.2 Time evolution

Here, we discuss the time evolution. From the diagonalized matrix X_0 and the band-diagonal matrices X_i, we can define the time evolution as follows.

We determine the band size n so that a collection of the elements $\{[X_i]_{pq} \,|\, |p-q| \leq n-1\}$ can include non-negligible elements in the band structure. The details of the determination are explained in appendix E, where the block size for the typical solution is determined as $n = 10$. We define $n \times n$ blocks $\bar{X}_i(k)$ with $k = 0, 1, \ldots, N_X - n$ as follows:

$$\left[\bar{X}_i(k)\right]_{\tilde{p}\tilde{q}} = [X_i]_{k+\tilde{p},\, k+\tilde{q}} \quad (\tilde{p}, \tilde{q} = 1, 2, \ldots, n) \ . \tag{5.2.2}$$

These $N_X - n + 1$ matrices are labeled by a variable t which is defined as the average of the n eigenvalues of X_0 within the k-th $n \times n$ block:

$$t = t\,(k) = \frac{1}{n} \sum_{\tilde{p}=1}^{n} \alpha_{k+\tilde{p}} \ . \tag{5.2.3}$$

Here, α_p is a series of the eigenvalues of X_0 in ascending order. Thus, $t(k)$ is monotonically (strictly) increasing:

$$\alpha_1 < \alpha_2 < \cdots < \alpha_{N_X} \quad \Longrightarrow \quad t\,(0) < t\,(1) < \cdots < t\,(N_X - n) \ . \tag{5.2.4}$$

It is naturally considered that the $n \times n$ matrices $\bar{X}_i(t) = \bar{X}_i(k)$ represent the space structure at the time t. We can extract some information of the time evolution of the 3-dimensional space from $\bar{X}_i(t)$. The solutions in $\mathcal{S}$ share common properties of the time evolution shown in the following sections.

5.2.3 Extent of space

One of important quantities of the time evolution is the extent of space, which represents the scale of the 3-dimensional space at the time t. For a given configuration X_i, the extent of space at t is defined by

$$R^2\,(t) = \frac{1}{n} \sum_{i=1}^{3} \mathrm{tr}\left(\bar{X}_i\,(t)\, \bar{X}_i\,(t)\right) \ . \tag{5.2.5}$$

Here, we note that 'tr' denotes the trace over an $n \times n$ matrix. In Fig. 5.3, we plot $R^2(t)$ for the typical solution given in section 5.2.1. From the plot of $R^2(t)$, one can find shrinking and expanding behavior, which reflects the time-reversal symmetry of the model. Note that this behavior is common for the solutions in $\mathcal{S}$. We identify the minimum point of $R^2(t)$ as the beginning of the time evolution of universe, and regard the time evolution of our universe at $t > 0$ regime. Namely, the beginning and the end of expansion of $R^2(t)$ corresponds to the earliest time and the latest time, respectively.

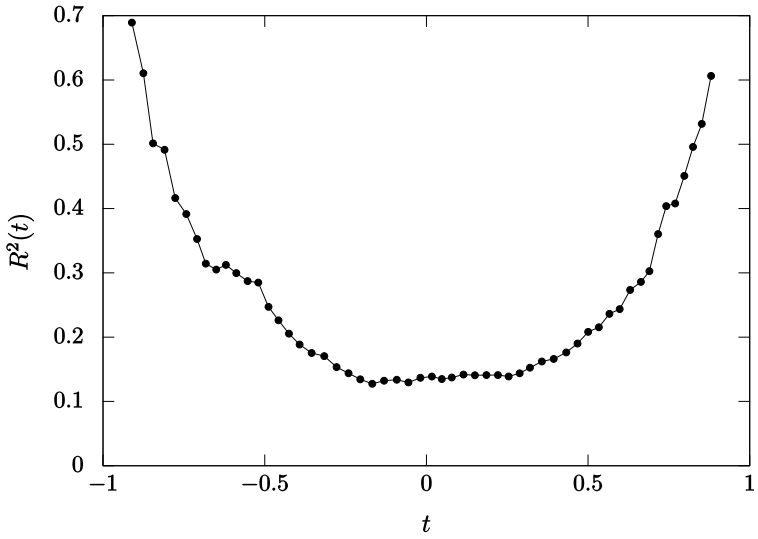

Figure 5.3: The extent of space $R^2(t)$ is plotted against t in the typical solution for $N_X = 64$. It is time-reversal symmetric. We find that the space is expanding in the $t > 0$ region.

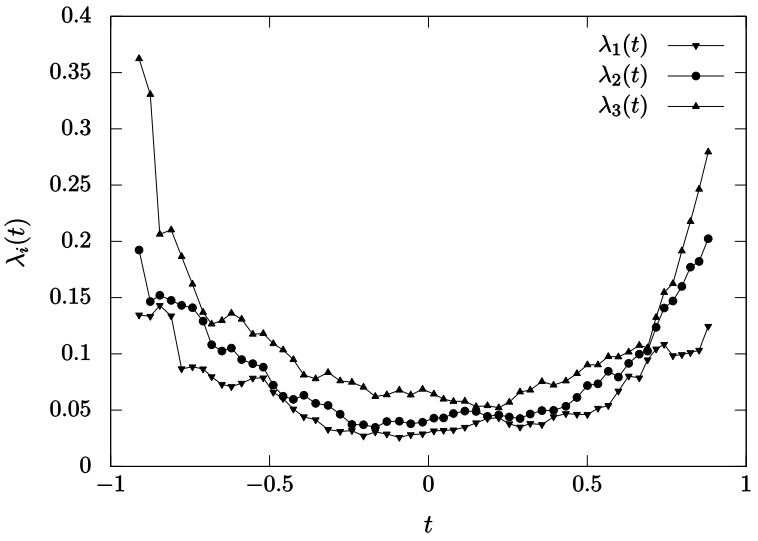

Figure 5.4: The eigenvalues of $T_{ij}(t)$ $(i, j = 1, 2, 3)$ denoted by $\lambda_i(t)$ are plotted against t in the typical solution for $N_X = 64$. Inverted triangles, circles, and triangles represent $\lambda_1(t), \lambda_2(t)$, and $\lambda_3(t)$, respectively.

5.2.4 Moment of inertia tensor

Next, we define a 3×3 (positive definite) real symmetric tensor

$$T_{ij}(t) = \frac{1}{n}\mathrm{tr}\left(\bar{X}_i(t)\,\bar{X}_j(t)\right) \ . \tag{5.2.6}$$

This is an analog of the moment of inertia tensor, and represents how the space extends in 3 dimensions. Each eigenvalue is the extent of space for each of three directions. Note that $R^2(t)$ is equivalent to the sum of the diagonal elements $T_{ii}(t)$:

$$R^2(t) = \sum_{i=1}^{3} T_{ii}(t) \ . \tag{5.2.7}$$

If our solution represents the present universe, SO(3) symmetry should be preserved. If the three eigenvalues are equivalent, the configuration represents an SO(3) symmetric space.

In Fig. 5.4, three eigenvalues of $T_{ij}(t)$, which are denoted $\lambda_i(t)$ arranged in ascending order $\lambda_1(t) \leq \lambda_2(t) \leq \lambda_3(t)$, for the typical solution are plotted. The behavior of $T_{ij}(t)$ is time-reversal symmetric as $R^2(t)$ is. Note that this is also common for the solutions in $\mathcal{S}$. We find from Fig. 5.4 that the 3-dimensional space represented by the typical solution is SO(3) symmetric except at late time. The breaking of the SO(3) can be caused by a finite size effect. In other words, N_X must be larger enough to fully keep SO(3) symmetry of the model. We actually confirm that the symmetry is expected to recover in the large-N_X limit.

5.2.5 Structure of the 3-dimensional space

We are interested in the structure of the 3-dimensional space described by the classical solutions. In order to see it, we define the following $n \times n$ matrix $Q(t)$:

$$Q(t) = \sum_{i=1}^{3} \bar{X}_i(t)\,\bar{X}_i(t) \ . \tag{5.2.8}$$

Since the eigenvalues of $\bar{X}_i(t)$ correspond to the spatial coordinates, the eigenvalues $q_{\tilde{p}}(t)$ of $Q(t)$ give the squared radial coordinates. In other words, the eigenvalues $q_{\tilde{p}}(t)$ represent the distribution in the radial direction of the points which describe the 3-dimensional space. Note that $R^2(t)$ is the average of the n eigenvalues:

$$R^2(t) = \frac{1}{n}\mathrm{tr}Q(t) = \frac{1}{n}\sum_{\tilde{p}=1}^{n} q_{\tilde{p}}(t) \ . \tag{5.2.9}$$

The eigenvalues of $Q(t)$ for the typical solution are plotted in Fig. 5.5. Since $n = 10$ for

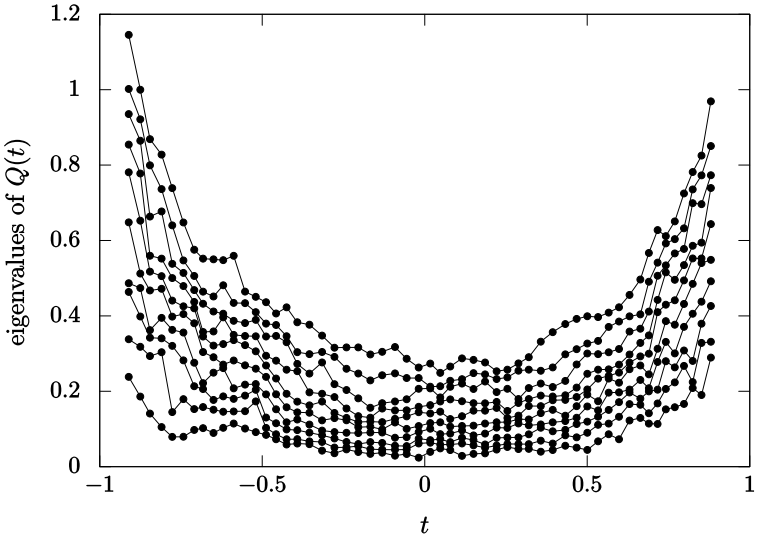

Figure 5.5: The 10 eigenvalues of $Q(t)$ are plotted against t in the typical solution for $N_X = 64$ whose block size is $n = 10$. All of the eigenvalues are growing almost uniformly.

the solution, there are ten lines corresponding to the ten eigenvalues $q_{\tilde{p}}(t)$ at each time. We find that all of the eigenvalues are growing and spreading almost uniformly. It means that the radial direction of the 3-dimensional space is uniformly expanding. This behavior is common for the solutions in $\mathcal{S}$.

5.3 Emergence of Dirac zero modes in the 6 dimensions

In this section, we discuss how chiral zero modes appear from the type IIB matrix model. A general discussion on the Dirac equation implies that it is necessary to have zero modes in the 6-dimensional Dirac operator. In fact, we show that the block-diagonal structure (5.1.14) of the typical solutions can be regarded as the emergence of intersecting D-branes. Indeed we find that zero modes appear in the limit where the matrix size goes to infinity if the dimensionality of the branes is chosen appropriately.

5.3.1 The 6-dimensional Dirac equation

From the fermionic action (2.3.3) of the type IIB matrix model, one obtains the 10-dimensional Dirac equation

$$\Gamma^M [A_M, \Psi] = 0 \ , \tag{5.3.1}$$

where Ψ satisfies the Weyl condition with the chirality operator in 10 dimensions Γ_χ:

$$\Gamma_\chi \Psi = +\Psi \ . \tag{5.3.2}$$

Here, we decompose the 10-dimensional Gamma matrices Γ^M into the 4-dimensional ones ρ^μ and the 6-dimensional ones γ^a:

$$\Gamma^\mu = \rho^\mu \otimes \mathbf{1}_8 \ , \quad \Gamma^a = \rho_\chi \otimes \gamma^a \ , \tag{5.3.3}$$

and the chirality operator Γ_χ is also decomposed as

$$\Gamma_\chi = \rho_\chi \otimes \gamma_\chi \ , \tag{5.3.4}$$

where ρ_χ and γ_χ are the chirality operators in 4 and 6 dimensions, respectively.

We require Ψ to be chiral in 4 dimensions:

$$(\rho_\chi \otimes \mathbf{1}_8)\, \Psi = \pm \Psi \ . \tag{5.3.5}$$

Due to the chirality (5.3.2) in 10 dimensions, (5.3.5) implies

$$(\mathbf{1}_4 \otimes \gamma_\chi)\, \Psi = \pm \Psi \ . \tag{5.3.6}$$

Namely, Ψ is chiral also in six dimensions. Let us next decompose (5.3.1) into two terms as

$$\Gamma^\mu \left[A_\mu, \Psi\right] + \Gamma^a \left[A_a, \Psi\right] = 0 \ . \tag{5.3.7}$$

Note that the first term and the second term have opposite chirality in 4-dimensions as well as in 6-dimensions, which implies that each term has to vanish separately. Thus, in order to obtain chiral fermions in 4 dimensions, we need to have Dirac zero modes in six dimensions:

$$\Gamma^a \left[A_a, \Psi\right] = 0 \ . \tag{5.3.8}$$

Let us now consider that A_M is a classical solution with the quasi direct-product structure (5.1.3). Since $A_a = \mathbf{1} \otimes Y_a$, the general solution to (5.3.8) can be obtained by decomposing Ψ as

$$\Psi = \psi^{(4\mathrm{d})} \otimes \psi^{(6\mathrm{d})} \ , \tag{5.3.9}$$

where the 4-dimensional and 6-dimensional gamma matrices act only on $\psi^{(4\mathrm{d})}$ and $\psi^{(6\mathrm{d})}$, respectively. Thus, in order to satisfy (5.3.8), we only need to require

$$\gamma^a \left[Y_a, \psi^{(6\mathrm{d})}\right] = 0, \quad \gamma_\chi \psi^{(6\mathrm{d})} = \pm \psi^{(6\mathrm{d})} \ . \tag{5.3.10}$$

5.3.2 Dirac zero modes

If Y_a are block-diagonal, it is expected from the following picture that zero modes, namely, solutions to the first equation in (5.3.10) arise from off-diagonal blocks. Here, we note that zero modes in 6 dimensions yield Dirac zero modes in 4 dimensions. Diagonal blocks of Y_a correspond to D-branes, and these D-branes can intersect each other. Open strings are stretched between intersecting D-branes. At an intersecting point, the string whose length is zero corresponds to the Dirac zero mode. The off-diagonal block of $\psi^{(6d)}$ corresponds to those open strings.

Assuming that Y_a have the block-diagonal structure, we solve (5.1.13) for each block of Y_a with a common ζ. In the following analysis, we set $\zeta = 1$ without loss of generality. We concentrate on two of the diagonal blocks of Y_a and the off-diagonal block of $\psi^{(6d)}$:

$$Y_a = \begin{pmatrix} Y_a^{(1)} & \\ & Y_a^{(2)} \end{pmatrix} , \tag{5.3.11}$$

$$\psi^{(6d)} = \begin{pmatrix} & \varphi \\ & \end{pmatrix} , \tag{5.3.12}$$

where the sizes of $Y_a^{(1)}$ and $Y_a^{(2)}$ are $N_Y^{(1)}$ and $N_Y^{(2)}$, respectively. Then, we solve the following eigenvalue problem:

$$\gamma^a_{\alpha\beta} \left[Y_a^{(1)} \varphi_\beta - \varphi_\beta Y_a^{(2)} \right] = \lambda \varphi_\alpha , \tag{5.3.13}$$

where φ_α ($\alpha = 1, \ldots, 8$) are eigenvectors, and eigenvalue λ corresponds to a mass in the (3+1) dimensions. If λ is eigenvalue of φ_α, $-\lambda$ is also eigenvalue of φ_α from the second equation in (5.3.10). Here, note that $\lambda = 0$ corresponds to a Dirac zero mode. In order to see the picture of intersecting D-branes, we consider wave functions. φ_α obtained in our numerical calculation contains the left-handed and the right-handed ones, so we extract $\varphi_{\mathrm{L}\alpha}$ and $\varphi_{\mathrm{R}\alpha}$:

$$\varphi_{\mathrm{L}\alpha} = \frac{1 - \gamma_\chi}{2} \varphi_\alpha , \quad \varphi_{\mathrm{R}\alpha} = \frac{1 + \gamma_\chi}{2} \varphi_\alpha . \tag{5.3.14}$$

Here, we choose $\mathcal{U}' = \mathbf{1}_{N_X} \otimes U'$ with $U' \in \mathrm{SU}(N_Y)$ as $\mathcal{U}$ in (2.3.4) such that SU(N) transformation preserves the quasi-direct-product structure (5.1.3). Then, M, Y_a and $\psi_\alpha^{(6d)}$ are transformed as follows:

$$M' = U' M U'^\dagger , \quad Y'_a = U' Y_a U'^\dagger , \quad \psi'^{(6d)}_\alpha = U' \psi^{(6d)}_\alpha U'^\dagger . \tag{5.3.15}$$

In particular, by restricting U' to

$$U' = \begin{pmatrix} U'' & 0 \\ 0 & V'' \end{pmatrix} \tag{5.3.16}$$

with $U'' \in \mathrm{SU}(N_Y^{(1)})$ and $V'' \in \mathrm{SU}(N_Y^{(2)})$, which keeps the structure (5.3.11), we transform the wave functions corresponding to the Dirac operator as

$$\varphi_{\mathrm{L}\alpha} \mapsto U'' \varphi_{\mathrm{L}\alpha} V''^{\dagger} \ , \quad \varphi_{\mathrm{R}\alpha} \mapsto U'' \varphi_{\mathrm{R}\alpha} V''^{\dagger} \ . \tag{5.3.17}$$

In the following sections, we use this transformation in order to see whether the wave function is localized.

5.3.3 Solving the Dirac equation in numerical calculation

We see from the statement below (5.3.13) that for each eigenvalue in (5.3.13) there is another eigenvalue with the same magnitude and the different sign. In this section, we concentrate on the lowest and the second lowest eigenvalues among $(8N_Y^{(1)}N_Y^{(2)}/2)$ positive eigenvalues[21]. From the picture of the intersecting D-branes, we expect the emergence of Dirac zero modes when the two branes intersect at a point. This requires generically that the dimensionality of the branes adds up to 6. If the sum of the dimensionality is less than 6, the two branes do not intersect, and if the sum is more than 6, the two branes intersect but not at a point. In order to specify the dimensionality of the brane, say to d, we set $6-d$ components of Y_a to zero. In the following, we replace $a = 4, \ldots, 9$ with $a = 1, \ldots, 6$.

3d and 4d solutions are generated numerically with the algorithm described in section 5.1. On the other hand, the 2d solutions can be constructed analytically as follows. By putting

$$\left[Y_1^{(1)}, Y_2^{(2)}\right] = iZ \ , \tag{5.3.18}$$

we reduce (5.1.13) with $\zeta = 1$ to

$$\left[Y_2^{(1)}, Z\right] = iY_1^{(1)} \ , \quad \left[Z, Y_1^{(1)}\right] = iY_2^{(1)} \ . \tag{5.3.19}$$

Here, (5.3.18) and (5.3.19) imply that $Y_a^{(1)}$ and Z are generators of the SU(2) algebra L_i $(i = 1, 2, 3)$:

$$Y_1^{(1)} = L_1 \ , \quad Y_2^{(1)} = L_2 \ , \quad Z = L_3 \ . \tag{5.3.20}$$

We use the irreducible representation for configurations of $Y_a^{(1)}$ without loss of generality because we can obtain spectra with the reducible representation from summation of those with the irreducible representations. The above construction suggests that the 2d brane is something like a "fuzzy disk", which can be obtained by projecting a fuzzy sphere onto a

[21] Note that φ_α is the element of $(8N_Y^{(1)}N_Y^{(2)})$-dimensional vector space and here we count the number of the eigenvalues including the degeneracy.

plane. More precisely, it should be regarded as two coinciding fuzzy disks corresponding to the two hemispheres of the fuzzy sphere.

We solve (5.3.13) for Y_a obtained numerically in this section. Except in the cases where 2d solutions are used, we obtain 4 solutions for each block, so we examine $4 \times 4 = 16$ cases. In the cases where 2d solutions are used, we also examine 16 cases, which are given by one solution for $Y_a^{(1)}$ and 16 solutions for $Y_a^{(2)}$. For simplicity, we set $N_Y^{(1)} = N_Y^{(2)}$ except in the 2d-4d ansatz.

3d-3d ansatz

We further make the following ansatz for $Y_a^{(1)}$ and $Y_a^{(2)}$. 3-dimensional manifolds intersect at a point in the 6-dimensional space, so we use 3d-3d ansatz, which implies that

$$Y_1^{(1)} \neq 0 \ , \ Y_2^{(1)} \neq 0 \ , \ Y_3^{(1)} \neq 0 \ , \ Y_4^{(1)} = Y_5^{(1)} = Y_6^{(1)} = 0 \ , \tag{5.3.21}$$

$$Y_1^{(2)} = Y_2^{(2)} = Y_3^{(2)} = 0 \ , \ Y_4^{(2)} \neq 0 \ , \ Y_5^{(2)} \neq 0 \ , \ Y_6^{(2)} \neq 0 \ . \tag{5.3.22}$$

Since there is the ambiguity of the scale (or normalization), we take the ratio of the average of the lowest eigenvalues, which are denoted by μ_0, to that of the second lowest ones, which are denoted by μ_1, for each $N_Y^{(1)}$ in order to fix this ambiguity. In Fig. 5.6, we plot the ratios against $1/N_Y^{(1)}$, and fit them to the quadratic function of $1/N_Y^{(1)}$, $s + t/N_Y^{(1)} + u/(N_Y^{(1)})^2$ with $s = -0.04(7)$, $t = 39(6)$, and $u = -5(1) \times 10^2$. The constant term, s, converges to 0 in the $N_Y^{(1)} \to \infty$ limit within error. Therefore, we can obtain Dirac zero modes in the $N_Y^{(1)} \to \infty$ limit.

Next, we consider the wave function corresponding to the lowest eigenvalue for one of the 16 cases with $N_Y^{(1)} = 64$. Here, we choose U'' and V'' in (5.3.17) such that

$$\varphi_{\mathrm{R1}} \mapsto U''^{\dagger} \varphi_{\mathrm{R1}} V'' \tag{5.3.23}$$

becomes the singular value decomposition (SVD). Namely, φ_{R1} is a diagonal matrix, where the diagonal elements are the singular values. In Fig. 5.7, we plot $|(\varphi_{\mathrm{R1}})_{pq}|^2$ and $|(\varphi_{\mathrm{L5}})_{pq}|^2$ $(p, q = 1, \ldots, N_Y^{(1)})$. The wave functions are localized at the $(1, 1)$ element, while other wave functions take almost 0. This is consistent with the picture that the right-handed zero mode is localized at a point where D-branes intersect.

2d-4d ansatz

We make 2d-4d ansatz in which $Y_a^{(1)}$ and $Y_a^{(2)}$ take the following configurations:

$$Y_1^{(1)} = L_1 \ , \ Y_2^{(1)} = L_2 \ , \ Y_3^{(1)} = Y_4^{(1)} = Y_5^{(1)} = Y_6^{(1)} = 0 \ , \tag{5.3.24}$$

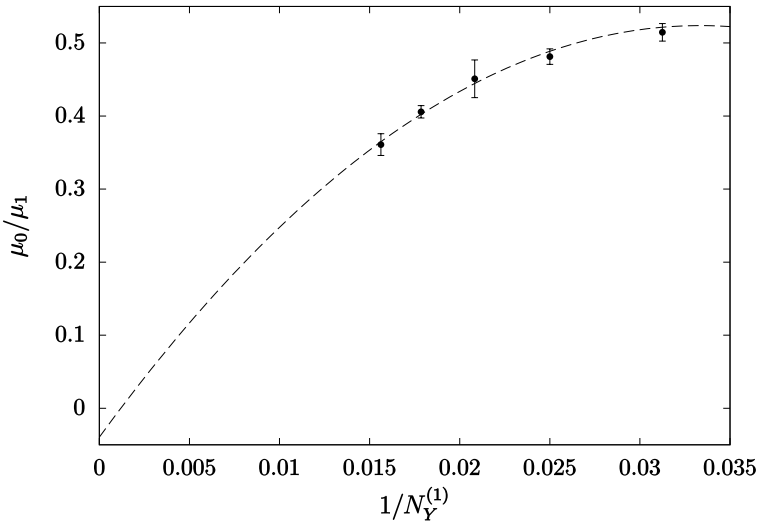

Figure 5.6: μ_0/μ_1 for $N_Y^{(1)} = 32$, 40, 48, 56, and 64 in the 3d-3d ansatz are plotted against $1/N_Y^{(1)}$. The dashed curve is a fit of ratios to $s + t/N_Y^{(1)} + u/(N_Y^{(1)})^2$ with $s = -0.04(7)$, $t = 34(6)$, and $u = -5(1) \times 10^2$.

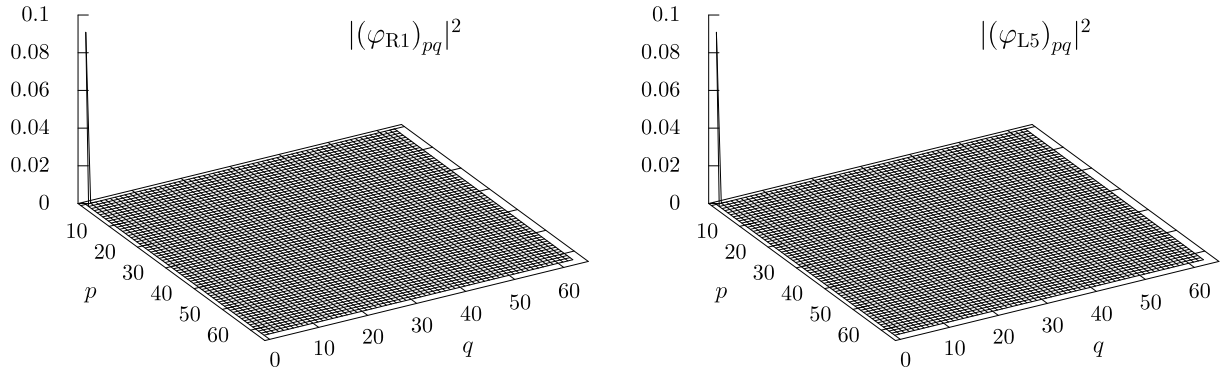

Figure 5.7: $|(\varphi_{\mathrm{R1}})_{pq}|^2$ and $|(\varphi_{\mathrm{L5}})_{pq}|^2$ $(p, q = 1, \ldots, N_Y^{(1)})$ for $N_Y^{(1)} = 64$ in the 3d-3d ansatz are plotted. The $(1, 1)$ element of them is non-zero and the other elements are almost zero. For other α, all the elements are almost zero.

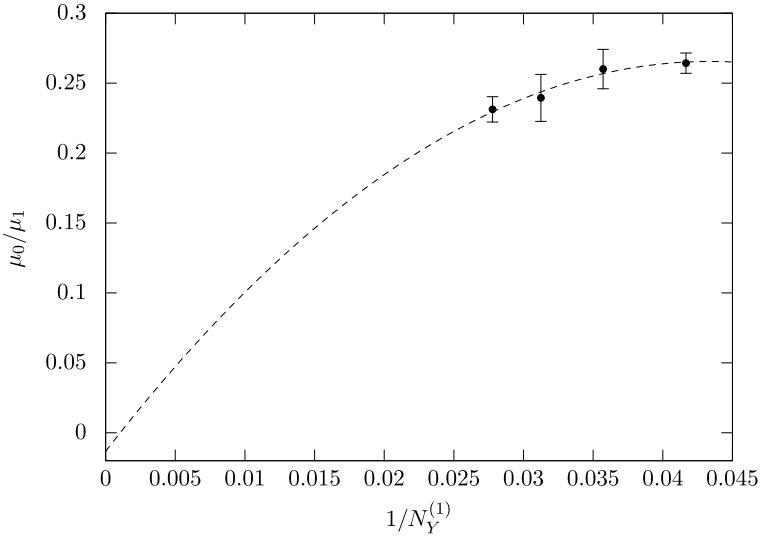

Figure 5.8: μ_0/μ_1 for $N_Y^{(1)} = 24$, 28, 32, and 36 with $N_Y^{(2)} = (N_Y^{(1)})^2/16$ in the 2d-4d ansatz are plotted against $1/N_Y^{(1)}$. The dashed curve is a fit of ratios to $s + t/N_Y^{(1)} + u/(N_Y^{(1)})^2$ with $s = -0.01(16)$, $t = 13(9)$, and $u = -1.3(1.3) \times 10^2$.

$$Y_1^{(2)} = Y_2^{(2)} = 0 \ , \ Y_3^{(2)} \neq 0 \ , \ Y_4^{(2)} \neq 0 \ , \ Y_5^{(2)} \neq 0 \ , \ Y_6^{(2)} \neq 0 \ . \tag{5.3.25}$$

For $Y_a^{(2)}$, we generate sixteen solutions obtained[22] with $N_Y^{(2)} = (N_Y^{(1)})^2/16$.

In the present case, the eigenvalues turn out to have two-fold degeneracy, which may be understood from the fact that the 2d brane is actually something like two coinciding fuzzy disks (see, (5.3.20) and the lines below.). We take the ratio between the average of the 32 lowest eigenvalues and that of the 32 second lowest ones. In Fig. 5.8, we plot the ratios against $1/N_Y^{(1)}$ for $N_Y^{(1)} = 24$, 28, 32, and 36. We see that ratio converge to 0 when $N_Y^{(1)}$ increases. Therefore, we can obtain Dirac zero modes in this ansatz.

We again consider the wave function corresponding to one of the 2 lowest eigenvalues[23] for one of the 16 cases with $N_Y^{(1)} = 64$. Here, we choose U'' and V'' in (5.3.17) such that (5.3.23) becomes the SVD. In Fig. 5.9, we plot $|(\varphi_{\mathrm{R}\alpha})_{pq}|^2$. For $\alpha = 1$, some elements are non-zero and other elements are almost zero. For other α, all the elements are non-zero. We also plot $|[(\varphi_{\mathrm{L}\alpha})_{pq}|^2$. For $\alpha = 5$, some elements are non-zero and other elements are almost zero. For other α, all the elements are non-zero. $|(\varphi_{\mathrm{R}1})_{pq}|^2$ and $|(\varphi_{\mathrm{L}5})_{pq}|^2$ are almost localized at the $(1, 1)$ element. These results are consistent with the picture that

[22]The chosen matrix size $N_Y^{(2)}$ for the 4d brane is motivated from the fact that the degrees of freedom on a lattice with a linear extent L grow as L^2 and L^4 for 2d and 4d cases, respectively. The factor of $1/16$ in $N_Y^{(2)} = (N_Y^{(1)})^2/16$ is introduced to avoid having too large $N_Y^{(2)}$ to perform explicit calculations.

[23]The situation with the other lowest eigenvalue is qualitatively the same. The same comment applies also to the case with the 2d-3d ansatz below.

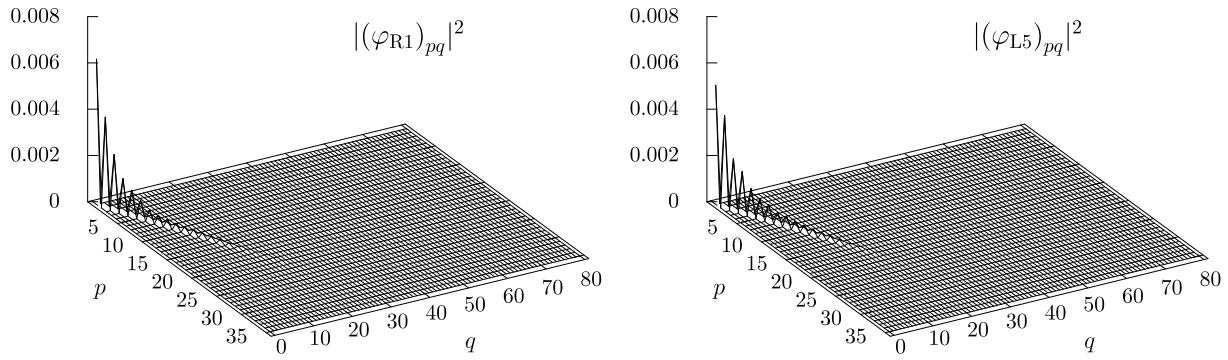

Figure 5.9: $|(\varphi_{\rm R1})_{pq}|^2$ and $|(\varphi_{\rm L5})_{pq}|^2$ ($p = 1, \ldots, N_Y^{(1)},\ q = 1, \ldots, N_Y^{(2)}$) for $N_Y^{(1)} = 36$ in the 2d-4d ansatz are plotted. For $|(\varphi_{\rm R1})|^2$ and $|(\varphi_{\rm L5})|^2$, (p, p) elements (p is less than 10) are non-zero and the other elements are almost zero. For other α, all the elements are almost zero.

the left-handed and right-handed zero modes appear from the intersecting D-branes.

3d-4d ansatz

We make 3d-4d ansatz in which $Y_a^{(1)}$ and $Y_a^{(2)}$ take the following configurations:

$$Y_1^{(1)} \neq 0\ ,\ Y_2^{(1)} \neq 0\ ,\ Y_3^{(1)} \neq 0\ ,\ Y_4^{(1)} = Y_5^{(1)} = Y_6^{(1)} = 0\ , \tag{5.3.26}$$

$$Y_1^{(2)} = Y_2^{(2)} = 0\ ,\ Y_3^{(2)} \neq 0\ ,\ Y_4^{(2)} \neq 0\ ,\ Y_5^{(2)} \neq 0\ ,\ Y_6^{(2)} \neq 0\ . \tag{5.3.27}$$

We again obtain a lowest eigenvalue and a second lowest one in each of the 16 cases. For each $N_Y^{(1)}$, we take the ratio between the average of the 16 lowest eigenvalues and that of the 16 second lowest ones. In Fig. 5.10, we plot the ratios against $1/N_Y^{(1)}$ for $N_Y^{(1)} = 32$, 48, and 64. They do not converge to 0 in the $N_Y^{(1)} \to \infty$ limit, so we cannot obtain Dirac zero modes in this ansatz. We again consider the wave function corresponding to the lowest eigenvalue for one of the 16 cases with $N_Y^{(1)} = 64$. Here, we choose U'' and V'' in (5.3.17) such that (5.3.23) becomes the SVD.

In Fig. 5.11, we plot $|(\varphi_{\rm R1})_{pq}|^2$ and $|(\varphi_{\rm L5})_{pq}|^2$. We find that the wave functions are not localized but have a long tail along the diagonal line. These results are consistent with the picture that the intersection does not occur at a point. The zero modes do not appear, and the wave functions corresponding to the lowest eigenvalue do not localize. Similar behaviors are observed for the 4d-4d ansatz.

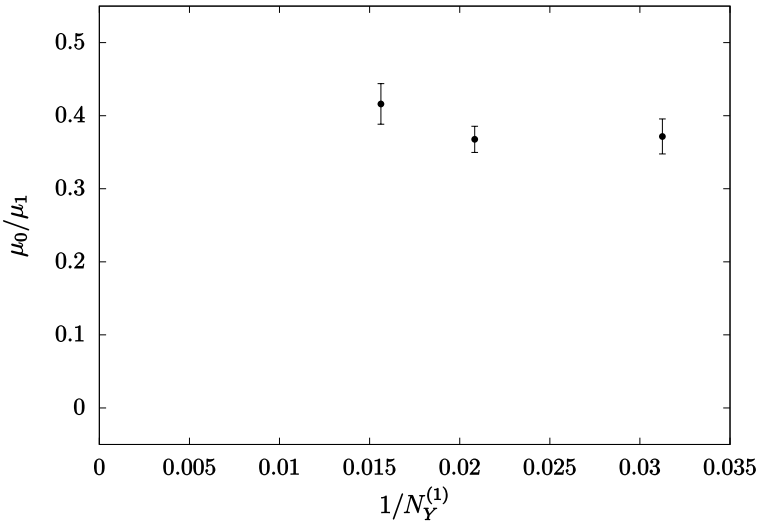

Figure 5.10: μ_0/μ_1 for $N_Y^{(1)} = 32$, 48, and 64 in the 3d-4d ansatz are plotted against $1/N_Y^{(1)}$.

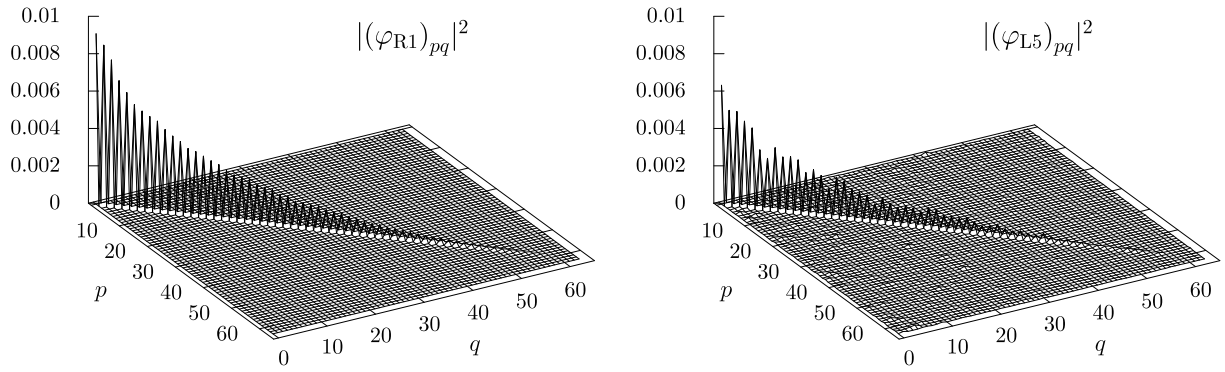

Figure 5.11: $|(\varphi_{\mathrm{R1}})_{pq}|^2$ and $|(\varphi_{\mathrm{L5}})_{pq}|^2$ $(p, q = 1, \ldots, N_Y^{(1)})$ for $N_Y^{(1)} = 64$ in the 3d-4d ansatz are plotted. A lot of diagonal elements of them are non-zero and the other elements are almost zero. For other α, all the elements are almost zero.

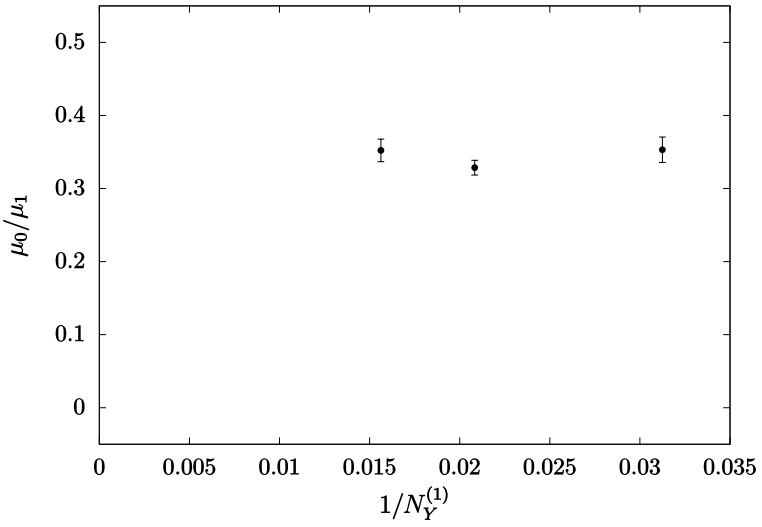

Figure 5.12: μ_0/μ_1 for $N_Y^{(1)} = 32$, 48, and 64 in the 2d-3d ansatz are plotted against $1/N_Y^{(1)}$.

2d-3d ansatz

We make 2d-3d ansatz in which $Y_a^{(1)}$ and $Y_a^{(2)}$ take the following configurations:

$$Y_1^{(1)} \neq 0 \ , \ Y_2^{(1)} \neq 0 \ , \ Y_3^{(1)} = Y_4^{(1)} = Y_5^{(1)} = Y_6^{(1)} = 0 \ , \tag{5.3.28}$$

$$Y_1^{(2)} = Y_2^{(2)} = Y_3^{(2)} = 0 \ , \ Y_4^{(2)} \neq 0 \ , \ Y_5^{(2)} \neq 0 \ , \ Y_6^{(2)} \neq 0 \ . \tag{5.3.29}$$

We obtain 2 lowest eigenvalues and 2 second lowest ones in each of the 16 cases as in the 2d-4d ansatz. We take the ratio between the average of the 32 lowest eigenvalues and that of the 32 second lowest ones. In Fig. 5.12, we plot the ratios against $1/N_Y^{(1)}$ for $N_Y^{(1)} = 32$, 48, and 64. we see that they do not converge to 0 in the $N_Y^{(1)} \to \infty$ limit, so that we cannot obtain Dirac zero modes in this ansatz.

We consider the wave function corresponding to one of the 2 lowest eigenvalues for one of the 16 cases with $N_Y^{(1)} = 64$. Here, we choose U'' and V'' in (5.3.17) such that (5.3.23) becomes the SVD. In Fig. 5.13, we plot $|(\varphi_{\mathrm{R}\alpha})_{pq}|^2$. For $\alpha = 1, 2$, the $(1, 1)$ element is non-zero and the other elements are almost zero. For $\alpha = 5, 6$, the $(1, 2)$ element is non-zero and the other elements are almost zero. For other α, all the elements are almost zero. We also plot $|(\varphi_{\mathrm{L}\alpha})_{pq}|^2$. For $\alpha = 1, 2$, the $(1, 2)$ element is non-zero and the other elements are almost zero. For $\alpha = 5, 6$, the $(1, 1)$ element is non-zero and the other elements are almost zero. For other α, all the elements are almost zero. Therefore, in this ansatz, we cannot see the picture that D-branes intersect.

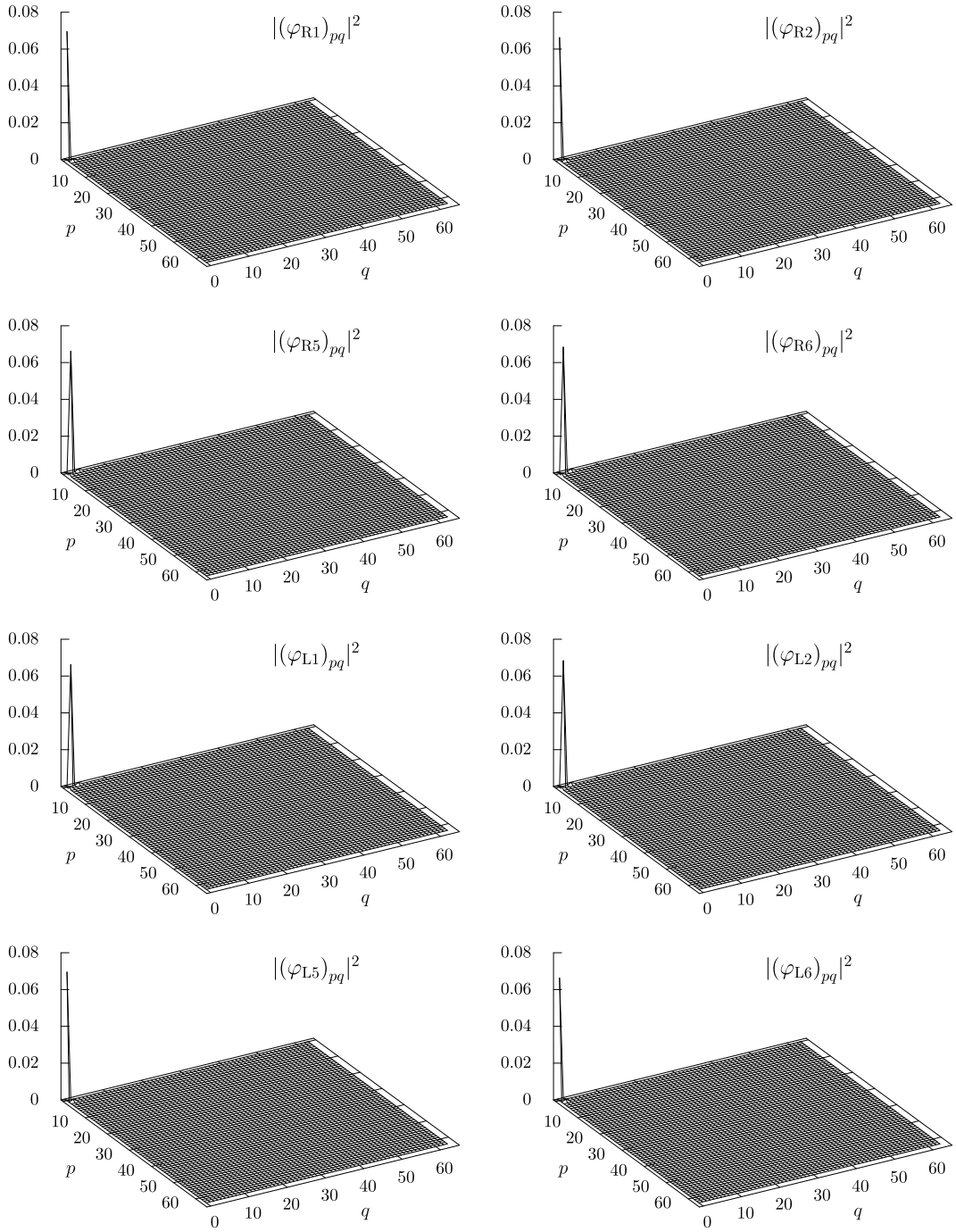

Figure 5.13: $|(\varphi_{\mathrm{R}\alpha})_{pq}|^2$ and $|(\varphi_{\mathrm{L}\alpha})_{pq}|^2$ ($\alpha = 1, 2, 5, 6,\ p, q = 1, \ldots, N_Y^{(1)}$) for $N_Y^{(1)} = 64$ in the 2d-3d ansatz are plotted. For $|(\varphi_{\mathrm{R}\alpha})|^2$ with $\alpha = 1, 2$, the $(1, 1)$ element is non-zero and the other elements are almost zero. For $|(\varphi_{\mathrm{R}\alpha})|^2$ with $\alpha = 5, 6$, the $(1, 2)$ element is non-zero and the other elements are almost zero. For other α, all the elements are almost zero. For $|(\varphi_{\mathrm{L}\alpha})|^2$ with $\alpha = 1, 2$, the $(1, 2)$ element is non-zero and the other elements are almost zero. For $|(\varphi_{\mathrm{L}\alpha})|^2$ with $\alpha = 5, 6$, the $(1, 1)$ element is non-zero and the other elements are almost zero. For other α, all the elements are almost zero.

Chapter 6

Conclusion and outlook

In this thesis, we have studied the three topics concerning space-times emerging from matrix models. We have seen the mechanism of emergence of space-times from the matrix models and properties of those emergent space-times in order to establish matrix models completely as non-perturbative formulations of superstring theory. In the following, we summarize the three topics studied in this thesis and show their outlook. Then, we conclude this thesis comprehensively and show a perspective of our studies.

Renormalization in a scalar filed theory on the fuzzy sphere

In chapter 3, we studied renormalization in a scalar filed theory on the fuzzy sphere by Monte Carlo simulation. We identified the Berezin symbol constructed from the Bloch coherent state as the field. It was shown that the 2-point and 4-point correlation functions are made independent of the UV cutoff, or the matrix size up to the wave function renormalization by tuning the mass parameter or the coupling constant. This strongly suggests that the theory is renormalizable non-perturbatively in the ordinary sense and that the theory is universal up to a parameter fine-tuning.

We also examined the 2-point and 4-point correlation functions on the phase boundary beyond which the Z_2 symmetry is spontaneously broken. We found that the 2-point and 4-point correlation functions at different points on the boundary agree up to the wave function renormalization. This implies that the critical theory is universal, which is consistent with the above universality in the disordered phase, because the phase boundary is obtained by a parameter fine-tuning. Furthermore, it was observed that the 2-point correlation functions behave as those in a CFT at short distances and deviate universally from those at long distances. The latter is considered to be due to the UV/IR anomaly.

The CFT observed at short distances seems to be different from the critical Ising model (the scaling dimension of the spin operator $\Delta = 0.125$), because the value of u in (3.3.8) disagrees with 2Δ. This suggests that the universality classes of the scalar field theory on the fuzzy sphere totally differs from those of an ordinary field theory[24].

[24]It should be noted that the scaling dimension we obtained, $\Delta \simeq 0.075 = 3/40$, coincides with that of

Indeed, it was reported in [15–19] that there exists a novel phase in the theory on the fuzzy sphere which is called the non-uniformly ordered phase, or the stripe phase [82, 83]. We hope to elucidate the universality classes by studying renormalization in the whole phase diagram.

The large-N volume independence on group manifolds

In chapter 4, we showed that a theory on a group manifold G is equivalent to the corresponding theory on G/H with H a subgroup of G in the large-N limit. The degrees of freedom on G are retrieved by the degrees of freedom of matrices in a consistent way with the dimensional reduction to G/H. An advantage of reduction to G/H with a finite volume compared to reduction to a matrix model is that one does not need to introduce k multiplicity and take the $k \to \infty$ limit to extract only planar contribution as in the latter case [35, 36], since the UV cutoff V'/v' plays the role of extracting planar contribution. While we showed the equivalence perturbatively, we can show it non-perturbatively based on the continuum Schwinger-Dyson equations as in [41], by assuming the stability of the background, which is a counterpart of the center symmetry.

An interesting application of the large-N equivalence in dimensional reduction on group manifolds is that the SU(2|4) symmetric gauge theory on $R \times S^2$ is equivalent to $\mathcal{N} = 4$ super Yang-Mills theory on $R \times S^3$ in the large-N limit. (For another large-N equivalence between these two theories, see [37, 84].) Both of the theories have gravity duals, so that the above equivalence would be seen on the gravity side. It is interesting to search for gravity duals of other large-N equivalences in dimensional reduction [85–89].

Classical solutions in the Lorentzian type IIB matrix model

In chapter 5, we solved classical equations of motion of the type IIB matrix model numerically because the classical approximation is expected to be valid since the action becomes large due to the cosmic expansion. We obtained classical solutions by assuming a quasi-direct-product structure (5.1.3). This structure is compatible with SO(3,1) symmetry, and favors a block-diagonal structure which can yield D-branes intersecting in extra dimensions. We examined a space-time structure in (3+1) dimensions and Dirac zero modes in extra dimensions.

First, we focused on the (3+1)-dimensional space-time structure, which is represented by X_μ in (5.1.3). When X_0 is diagonalized, X_i become band-diagonal, which ensures the locality of the time. We defined the time t from eigenvalues of X_0 to derive the

the spin operator in the tricritical Ising model which is the $(4, 5)$ unitary minimal model.

time evolution of the space. Then, we found that the 3-dimensional space obtained in our solutions is smooth and SO(3) symmetry is respected at almost all of late time[25]. Breaking of the SO(3) symmetry at the last regime is considered to be a finite matrix size effect, so it is expected to be disappeared in the $N_X \to \infty$ limit. In [61], it was shown that the space-time structure is singular one which is represented by the Pauli matrices. This is attributed to approximation used in the simulation. From the results in [62] obtained by using the complex Langevin method, it is conjectured that the smooth space-time is obtained in the $N \to \infty$ limit. Our results strongly support this conjecture.

Next, we examined Dirac zero modes in extra dimensions numerically by focusing on the structure in the extra dimensions. For simplicity, we concentrated on two of the blocks of Y_a in (5.1.3); $Y_a^{(1)}$ and $Y_a^{(2)}$. We further made ansatz for $Y_a^{(1)}$ and $Y_a^{(2)}$ in numerical solutions. In the 3d-3d and 2d-4d ansatz, we found solutions that give Dirac zero modes in the $N_Y^{(1)} \to \infty$ limit. We fitted the ratios of the average of the lowest eigenvalues to that of the second lowest ones to the quadratic function in $1/N_Y^{(1)}$, and found that the ratio converges to 0 within error in the $N_Y^{(1)} \to \infty$ limit. We also found that the wave functions corresponding to the lowest eigenvalues are localized at a point, which is consistent with the picture of intersecting D-branes. In other ansatz, we did not obtain Dirac zero modes and localized wave functions. What is important is that Dirac zero modes were obtained as solutions of classical equations of motion of the type IIB matrix model. In previous studies [69, 71, 73, 79], matrix configurations in extra dimensions are given by hand.

It is important to obtain solutions with larger N_X and see whether 3-dimensional space is completely uniform and SO(3) symmetric. Furthermore, from a viewpoint of cosmology, we would like to see whether the 3-dimensional space obtained in such solutions expands obeying a power low. We would also like to identify Higgs modes in the spectra of fluctuation of Y_a, and determine the Yukawa coupling from the overlap of wave functions between Dirac zero modes and Higgs modes. By using the information of the Yukawa coupling and the renormalization group, we see whether chiral fermions are obtained at the low energy in (3+1) dimensions.

Conclusion and perspective

Throughout this thesis, we studied a mechanism of emergence of space-times from matrix models and properties of those emergent space-times. We showed that it is possible that field theories on non-commutative spaces describe the real world because renormalization is performed as in the ordinary field theories. We drew a lesson on the emergence of the

[25] In [90], the emergence of 3-dimensional space obtained in our study was checked by using the same model.

curved space-times from the large-N volume independence on group manifolds. We took a first step to verify a conjecture that the type IIB matrix model describes the real world by showing that one can obtain classical solutions which give rise to the (3+1)-dimensional expanding space-time and Dirac zero modes. It is expected that insights on field theories on non-commutative spaces and the curve space-times in matrix models can be used to verify the conjecture.

Superstring theory has not been established completely, and there remain a lot of aspects to be understood. In this thesis, we tried to understand some aspects through matrix models. We would like to not only develop the above studies but also study other aspects by using insights gained in this thesis. In particular, we would like to continue to study the type IIB matrix model. We hope to establish that superstring theory is indeed the unified theory including quantum gravity by obtaining both the Big-Bang universe and the Standard Model from the matrix model.

Acknowledgements

First of all, I would like to thank my supervisor, Prof. Asato Tsuchiya, for his continuous encouragements, kind advice, and his collaborations with me, and for reading the manuscript carefully. I would also like to thank my collaborators, Prof. Jun Nishimura, Mr. Kazushi Yamashiro, Mr. Akira Matsumoto, and Mr. Atis Yosprakob, for discussions and their kind help through their collaborations, and Prof. Takeshi Morita for helpful comments and encouragement. I wish to thank people giving me comments and arguing with me at various occasions. I am also obliged to other colleagues at the particle theory group in Shizuoka University and the secretary. I would like to thank people in the Katayama dormitory, my friends, and my family. Numerical computation was carried out on PC clusters at KEK and XC40 at YITP in Kyoto University. I have been supported in part by Grant-in-Aid for JSPS Fellows (No. 19J10002).

Appendix A

Bloch coherent state and Berezin symbol

In this appendix, we summarize the basic properties of the Bloch coherent state [76] and the Berezin symbol [75].

The highest weight state $|jj\rangle$[26] is considered to correspond to the north pole (see, Fig. A.1). Thus, the state $|\Omega\rangle$ that corresponds to a point $\Omega = (\theta, \varphi)$ is obtained by acting a rotation operator on $|jj\rangle$:

$$|\Omega\rangle = e^{i\theta(\sin\varphi L_1 - \cos\varphi L_2)} |jj\rangle \ . \tag{A.0.1}$$

(A.0.1) implies that

$$n_i L_i |\Omega\rangle = j |\Omega\rangle \ , \tag{A.0.2}$$

where $\vec{n} = (\sin\theta\cos\varphi, \sin\theta\sin\varphi, \cos\theta)$. It is easy to show from (A.0.2) that $|\Omega\rangle$ minimizes $\sum_i (\Delta L_i)^2$ with $(\Delta L_i)^2$ being the standard deviation of L_i.

It is convenient to introduce the stereographic projection, $z = R\tan\frac{\theta}{2}e^{i\varphi}$. Then, (A.0.1) is rewritten as

$$|\Omega\rangle = e^{zL_-/R} e^{-L_3\log(1+|z/R|^2)} e^{-\bar{z}L_+/R} |jj\rangle \ , \tag{A.0.3}$$

which gives an explicit form of $|\Omega\rangle$ as

$$|\Omega\rangle = \sum_{m=-j}^{j} \begin{pmatrix} 2j \\ j+r \end{pmatrix}^{1/2} \left(\cos\frac{\theta}{2}\right)^{j+r} \left(\sin\frac{\theta}{2}\right)^{j-r} e^{i(j-r)\varphi} |jr\rangle \ . \tag{A.0.4}$$

By using (A.0.4), one can easily show the following relations:

$$\langle\Omega_1|\Omega_2\rangle = \left[\cos\frac{\theta_1}{2}\cos\frac{\theta_2}{2} + e^{i(\varphi_2-\varphi_1)}\sin\frac{\theta_1}{2}\sin\frac{\theta_2}{2}\right]^{2j} \ , \tag{A.0.5}$$

$$\left|\langle\Omega_1|\Omega_2\rangle\right| = \left(\cos\frac{\chi}{2}\right)^{2j} \ \text{with} \ \chi = \arccos(\vec{n}_1\cdot\vec{n}_2) \ , \tag{A.0.6}$$

$$(2j+1)\int \frac{d\Omega}{4\pi} |\Omega\rangle\langle\Omega| = 1 \ . \tag{A.0.7}$$

[26] $|jr\rangle$ are standard basis in (2.1.41).

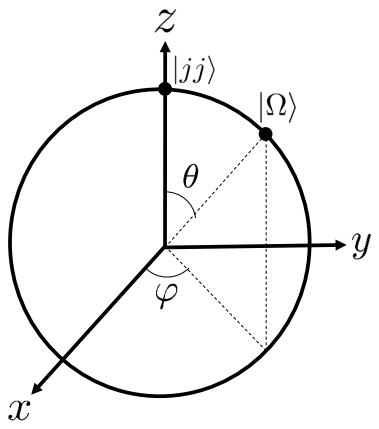

Figure A.1: Bloch coherent state.

(A.0.6) implies that the width of the Bloch coherent state is $R/\sqrt{j}$ for large j.

Denoting the Bloch coherent state $|\Omega\rangle$ by $|z\rangle$, we rewrite (A.0.4) and (A.0.7) as

$$|z\rangle = \left(\frac{z/R}{1+|z/R|^2}\right)^j \sum_{r=-j}^{j} \binom{2j}{j+r}^{1/2} \left(\frac{R}{z}\right)^r |jr\rangle \ , \tag{A.0.8}$$

$$\frac{2j+1}{4\pi} 4R^2 \int \frac{d^2z}{(1+|z/R|^2)^2} \ |z\rangle\langle z| = 1 \ , \tag{A.0.9}$$

respectively.

The Berezin symbol for a matrix Φ with the matrix size $2j+1$ is defined by

$$f_\Phi(\Omega) = f_\Phi(z,\bar{z}) = \big\langle \Omega \big| \Phi \big| \Omega \big\rangle = \big\langle z \big| \Phi \big| z \big\rangle \ . \tag{A.0.10}$$

By using (A.0.4), it is easy to show that

$$f_{[L_i,\Phi]}(\Omega) = \mathcal{L}_i f_\Phi(\Omega) \ . \tag{A.0.11}$$

(A.0.7) implies that

$$\frac{1}{N}\mathrm{Tr}(\Phi) = \int \frac{d\Omega}{4\pi} f_\Phi(\Omega) \ . \tag{A.0.12}$$

The definition of the star product for Φ and Φ' is

$$f_\Phi \star f_{\Phi'}(\Omega) = f_\Phi \star f_{\Phi'}(z,\bar{z}) = \big\langle \Omega \big| \Phi\Phi' \big| \Omega \big\rangle = \big\langle z \big| \Phi\Phi' \big| z \big\rangle \ . \tag{A.0.13}$$

Here let us consider a quantity

$$\frac{\langle w|\Phi|z\rangle}{\langle w|z\rangle} \ , \tag{A.0.14}$$

which is holomorphic in z and anti-holomorphic in w. Then, one can deform this quantity as follows:

$$\begin{aligned}\frac{\langle w|\Phi|z\rangle}{\langle w|z\rangle} &= e^{-w\frac{\partial}{\partial z}}\frac{\langle w|\Phi|z+w\rangle}{\langle w|z+w\rangle} \\ &= e^{-w\frac{\partial}{\partial z}}e^{z\frac{\partial}{\partial w}}\frac{\langle w|\Phi|w\rangle}{\langle w|w\rangle} \\ &= e^{-w\frac{\partial}{\partial z}}e^{z\frac{\partial}{\partial w}}\langle w|\Phi|w\rangle \\ &= e^{-w\frac{\partial}{\partial z}}e^{z\frac{\partial}{\partial w}}f_\Phi(w,\bar{w})\ . \end{aligned} \tag{A.0.15}$$

Similarly, one obtains

$$\frac{\langle z|\Phi|w\rangle}{\langle z|w\rangle} = e^{-\bar{w}\frac{\partial}{\partial \bar{z}}}e^{\bar{z}\frac{\partial}{\partial \bar{w}}}f_\Phi(w,\bar{w})\ . \tag{A.0.16}$$

By using (A.0.9), (A.0.15) and (A.0.16), one can express the star product as

$$\begin{aligned}& f_\Phi \star f_{\Phi'}(w,\bar{w}) \\ &= \langle w|\Phi\Phi'|w\rangle \\ &= \frac{2j+1}{4\pi}4R^2\int\frac{d^2z}{(1+|z/R|^2)^2}\frac{\langle w|\Phi|z\rangle}{\langle w|z\rangle}\frac{\langle z|\Phi'|w\rangle}{\langle z|w\rangle}|\langle w|z\rangle|^2 \\ &= \frac{2j+1}{4\pi}4R^2\int\frac{d^2z}{(1+|z/R|^2)^2}\left(e^{-w\frac{\partial}{\partial z}}e^{z\frac{\partial}{\partial w}}f_\Phi(w,\bar{w})\right)\left(e^{-\bar{w}\frac{\partial}{\partial \bar{z}}}e^{\bar{z}\frac{\partial}{\partial \bar{w}}}f_{\Phi'}(w,\bar{w})\right)|\langle w|z\rangle|^2\ , \end{aligned} \tag{A.0.17}$$

which indicates that the star product is non-commutative and non-local. Furthermore, one can easily show that in the $j\to\infty$ limit

$$\frac{2j+1}{4\pi}\frac{4R^2}{(1+|z/R|^2)^2}|\langle w|z\rangle|^2 \to \delta^(2)(z-w)\ . \tag{A.0.18}$$

This implies that the star product coincides with the ordinary product in the $j\to\infty$ limit. Namely,

$$f_\Phi \star f_{\Phi'}(w,\bar{w}) \to f_\Phi(w,\bar{w})f_{\Phi'}(w,\bar{w}) \tag{A.0.19}$$

or

$$f_\Phi \star f_{\Phi'}(\Omega) \to f_\Phi(\Omega)f_{\Phi'}(\Omega)\ . \tag{A.0.20}$$

We see from (A.0.11), (A.0.12) and (A.0.20) that the theory (3.1.1) reduces to the one (3.1.3) in the $N\to\infty$ limit at the classical level if one identifies $f_\Phi(\Omega)$ with $\phi(\Omega)$. However, the authors of [13,14] showed that the 1-loop effective action in (3.1.1) differs from that in (3.1.3) by finite and non-local terms since the UV cutoff N is kept finite in calculating loop corrections. This phenomenon is sometimes called the UV/IR anomaly, which is explained in Appendix B.

Appendix B

UV/IR anomaly

There is no UV/IR mixing in a field theory on the fuzzy sphere. However, there exist finite differences between a theory on the fuzzy sphere and the corresponding theory on an ordinary sphere at the quantum level even in a continuum and commutative limit. These differences are the UV/IR anomaly [13]. In this appendix, we briefly review it.

From (2.1.60), Φ is expanded in terms of the fuzzy spherical harmonics $\hat{Y}_{lm}^{[j]}$:

$$\Phi = \sum_{l=0}^{2j} \sum_{m=-l}^{l} \phi_{lm} \hat{Y}_{lm}^{[j]} \ , \quad \phi_{lm}^* = (-1)^m \phi_{l\,-m} \ . \tag{B.0.1}$$

n-point correlation functions are given by

$$\langle \phi_{l_1 m_1} \cdots \phi_{l_n m_n} \rangle = \frac{\int \mathcal{D}\Phi e^{-S_{\text{fuzzy}}} \phi_{l_1 m_1} \cdots \phi_{l_n m_n}}{\int \mathcal{D}\Phi e^{-S_{\text{fuzzy}}}} \ , \tag{B.0.2}$$

and in particular 2-point correlation functions take the form

$$\langle \phi_{l\,m} \phi_{l'\,m'}^* \rangle = (-1)^m \langle \phi_{l\,m} \phi_{l'\,-m'} \rangle = \frac{1}{l(l+1)+\mu^2} \delta_{l,l'} \delta_{m,m'} \ . \tag{B.0.3}$$

The vertex in the ϕ^4 theory is given by

$$\phi_{l_1\,m_1} \cdots \phi_{l_4\,m_4} V(l_1, m_1; \ldots; l_4, m_4) \ , \tag{B.0.4}$$

where

$$\begin{aligned} V(l_1, m_1; \ldots; l_4, m_4) = \frac{\lambda}{4}(2j+1)(-1)^{l_1+l_2+l_3+l_4} \prod_{i=1}^{4} \sqrt{2l_i+1} \sum_{l=0}^{2j} \sum_{m=-l}^{l} (-1)^m (2l+1) \\ \times \begin{pmatrix} l_1 & l_2 & l \\ m_1 & m_2 & m \end{pmatrix} \begin{pmatrix} l_3 & l_4 & l \\ m_3 & m_4 & -m \end{pmatrix} \begin{Bmatrix} l_1 & l_2 & l \\ j & j & j \end{Bmatrix} \begin{Bmatrix} l_3 & l_4 & l \\ j & j & j \end{Bmatrix} \end{aligned} \tag{B.0.5}$$

is symmetric under cyclic permutations of (l_i, m_i). Here, $\begin{pmatrix} * & * & * \\ * & * & * \end{pmatrix}$ denotes $3j$ symbol.

Using (B.0.3), we calculate counter part of Fig. 2.1 and Fig. 2.2. The planar contribution $\left(\Gamma^{(2)}_{\text{planar}}\right)^{l,l'}_{m,m'}$ is

$$\left(\Gamma^{(2)}_{\text{planar}}\right)^{l,l'}_{m,m'} = 2\lambda\delta_{l,l'}\delta_{m,-m'}(-1)^m I^{\text{P}} \ , \tag{B.0.6}$$

$$I^{\text{P}} \equiv \sum_{K=0}^{2j} \frac{2K+1}{K(K+1)+\mu^2} \sim \log j + O(1) \ . \tag{B.0.7}$$

I^{P} exactly agrees with the corresponding term on the classical sphere in the $j \to \infty$ limit. The non-planar contribution $\left(\Gamma^{(2)}_{\text{non-planar}}\right)^{l,l'}_{m,m'}$ is

$$\left(\Gamma^{(2)}_{\text{non-planar}}\right)^{l,l'}_{m,m'} = \lambda\delta_{l,l'}\delta_{m,-m'}(-1)^m I^{\text{NP}} \ , \tag{B.0.8}$$

$$I^{\text{NP}} \equiv \sum_{K=0}^{2j} (-1)^{l+K+2j} \frac{(2K+1)(2j+1)}{K(K+1)+\mu^2} \begin{Bmatrix} j & j & l \\ j & j & K \end{Bmatrix} \ . \tag{B.0.9}$$

We rewrite I^{NP} as follows:

$$I^{\text{NP}} = \sum_{K=0}^{2j} \frac{2K+1}{K(K+1)+\mu^2} f_K \ , \quad f_K \equiv (-1)^{l+K+2j}(2j+1) \begin{Bmatrix} j & j & l \\ j & j & K \end{Bmatrix} \ . \tag{B.0.10}$$

For $l = 0$, the planar contribution in the 2-point functions agree with the non-planar ones since $f_K = 1$ $(0 \le K \le 2j)$. For $l = 1$,

$$f_K = 1 - \frac{K(K+1)}{2j(j+1)} \ , \tag{B.0.11}$$

and then we obtain

$$I^{\text{NP}} = I^{\text{P}} - \frac{1}{2j(j+1)} \sum_{K=0}^{2j} \frac{K(K+1)(2K+1)}{K(K+1)+\mu^2} \ . \tag{B.0.12}$$

Summation with respect to K in the second term of RHS in (B.0.12) diverges j^2, but thanks to $1/2j(j+1)$, this term becomes finite. This implies that these is no IR singularity in the non-planar contribution unlike in the case of the non-commutative plane.

For general l, we evaluate the non-planar contribution by using the approximation for the $6j$ symbol:

$$\begin{Bmatrix} j & j & l \\ j & j & K \end{Bmatrix} \approx \frac{(-1)^{l+2j+K}}{2j} P_l\left(1 - \frac{K^2}{2j^2}\right) \tag{B.0.13}$$

with $l \ll j$ and $0 \le K \le 2j$. Here, $P_l(x)$ is the Legendre polynomial[27]. Then, we obtain

$$I^{\text{NP}} - I^{\text{P}} = \sum_{K=0}^{2j} \frac{2K+1}{K(K+1)+\mu^2} \left[(-1)^{l+K+2j}(2j+1) \begin{Bmatrix} j & j & l \\ j & j & K \end{Bmatrix} - 1 \right]$$

[27] $P_l(x) = \dfrac{1}{2^l l!} \dfrac{d^l}{dx^l}(x^2-1)^l$.

$$\approx \sum_{K=0}^{2j} \frac{2K+1}{K(K+1)+\mu^2} \left[P_l \left(1 - \frac{K^2}{2j^2} \right) - 1 \right] \ . \tag{B.0.14}$$

Because $P_l(1) = 1$ for all l, only $K \gg 1$ contributes, and the summation is approximated by the integral:

$$I^{\mathrm{NP}} - I^{\mathrm{P}} \approx \int_0^2 du \frac{2u + \frac{1}{j}}{u^2 + \frac{u}{j} + \left(\frac{\mu}{j}\right)^2} \left[P_l \left(1 - \frac{u^2}{2} \right) - 1 \right] = \int_{-1}^{1} dt \frac{P_l(t) - 1}{1 - t} + O\left(\frac{1}{j}\right) \tag{B.0.15}$$

with change of variables $1 - u^2/2 = t$ and $\mu \ll j$. One can show

$$\int_{-1}^{1} dt \frac{P_l(t) - 1}{1 - t} = -2 \sum_{k=1}^{l} \frac{1}{k} = -2h(l) \ , \tag{B.0.16}$$

where $h(l)$ is the harmonic number and $h(0) = 0$. $h(l)$ is finite for small l, while $h(l) \approx \log l$ for large l. Therefore, the 1-loop effective action is obtained as follows:

$$S_{\text{1-loop}} = S_{\text{fuzzy}} + \frac{1}{2j+1} \mathrm{Tr} \left(\frac{1}{2} \Phi \left[\delta\mu^2 - 2\lambda h\left(\tilde{\Delta}\right) \right] \Phi \right) + O\left(\frac{1}{j}\right), \tag{B.0.17}$$

where

$$\delta\mu^2 = 3\lambda \sum_{K=0}^{2j} \frac{2K+1}{K(K+1)+\mu^2} \tag{B.0.18}$$

is the renormalized mass squared and $\tilde{\Delta}$ is the function of the Laplacian whose eigenvalues are l on $\hat{Y}_{lm}^{[j]}$. Thus, it turns out that a non-commutative effect is analytic in $1/j$. This is a non-trivial finite quantum effect and has an l-dependence.

A field theory in the commutative limit is defined in the $j \to \infty$ limit with fixed R, λ, and μ^2. In this limit, the 1-loop effective action on the fuzzy sphere differs from that on the commutative sphere by amount

$$\Gamma^{(2)}_{\text{anomaly}} = -\frac{\lambda}{2j+1} \mathrm{Tr} \left[\Phi h(\tilde{\Delta}) \Phi \right] \ . \tag{B.0.19}$$

This is non-local due to $h(l) \approx \log l$ for large l. This effect does not appear in an ordinary field theory, and is called the UV/IR anomaly.

Appendix C

$3nj$ symbol

In this appendix, we present concrete expressions for the $3j$ and the $6j$ symbols [91].

The Clebsch-Gordan coefficient is represented as

$$C^{l'\,-m'}_{l_1\,m_1\;l_2\,-m_2} = (-1)^{l_1-l_2-m'}\sqrt{2l'+1}\begin{pmatrix} l_1 & l_2 & l' \\ m_1 & -m_2 & m' \end{pmatrix} \tag{C.0.1}$$

in terms of the $3j$ symbol. From (C.0.1), one can show the following relations:

$$\begin{pmatrix} l_3 & l_3 & l'' \\ m_3 & -m_3 & -m'' \end{pmatrix} = \frac{(-1)^{l''+m''+l_3-m_3}}{\sqrt{2l_3+1}} C^{l_3\,-m_3}_{l_3\,-m_3\;l''\,m''} \ , \tag{C.0.2}$$

$$\begin{pmatrix} l & l' & 0 \\ m & m' & 0 \end{pmatrix} = \frac{(-1)^{l-m}}{\sqrt{2l+1}}\delta_{l,l'}\delta_{m,-m'} \ , \tag{C.0.3}$$

$$\begin{pmatrix} l & l_4 & l'' \\ -m & -m_4 & m'' \end{pmatrix} = \frac{(-1)^{l''+m''+l-m}}{\sqrt{2l_4+1}} C^{l_4\,m_4}_{l''\,m''\;l\,-m} \ , \tag{C.0.4}$$

$$\begin{pmatrix} l' & l_4 & l'' \\ m' & m_4 & -m'' \end{pmatrix} = \frac{(-1)^{-l_4+m''-m'}}{\sqrt{2l_4+1}} C^{l_4\,m_4}_{l''\,m''\;l'\,-m'} \ . \tag{C.0.5}$$

One can also show the following relations:

$$\sum_{m_3} C^{l_3\,-m_3}_{l_3\,-m_3\;l''\,m''} = (2l_3+1)\delta_{l'',0} \ , \tag{C.0.6}$$

$$\sum_{m_4,m''} C^{l_4\,m_4}_{l''\,m''\;l\,-m} C^{l_4\,m_4}_{l''\,m''\;l'\,-m'} = \frac{2l_4+1}{2l+1}\delta_{l,l'}\delta_{m,-m'} \ , \tag{C.0.7}$$

$$\begin{Bmatrix} l & l' & 0 \\ j & j & j \end{Bmatrix} = \frac{(-1)^{l+2j}}{\sqrt{(2l'+1)(2j+1)}}\delta_{l,l'} \ , \tag{C.0.8}$$

$$\begin{Bmatrix} l_3 & l_3 & 0 \\ j & j & j \end{Bmatrix} = \frac{(-1)^{l_3+2j}}{\sqrt{(2l_3+1)(2j+1)}} \ , \tag{C.0.9}$$

$$\sum_{l''}(-1)^{2j+l''}(2l''+1)\begin{Bmatrix} l & l_4 & l'' \\ j & j & j \end{Bmatrix}\begin{Bmatrix} l & l_4 & l'' \\ j & j & j \end{Bmatrix} = \begin{Bmatrix} j & j & l \\ j & j & l_4 \end{Bmatrix} \ . \tag{C.0.10}$$

Appendix D

Method of a numerical simulation

In this appendix, we describe a numerical method and an error estimation used in chapter 3.

D.1 Hybrid Monte Carlo algorithm

To study renormalization on the fuzzy sphere, we use the Hybrid Monte Carlo (HMC) algorithm [92], which enables us to perform Monte Carlo simulations efficiently. Here, we briefly review the HMC algorithm.

We consider a system described by a set of dynamical variables denoted ϕ. Suppose that the probability distribution is given by $e^{-S(\phi)}$. Then, the detailed balance is satisfied if a stochastic process is generated by the following procedure.

1. Take ϕ as an initial state, and generate the conjugate momentum π with the following probability:
$$P(\pi) \propto e^{-\pi^2/2} \ . \tag{D.1.1}$$

2. Update ϕ and π by using the molecular dynamics as follows:
$$\dot{\phi}(t) = \frac{\partial H\left[\phi(t), \pi(t)\right]}{\partial \pi(t)} = \pi(t) \ , \tag{D.1.2}$$
$$\dot{\pi}(t) = -\frac{\partial H\left[\phi(t), \pi(t)\right]}{\partial \phi(t)} = -\frac{\partial S(\phi(t))}{\partial \phi(t)} \ , \tag{D.1.3}$$
$$H\left[\phi(t), \pi(t)\right] = \frac{\pi^2}{2} + S(\phi(t)) \ . \tag{D.1.4}$$

   This expression is valid for the continuum time t in the range $0 \leq t \leq \tau$. However, time must be discretized to perform numerical simulations discretely. We divide τ into N_τ steps. Here, we define $\varepsilon = \tau/N_\tau$. The equations of motion for molecular dynamics become difference equations. To discretize the time, we use a leap-frog method. In the following, $\phi(n)$ and $\pi(n)$ denotes $\phi(t = n\varepsilon)$ and $\pi(t = n\varepsilon)$, respectively.

Set initial conditions as follows:

$$\phi(0) = 0 \ , \quad \pi(0) = \pi \ , \tag{D.1.5}$$

then at the first step, take

$$\pi\left(\frac{1}{2}\right) = \pi(0) - \frac{\varepsilon}{2}\frac{\partial S\left(\phi(0)\right)}{\partial\phi(0)} \ . \tag{D.1.6}$$

At main steps ($n = 0, 1, \ldots, N_\tau - 2$), update ϕ and π:

$$\phi(n+1) = \phi(n) + \varepsilon\pi\left(n + \frac{1}{2}\right) \ , \quad \pi\left(n + \frac{3}{2}\right) = \pi\left(n + \frac{1}{2}\right) - \varepsilon\frac{\partial S(\phi(n+1))}{\partial\phi(n+1)} \ . \tag{D.1.7}$$

At the final step, ϕ' and π', which are new ϕ and π, are

$$\phi' = \phi(N_\tau) = \phi(N_\tau - 1) + \varepsilon\pi\left(N_\tau - \frac{1}{2}\right) \tag{D.1.8}$$

$$\pi' = \pi(N_\tau) = \pi\left(N_\tau - \frac{1}{2}\right) - \frac{\varepsilon}{2}\frac{\partial S(\phi(N_\tau))}{\partial\phi(N_\tau)} \ . \tag{D.1.9}$$

3. Accept ϕ' and π' with the following probability, which is called the Metropolis test [93].

$$P(\{\phi, \pi\} \to \{\phi', \pi'\}) = \min\left\{1, e^{-\Delta H}\right\} \quad \text{with} \quad \Delta H = H[\phi', \pi'] - H[\phi, \pi] \ , \tag{D.1.10}$$

where

$$\min\left\{1, e^{-\Delta H}\right\} = \begin{cases} \text{accept for } \Delta H < 0 \ , \\ \text{accept with probability } e^{-\Delta H} \text{ for } \Delta H > 0 \ . \end{cases} \tag{D.1.11}$$

If ϕ' and π' are rejected by the Metropolis test, ϕ and π (old ones) are kept. In practice, we use a random number for the Metropolis test in numerical simulations.

4. Return to 1.

D.2 Error estimation

Quantities calculated in numerical simulations have errors. In this appendix, we show how to estimate errors.

For observed quantities $\mathcal{O}_i$ ($i = 1, \ldots, N$), their average and statistical error are given as follows:

$$\langle\mathcal{O}\rangle = \frac{1}{N}\sum_{i=1}^{N}\mathcal{O}_i \ , \quad \delta\langle\mathcal{O}\rangle = \sqrt{\frac{\langle\mathcal{O}^2\rangle - \langle\mathcal{O}\rangle^2}{N-1}} \ . \tag{D.2.1}$$

For more complicated physical quantities, we use the following error-propagation relation:

$$\delta \langle f(\{\mathcal{O}_a\}) \rangle = \sum_a \left| \left\langle \frac{\partial f}{\partial \mathcal{O}_a} \right\rangle \delta \langle \mathcal{O}_a \rangle \right| \ , \tag{D.2.2}$$

where $\{\mathcal{O}_a\}$ denotes a set of physical quantities, and f is an arbitrary function of them. However, in general, we excessively estimate an error for complicated quantities by using the above relation due to correlations among $\mathcal{O}_a$.

We can overcome the problem by using the jackknife method. We show a procedure of the method for a bin size n.

1. Divide N data into $N_n (\equiv N/n)$ equal parts. Each bin contains n data.

2. Define the average except data in a bin b:

$$\langle \mathcal{O} \rangle_b = \frac{1}{N-n} \sum_{k \notin B_b} \mathcal{O}_k \ , \tag{D.2.3}$$

   where B_b denotes a set of indices for data in b.

3. By using $\langle \mathcal{O} \rangle_b$, one can calculate the average and the error of f:

$$\langle f(\mathcal{O}) \rangle = \frac{1}{N_n} \sum_{b=1}^{N_n} f\left(\langle \mathcal{O} \rangle_b \right) \ , \quad \delta \langle f(\mathcal{O}) \rangle = \sqrt{(N_n - 1) \left(\langle f(\mathcal{O})^2 \rangle - \langle f(\mathcal{O}) \rangle^2 \right)} \ . \tag{D.2.4}$$

Appendix E

Determination of the band size

We note here how we determine the band size n for the classical solutions in section 5.2.2. Our model has a time reversal symmetry $t \to -t$, which comes from the invariance of the bosonic action $S_{\rm b}$ under $X_0 \to -X_0$. Since Δ defined in (5.2.1) reflects this symmetry, it is almost symmetric under the exchange of the left-upper and the right-lower triangle:

$$\Delta_{pq} \longrightarrow \Delta_{N_X+1-q,\, N_X+1-p} \ . \tag{E.0.1}$$

In order to determine the band size, we evaluate an average of Δ and its time reversal:

$$\bar{\Delta}_{pq} = \frac{1}{2} \left(\Delta_{pq} + \Delta_{N_X+1-q,\, N_X+1-p} \right) \ . \tag{E.0.2}$$

$\bar{\Delta}$ in the typical solution for $N_X = 64$ is plotted against "a time separation" $\alpha_q - \alpha_p$ in Fig. E.1. Due to the (strict) monotonicity of the eigenvalues α_p, the time separation is in one-to-one correspondence to "a distance" $q - p$ from the diagonal elements. In this plot, there are 20 series of points which correspond to $p + q = 4, 6, \ldots, 42$. We find that Δ scales only in a sufficiently large $\alpha_q - \alpha_p$ region. We determine the block size n so that $\bar{X}_i(t)$ can cover a region where the scaling behavior is violated. In fact, this criterion is the same as the one adopted to determine n in the previous studies [57–60] . From Fig. E.1, we determine $n = 10$ for the typical solution.

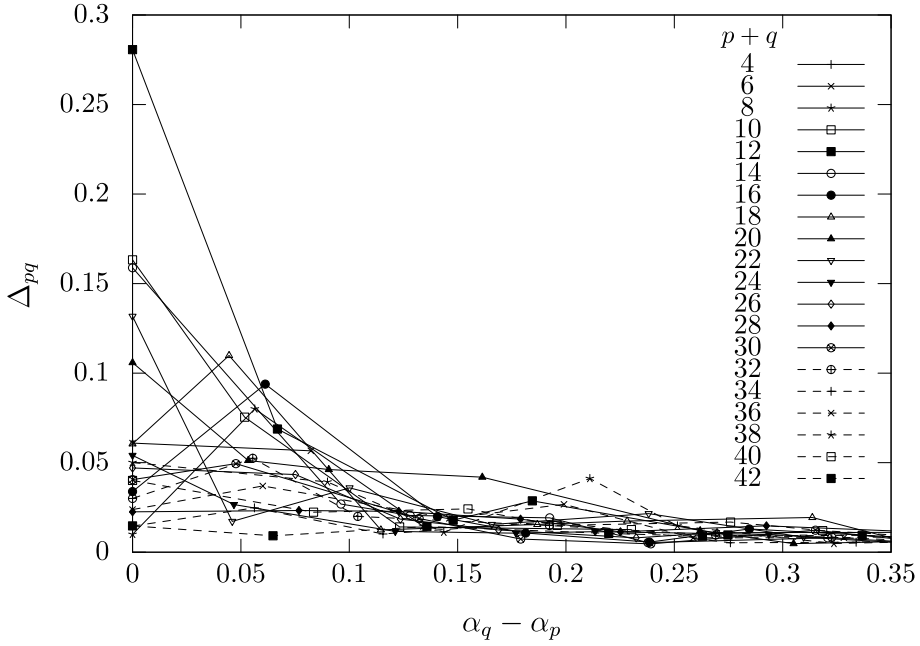

Figure E.1: Δ_{pq} are plotted against the time separation $\alpha_q - \alpha_p$. Each symbol corresponds to the label of "a slice of the band" $p+q-1 = 3, 5, \ldots, 41$. The scaling behavior is violated in the region $\alpha_q - \alpha_p \lesssim 0.15$

Appendix F

Detail calculations

In this appendix, we show detail calculations in this thesis.

F.1 Appendix A

(A.0.5) is calculated as follows:

$$\begin{aligned}\langle\Omega_1|\Omega_2\rangle &= \sum_{r=-j}^{j}\binom{2j}{j+r}\left(\cos\frac{\theta_1}{2}\cos\frac{\theta_2}{2}\right)^{j+r}\left(sin\frac{\theta_1}{2}\sin\frac{\theta_2}{2}\right)^{j-r}e^{i(j-r)(\varphi_2-\varphi_1)}\langle jr|jr\rangle \\ &= \sum_{r=-j}^{j}\binom{2j}{j+r}\left(\cos\frac{\theta_1}{2}\cos\frac{\theta_2}{2}\right)^{j+r}\left(e^{i(\varphi_2-\varphi_1)}\sin\frac{\theta_1}{2}\sin\frac{\theta_2}{2}\right)^{j-r} \\ &= \left[\cos\frac{\theta_1}{2}\cos\frac{\theta_2}{2}+\sin\frac{\theta_1}{2}\sin\frac{\theta_2}{2}e^{i(\varphi_2-\varphi_1)}\right]^{2j}. \qquad \text{(F.1.1)}\end{aligned}$$

We consider the square of $\langle\Omega_1|\Omega_2\rangle$:

$$\begin{aligned}|\langle\Omega_1|\Omega_2\rangle|^2 &= \left[\cos\frac{\theta_1}{2}\cos\frac{\theta_2}{2}+\sin\frac{\theta_1}{2}\sin\frac{\theta_2}{2}e^{i(\varphi_2-\varphi_1)}\right]^{2j\cdot 2} \\ &= \left[\cos^2\frac{\theta_1}{2}\cos^2\frac{\theta_2}{2}+\sin^2\frac{\theta_1}{2}\sin^2\frac{\theta_2}{2}+2\cos\frac{\theta_1}{2}\cos\frac{\theta_2}{2}\sin\frac{\theta_1}{2}\sin\frac{\theta_2}{2}e^{i(\varphi_2-\varphi_1)}\right]^{2j} \\ &= \left[\frac{1+\cos\theta_1}{2}\frac{1+\cos\theta_2}{2}+\frac{1-\cos\theta_1}{2}\frac{1-\cos\theta_2}{2}+\frac{\sin\theta_1\sin\theta_2}{4}\cdot 2\cos(\varphi_2-\varphi_1)\right]^{2j} \\ &= \left[\frac{1+\cos\theta_1\cos\theta_2+\sin\theta_1\sin\theta_2\cos(\varphi_2-\varphi_1)}{2}\right]^{2j} \\ &= \left(\frac{1+\cos\chi}{2}\right)^{2j} = \left(\cos^2\frac{\chi}{2}\right)^{2j}. \qquad \text{(F.1.2)}\end{aligned}$$

Thus, one obtains (A.0.6):

$$|\langle\Omega_1|\Omega_2\rangle| = \left(\cos\frac{\chi}{2}\right)^{2j}. \qquad \text{(F.1.3)}$$

Here, angle χ is defined as follows:

$$\vec{n}_1\cdot\vec{n}_2 = (\sin\theta_1\cos\varphi_1, \sin\theta_1\sin\varphi_1, \cos\theta_1)\cdot(\sin\theta_2\cos\varphi_2, \sin\theta_2\sin\varphi_2, \cos\theta_2)$$

$$= \sin\theta_1 \cos\varphi_1 \sin\theta_2 \cos\varphi_2 + \sin\theta_1 \sin\varphi_1 \sin\theta_2 \sin\varphi_2 + \cos\theta_1 \cos\theta_2$$
$$= \sin\theta_1 \sin\theta_2 (\cos\varphi_1 \cos\varphi_2 + \sin\varphi_1 \sin\varphi_2) + \cos\theta_1 \cos\theta_2$$
$$= \sin\theta_1 \sin\theta_2 \cos(\varphi_2 - \varphi_1) + \cos\theta_1 \cos\theta_2 \equiv \cos\chi \ . \tag{F.1.4}$$

Here, we show (A.0.7):

$$\begin{aligned}
&(2j+1) \int \frac{d\Omega}{4\pi} |\Omega\rangle \langle\Omega| \\
&= \frac{2j+1}{4\pi} \int_{-1}^{1} d(\cos\theta) \int_0^{2\pi} d\varphi \\
&\quad \times \sum_{r,r'=-j}^{j} \binom{2j}{j+r}^{\frac{1}{2}} \binom{2j}{j+r'}^{\frac{1}{2}} \left(\cos\frac{\theta}{2}\right)^{2j+r+r'} \left(\sin\frac{\theta}{2}\right)^{2j-r-r'} e^{i(-r+r')\varphi} |jr\rangle \langle jr'| \\
&= \frac{2j+1}{2} \int_{-1}^{1} d(\cos\theta) \sum_{r=-j}^{j} \binom{2j}{j+r} \left(\cos^2\frac{\theta}{2}\right)^{j+r} \left(\sin^2\frac{\theta}{2}\right)^{j-r} |jr\rangle \langle jr| \qquad \text{(F.1.5)} \\
&= \frac{2j+1}{2^{2j+1}} \sum_{r=-j}^{j} \frac{1}{(2j)!} \int_{-1}^{1} dx (1+x)^{2j} (-1)^{2j} \frac{d^{2j}}{dx^{2j}} (1-x)^{2j} |jr\rangle \langle jr| \qquad \text{(F.1.6)} \\
&= \frac{2j+1}{2^{2j+1}} \sum_{r=-j}^{j} \frac{1}{(2j)!} \int_{-1}^{1} dx (1+x)^{2j} |jr\rangle \langle jr| = \sum_{r=-j}^{j} |jr\rangle \langle jr| = 1 \ , \qquad \text{(F.1.7)}
\end{aligned}$$

where we change $\cos\theta$ to x and integrate by parts from (F.1.5) to (F.1.6).

Finally, we show (A.0.11). First of all, we derive $f_{[L_3,\Phi]}(\Omega)$:

$$\begin{aligned}
f_{[L_3,\Phi]}(\Omega) &= \big\langle\Omega\big| \left[L_3, \Phi\right] \big|\Omega\big\rangle \\
&= \big\langle\Omega\big| (L_3\Phi - \Phi L_3) \big|\Omega\big\rangle \\
&= \sum_{r,r'=-j}^{j} \binom{2j}{j+r}^{\frac{1}{2}} \binom{2j}{j+r'}^{\frac{1}{2}} \left(\cos\frac{\theta}{2}\right)^{2j+r+r'} \left(\sin\frac{\theta}{2}\right)^{2j-r-r'} e^{i(r-r')\varphi} \big\langle jr\big|\Phi\big|jr'\big\rangle \\
&= -i\frac{\partial}{\partial\varphi} \big\langle\Omega\big|\Phi\big|\Omega\big\rangle = \mathcal{L}_3 f_\Phi(\Omega) \ . \qquad \text{(F.1.8)}
\end{aligned}$$

Next, $f_{[L_+,\Phi]}(\Omega)$ is derived as

$$\begin{aligned}
&f_{[L_+,\Phi]}(\Omega) \\
&= \big\langle\Omega\big| \left[L_+, \Phi\right] \big|\Omega\big\rangle \\
&= \sum_{r,r'=-j}^{j} \binom{2j}{j+r}^{\frac{1}{2}} \binom{2j}{j+r'}^{\frac{1}{2}} \left(\cos\frac{\theta}{2}\right)^{2j+r+r'} \left(\sin\frac{\theta}{2}\right)^{2j-r-r'} e^{i(r-r')\varphi} \big\langle jr\big|(L_+\Phi - \Phi L_+)\big|jr'\big\rangle
\end{aligned} \tag{F.1.9}$$

Here,

$$\langle jr|\, L_+ = \sqrt{(j+r)(j-r+1)}\,\langle j\, r-1|\ , \quad L_+\,|jr'\rangle = \sqrt{(j-r')(j+r'+1)}\,|j\, r'+1\rangle\ , \tag{F.1.10}$$

so that

$$\begin{aligned}
(\text{F.1.9}) = &\sum_{r,r'=-j}^{j}\binom{2j}{j+r}^{\frac{1}{2}}\binom{2j}{j+r'}^{\frac{1}{2}}\left(\cos\frac{\theta}{2}\right)^{2j+r+r'+1}\left(\sin\frac{\theta}{2}\right)^{2j-r-r'-1}\\
&\quad\times e^{i(r-r')\varphi}\sqrt{(j+r)(j-r+1)}\,\big\langle j\, r-1\big|\Phi\big|jr'\big\rangle\\
&-\sum_{r,r'=-j}^{j}\binom{2j}{j+r}^{\frac{1}{2}}\binom{2j}{j+r'}^{\frac{1}{2}}\left(\cos\frac{\theta}{2}\right)^{2j+r+r'-1}\left(\sin\frac{\theta}{2}\right)^{2j-r-r'+1}\\
&\quad\times e^{i(r-r')\varphi}\sqrt{(j-r')(j+r'+1)}\,\big\langle jr\big|\Phi\big|j\, r'+1\big\rangle\\
=&\sum_{r=-j-1}^{j-1}\sum_{r'=-j}^{j}\binom{2j}{j+r+1}^{\frac{1}{2}}\binom{2j}{j+r'}^{\frac{1}{2}}\left(\cos\frac{\theta}{2}\right)^{2j+r+r'+1}\left(\sin\frac{\theta}{2}\right)^{2j-r-r'-1}\\
&\quad\times e^{i(r-r'+1)\varphi}\sqrt{(j-r)(j+r+1)}\,\big\langle jr\big|\Phi\big|jr'\big\rangle\\
&-\sum_{r=-j}^{j}\sum_{r'=-j+1}^{j+1}\binom{2j}{j+r}^{\frac{1}{2}}\binom{2j}{j+r'-1}^{\frac{1}{2}}\left(\cos\frac{\theta}{2}\right)^{2j+r+r'-1}\left(\sin\frac{\theta}{2}\right)^{2j-r-r'+1}\\
&\quad\times e^{i(r-r'+1)\varphi}\sqrt{(j+r')(j-r'+1)}\,\big\langle jr\big|\Phi\big|jr'\big\rangle\\
=&\sum_{r=-j-1}^{j-1}\sum_{r'=-j}^{j}\sqrt{\frac{j-r}{j+r+1}}\binom{2j}{j+r}^{\frac{1}{2}}\binom{2j}{j+r'}^{\frac{1}{2}}\left(\cos\frac{\theta}{2}\right)^{2j+r+r'+1}\left(\sin\frac{\theta}{2}\right)^{2j-r-r'-1}\\
&\quad\times e^{i(r-r'+1)\varphi}\sqrt{(j-r)(j+r+1)}\,\big\langle jr\big|\Phi\big|jr'\big\rangle\\
&-\sum_{r=-j}^{j}\sum_{r'=-j+1}^{j+1}\binom{2j}{j+r}^{\frac{1}{2}}\sqrt{\frac{j-r'}{j-r'+1}}\binom{2j}{j+r'}^{\frac{1}{2}}\left(\cos\frac{\theta}{2}\right)^{2j+r+r'+1}\left(\sin\frac{\theta}{2}\right)^{2j-r-r'-1}\\
&\quad\times e^{i(r-r'+1)\varphi}\sqrt{(j+r')(j-r'+1)}\,\big\langle jr\big|\Phi\big|jr'\big\rangle\\
=&\sum_{r=-j-1}^{j-1}\sum_{r'=-j}^{j}\binom{2j}{j+r}^{\frac{1}{2}}\binom{2j}{j+r'}^{\frac{1}{2}}\left(\cos\frac{\theta}{2}\right)^{2j+r+r'+1}\left(\sin\frac{\theta}{2}\right)^{2j-r-r'-1}\\
&\quad\times e^{i(r-r'+1)\varphi}(j-r)\,\big\langle jr\big|\Phi\big|jr'\big\rangle\\
&-\sum_{r=-j}^{j}\sum_{r'=-j+1}^{j+1}\binom{2j}{j+r}^{\frac{1}{2}}\binom{2j}{j+r'}^{\frac{1}{2}}\left(\cos\frac{\theta}{2}\right)^{2j+r+r'-1}\left(\sin\frac{\theta}{2}\right)^{2j-r-r'+1}\\
&\quad\times e^{i(r-r'+1)\varphi}(j+r')\,\big\langle jr\big|\Phi\big|jr'\big\rangle\ .
\end{aligned}\tag{F.1.11}$$

On the other hand, $\mathcal{L}_+\,\big\langle\Omega\big|\Phi\big|\Omega\big\rangle$ is

$$\mathcal{L}_+\,\big\langle\Omega\big|\Phi\big|\Omega\big\rangle \tag{F.1.12}$$

$$
\begin{aligned}
&= e^{i\varphi}\left(\frac{\partial}{\partial\theta}+i\cot\theta\frac{\partial}{\partial\varphi}\right)\left\langle\Omega\middle|\Phi\middle|\Omega\right\rangle \\
&= e^{i\varphi}\left(\frac{\partial}{\partial\theta}+i\cot\theta\frac{\partial}{\partial\varphi}\right)\sum_{r,r'=-j}^{j}\binom{2j}{j+r}^{\frac{1}{2}}\binom{2j}{j+r'}^{\frac{1}{2}}e^{i(r-r')\varphi} \\
&\quad\times\left(\cos\frac{\theta}{2}\right)^{2j+r+r'}\left(\sin\frac{\theta}{2}\right)^{2j-r-r'}\left\langle jr\middle|\Phi\middle|jr'\right\rangle \\
&= \sum_{r,r'=-j}^{j}\binom{2j}{j+r}^{\frac{1}{2}}\binom{2j}{j+r'}^{\frac{1}{2}} \\
&\quad\times\left[\left(-\frac{1}{2}\right)^{2j+r+r'}\left(\cos\frac{\theta}{2}\right)^{2j+r+r'-1}\left(\sin\frac{\theta}{2}\right)^{2j-r-r'+1}\right. \\
&\qquad\left.+\left(\frac{1}{2}\right)^{2j-r-r'}\left(\cos\frac{\theta}{2}\right)^{2j+r+r'+1}\left(\sin\frac{\theta}{2}\right)^{2j-r-r'-1}\right]e^{i(r-r'+1)\varphi}\left\langle jr\middle|\Phi\middle|jr'\right\rangle \\
&\quad+\sum_{r,r'=-j}^{j}\binom{2j}{j+r}^{\frac{1}{2}}\binom{2j}{j+r'}^{\frac{1}{2}} \\
&\qquad\times\left[-\frac{r-r'}{2}\left(\cos\frac{\theta}{2}\right)^{2j+r+r'+1}\left(\sin\frac{\theta}{2}\right)^{2j-r-r'-1}\right. \\
&\qquad\left.+\frac{r-r'}{2}\left(\cos\frac{\theta}{2}\right)^{2j+r+r'-1}\left(\sin\frac{\theta}{2}\right)^{2j-r-r'+1}\right]e^{i(r-r'+1)\varphi}\left\langle jr\middle|\Phi\middle|jr'\right\rangle \\
&= \sum_{r,r'=-j}^{j}\binom{2j}{j+r}^{\frac{1}{2}}\binom{2j}{j+r'}^{\frac{1}{2}} \\
&\qquad\times\left[-\frac{2j+r+r'-r+r'}{2}\left(\cos\frac{\theta}{2}\right)^{2j+r+r'-1}\left(\sin\frac{\theta}{2}\right)^{2j-r-r'+1}\right. \\
&\qquad\left.+\frac{2j-r-r'-r+r'}{2}\left(\cos\frac{\theta}{2}\right)^{2j+r+r'+1}\left(\sin\frac{\theta}{2}\right)^{2j-r-r'-1}\right] \\
&\qquad\qquad\times e^{i(r-r'+1)\varphi}\left\langle jr\middle|\Phi\middle|jr'\right\rangle \\
&= \sum_{r,r'=-j}^{j}\binom{2j}{j+r}^{\frac{1}{2}}\binom{2j}{j+r'}^{\frac{1}{2}} \\
&\qquad\times\left[(j-r)\left(\cos\frac{\theta}{2}\right)^{2j+r+r'+1}\left(\sin\frac{\theta}{2}\right)^{2j-r-r'-1}\right. \\
&\qquad\left.-(j+r')\left(\cos\frac{\theta}{2}\right)^{2j+r+r'-1}\left(\sin\frac{\theta}{2}\right)^{2j-r-r'+1}\right]e^{i(r-r'+1)\varphi}\left\langle jr\middle|\Phi\middle|jr'\right\rangle\ . \qquad \text{(F.1.13)}
\end{aligned}
$$

Thus, one obtains $\mathcal{L}_+\left\langle\Omega\middle|\Phi\middle|\Omega\right\rangle = f_{[L_+,\Phi]}(\Omega)$. Similarly, one can show $\mathcal{L}_-\left\langle\Omega\middle|\Phi\middle|\Omega\right\rangle =$

$f_{[L_-,\Phi]}(\Omega)$.

F.2 Appendix B

First of all, let us consider

$$\frac{\lambda}{4}\frac{1}{2j+1}\mathrm{Tr}\left(\Phi^4\right)=\sum_{l_1,\ldots,l_4}\sum_{m_1,\ldots,m_4}\phi_{l_1m_1}\cdots\phi_{l_4m_4}\frac{\lambda}{4}\frac{1}{2j+1}\mathrm{Tr}\left(\hat{Y}_{l_1m_1}\cdots\hat{Y}_{l_4m_4}\right)\ , \tag{F.2.1}$$

and the fuzzy spherical harmonics $\hat{Y}^{[j]}_{lm}$ are abbreviated as $\hat{Y}_{lm}$. The vertex (B.0.5) is calculated as

$$\begin{aligned}
&V(l_1,m_1;\ldots;l_4,m_4)\\
&\equiv\frac{\lambda}{4}\frac{1}{2j+1}\mathrm{Tr}\left(\hat{Y}_{l_1m_1}\hat{Y}_{l_2m_2}\hat{Y}_{l_3m_3}\hat{Y}_{l_4m_4}\right)\\
&=\frac{\lambda}{4}\sum_{l,l'}\sum_{m,m'}\hat{C}^{l\,m}_{l_1\,m_1\ l_2\,m_2}\hat{C}^{l'\,m'}_{l_3\,m_3\ l_4\,m_4}\frac{1}{2j+1}\mathrm{Tr}\left(\hat{Y}_{lm}\hat{Y}_{l'm'}\right)\\
&=\frac{\lambda}{4}\sum_{l,l'}\sum_{m,m'}\hat{C}^{l\,m}_{l_1\,m_1\ l_2\,m_2}\hat{C}^{l'\,m'}_{l_3\,m_3\ l_4\,m_4}(-1)^m\delta_{l,l'}\delta_{-m,m'}\\
&=\frac{\lambda}{4}\sum_{l',m'}(-1)^{m'}\hat{C}^{l'\,-m'}_{l_1\,m_1\ l_2\,m_2}\hat{C}^{l'\,m'}_{l_3\,m_3\ l_4\,m_4}\\
&=\frac{\lambda}{4}(2j+1)\prod_{i=1}^{4}\sqrt{2l_i+1}\sum_{l',m'}(-1)^{m'}C^{l'\,-m'}_{l_1\,m_1\ l_2\,m_2}C^{l'\,m'}_{l_3\,m_3\ l_4\,m_4}\begin{Bmatrix}l_1&l_2&l'\\j&j&j\end{Bmatrix}\begin{Bmatrix}l_3&l_4&l'\\j&j&j\end{Bmatrix}\\
&=\frac{\lambda}{4}(2j+1)(-1)^{\sum_{i=1}^4 l_i}\prod_{i=1}^{4}\sqrt{2l_i+1}\\
&\quad\times\sum_{l,m}(-1)^m(2l+1)\begin{pmatrix}l_1&l_2&l\\m_1&m_2&m\end{pmatrix}\begin{pmatrix}l_3&l_4&l\\m_3&m_4&-m\end{pmatrix}\begin{Bmatrix}l_1&l_2&l'\\j&j&j\end{Bmatrix}\begin{Bmatrix}l_3&l_4&l\\j&j&j\end{Bmatrix}\ ,
\end{aligned}\tag{F.2.2}$$

where we use (2.1.46)–(2.1.49) and (C.0.1).

In Fig. F.1, we contract ϕ_{lm} with $\phi_{l_1m_1}$, $\phi^*_{l'm'}$ with $\phi_{l_2m_2}$, and $\phi_{l_3m_3}$ with $\phi_{l_4m_4}$. 8 possible contractions are the same contribution. (B.0.6) is obtained as follows:

$$\begin{aligned}
&8\sum_{l_1,\ldots,l_4}\sum_{m_1,\ldots,m_4}(-1)^m\frac{\delta_{l_1,l}\delta_{m_1,-m}}{l_1(l_1+1)+\mu^2}\frac{\delta_{l',l_2}\delta_{m',m_2}}{l'(l'+1)+\mu^2}\\
&\times(-1)^{m_4}\frac{\delta_{l_3,l_4}\delta_{m_3,-m_4}}{l_3(l_3+1)+\mu^2}\frac{\lambda}{4}(2j+1)(-1)^{\sum_{i=1}^4 l_i}\prod_{i=1}^{4}\sqrt{2l_i+1}
\end{aligned}$$

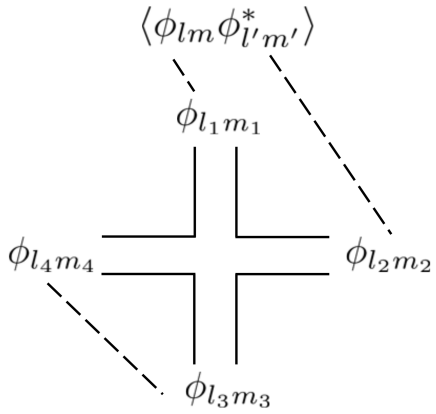

Figure F.1: Contraction of planar diagram.

$$
\begin{aligned}
&\times \sum_{l'',m''} (-1)^{m''}(2l''+1)
\begin{pmatrix} l_1 & l_2 & l'' \\ m_1 & m_2 & m'' \end{pmatrix}
\begin{pmatrix} l_3 & l_4 & l'' \\ m_3 & m_4 & -m'' \end{pmatrix}
\begin{Bmatrix} l_1 & l_2 & l'' \\ j & j & j \end{Bmatrix}
\begin{Bmatrix} l_3 & l_4 & l'' \\ j & j & j \end{Bmatrix} \\
&= 2\lambda(2j+1)\frac{(-1)^m}{l(l+1)+\mu^2}\frac{\sqrt{(2l+1)(2l'+1)}}{l'(l'+1)+\mu^2}\sum_{l_3,m_3}\frac{(-1)^{-m_3}}{l_3(l_3+1)+\mu^2}(-1)^{l+l'+2l_3}(2l_3+1) \\
&\times \sum_{l'',m''} (-1)^{m''}(2l''+1)
\begin{pmatrix} l & l' & l'' \\ -m & m' & m'' \end{pmatrix}
\begin{pmatrix} l_3 & l_3 & l'' \\ m_3 & -m_3 & -m'' \end{pmatrix}
\begin{Bmatrix} l & l' & l'' \\ j & j & j \end{Bmatrix}
\begin{Bmatrix} l_3 & l_3 & l'' \\ j & j & j \end{Bmatrix} \\
&= 2\lambda(2j+1)\frac{(-1)^m}{l_1(l_1+1)+\mu^2}(-1)^{l+l'}\frac{\sqrt{(2l+1)(2l'+1)}}{l'(l'+1)+\mu^2}\sum_{l_3,m_m}\frac{\sqrt{2l_3+1}}{l_3(l_3+1)+\mu^2}(-1)^{l''+m''+l_3-m_3} \\
&\times C^{l_3\,-m_3}_{l_3\,-m_3\;\;l''\,m''}\delta_{m'',0}
\begin{pmatrix} l & l' & l'' \\ -m & m' & m'' \end{pmatrix}
\begin{Bmatrix} l & l' & 0 \\ j & j & j \end{Bmatrix}
\begin{Bmatrix} l_3 & l_3 & 0 \\ j & j & j \end{Bmatrix} \\
&= 2\lambda(2j+1)\frac{(-1)^m}{l(l+1)+\mu^2}\frac{\delta_{l,l'}\delta_{m,-m'}}{l'(l'+1)+\mu^2}(-1)^{4l+l'}\sqrt{2l'+1} \\
&\times \sum_{l_3}\frac{2l_3+1}{l_3(l_3+1)+\mu^2}(-1)^{l_3}\sqrt{2l_3+1}
\begin{Bmatrix} l & l' & 0 \\ j & j & j \end{Bmatrix}
\begin{Bmatrix} l_3 & l_3 & 0 \\ j & j & j \end{Bmatrix} \\
&= \left[2\lambda(2j+1)\delta_{l,l'}\delta_{m,-m'}(-1)^m\sum_{l_3}\frac{2l_3+1}{l_3(l_3+1)+\mu^2}\right]\times\frac{1}{l(l+1)+\mu^2}\frac{1}{l'(l'+1)+\mu^2} \\
&= \left(\Gamma^{(2)}_{\text{planar}}\right)^{l,l'}_{m,m'}\times\frac{1}{l(l+1)+\mu^2}\frac{1}{l'(l'+1)+\mu^2}\,,
\end{aligned}
\tag{F.2.3}
$$

where $l, l', l'', l_i, m, m', m'', m_i$ $(i = 1, \ldots, 4)$ are integers and j is half integer. To derive the above, we use (C.0.2)–(C.0.3), (C.0.8), and (C.0.9).

In Fig. F.2, we contract ϕ_{lm} with $\phi_{l_1m_1}$, $\phi^*_{l'm'}$ with $\phi_{l_3m_3}$, and $\phi_{l_2m_2}$ with $\phi_{l_4m_4}$. If one of $\phi_{l_im_i}$ $(i = 1, \ldots, 4)$ contracted with ϕ_{lm} is chosen, another contracted with $\phi^*_{l'm'}$ is

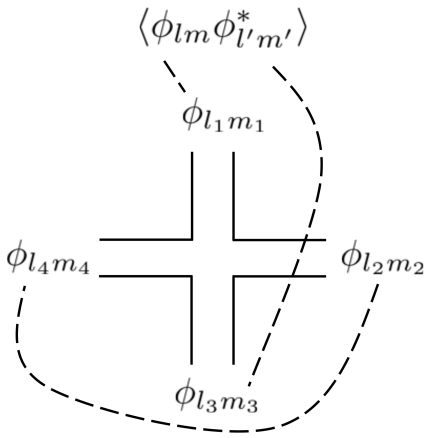

Figure F.2: Contraction of non-planar diagram.

consequently chosen, so that there are 4 possible contractions to be the same contribution.

$$
\begin{aligned}
&4\sum_{l_1,\ldots,l_4}\sum_{m_1,\ldots,m_4}(-1)^m\frac{\delta_{l_1,l}\delta_{m_1,-m}}{l_1(l_1+1)+\mu^2}\frac{\delta_{l',l_3}\delta_{m',m_3}}{l_3(l_3+1)+\mu^2}\\
&\times(-1)^{m_4}\frac{\delta_{l_2,l_4}\delta_{m_2,-m_4}}{l_2(l_2+1)+\mu^2}\frac{\lambda}{4}(2j+1)(-1)^{\sum_{i=1}^4 l_i}\prod_{i=1}^4\sqrt{2l_i+1}\\
&\times\sum_{l'',m''}(-1)^{m''}(2l''+1)\begin{pmatrix}l_1&l_2&l''\\m_1&m_2&m''\end{pmatrix}\begin{pmatrix}l_3&l_4&l''\\m_3&m_4&-m''\end{pmatrix}\begin{Bmatrix}l_1&l_2&l''\\j&j&j\end{Bmatrix}\begin{Bmatrix}l_3&l_4&l''\\j&j&j\end{Bmatrix}\\
=\;&\lambda(2j+1)\frac{(-1)^m}{l(l+1)+\mu^2}\frac{\sqrt{(2l+1)(2l'+1)}}{l'(l'+1)+\mu^2}\sum_{l_4,m_4}\frac{(-1)^{-m_4}}{l_4(l_4+1)+\mu^2}(-1)^{l+l'+2l_4}(2l_4+1)\\
&\times\sum_{l'',m''}(-1)^{m''}(2l''+1)\begin{pmatrix}l&l_4&l''\\-m&-m_4&m''\end{pmatrix}\begin{pmatrix}l'&l_4&l''\\m'&m_4&-m''\end{pmatrix}\begin{Bmatrix}l&l_4&l''\\j&j&j\end{Bmatrix}\begin{Bmatrix}l'&l_4&l''\\j&j&j\end{Bmatrix}\\
=\;&\lambda(2j+1)\frac{(-1)^m}{l(l+1)+\mu^2}\frac{\sqrt{(2l+1)(2l'+1)}}{l'(l'+1)+\mu^2}\sum_{l_4,m_4}\frac{2l_4+1}{l_4(l_4+1)+\mu^2}(-1)^{m+l+l'+2l_4}\\
&\times\sum_{l'',m''}(-1)^{2l+l'+3l''+3l_4+m''}\frac{2l''+1}{2l_4+1}C^{l_4\,m_4}_{l''\,m''\;\,l\,-m}C^{l_4\,m_4}_{l''\,m''\;\,l'\,-m'}\begin{Bmatrix}l&l_4&l''\\j&j&j\end{Bmatrix}\begin{Bmatrix}l'&l_4&l''\\j&j&j\end{Bmatrix}\\
=\;&\lambda(2j+1)\frac{(-1)^m}{l(l+1)+\mu^2}\frac{1}{l'(l'+1)+\mu^2}\sqrt{\frac{2l'+1}{2l+1}}\delta_{l,l'}\delta_{m,-m'}(-1)^{m+3l+2l'}\\
&\times\sum_{l_4,l''}\frac{2l_4+1}{l_4(l_4+1)+\mu^2}(2l''+1)(-1)^{5l_4+l''}\begin{Bmatrix}l&l_4&l''\\j&j&j\end{Bmatrix}\begin{Bmatrix}l'&l_4&l''\\j&j&j\end{Bmatrix}\\
=\;&\left[\lambda(2j+1)\delta_{l,l'}\delta_{m,-m'}(-1)^m\sum_{l_4}(-1)^{l+l_4+2j}\frac{(2l_4+1)(2j+1)}{l_4(l_4+1)+\mu^2}\begin{Bmatrix}j&j&l\\j&j&l_4\end{Bmatrix}\right]
\end{aligned}
$$

$$\times \frac{1}{l(l+1)+\mu^2}\frac{1}{l'(l'+1)+\mu^2}\sqrt{\frac{2l'+1}{2l+1}}$$

$$= \left(\Gamma^{(2)}_{\text{non-planar}}\right)^{l,l'}_{m,m'} \times \frac{1}{l(l+1)+\mu^2}\frac{1}{l'(l'+1)+\mu^2}\sqrt{\frac{2l'+1}{2l+1}}\ . \tag{F.2.4}$$

To derive the above, we use (C.0.4)–(C.0.7), and (C.0.10). (B.0.8) is derived in this way.

References

[1] A. Lawrence, *On the Instability of 3-D null singularities*, *JHEP* **11** (2002) 019 [hep-th/0205288].

[2] H. Liu, G.W. Moore and N. Seiberg, *Strings in time dependent orbifolds*, *JHEP* **10** (2002) 031 [hep-th/0206182].

[3] G.T. Horowitz and J. Polchinski, *Instability of space - like and null orbifold singularities*, *Phys. Rev.* **D66** (2002) 103512 [hep-th/0206228].

[4] M. Berkooz, B. Craps, D. Kutasov and G. Rajesh, *Comments on cosmological singularities in string theory*, *JHEP* **03** (2003) 031 [hep-th/0212215].

[5] N. Ishibashi, H. Kawai, Y. Kitazawa and A. Tsuchiya, *A Large N reduced model as superstring*, *Nucl. Phys.* **B498** (1997) 467 [hep-th/9612115].

[6] T. Banks, W. Fischler, S.H. Shenker and L. Susskind, *M theory as a matrix model: A Conjecture*, *Phys. Rev.* **D55** (1997) 5112 [hep-th/9610043].

[7] R. Dijkgraaf, E.P. Verlinde and H.L. Verlinde, *Matrix string theory*, *Nucl. Phys.* **B500** (1997) 43 [hep-th/9703030].

[8] M. Hanada, H. Kawai and Y. Kimura, *Describing curved spaces by matrices*, *Prog. Theor. Phys.* **114** (2006) 1295 [hep-th/0508211].

[9] A. Connes, M.R. Douglas and A.S. Schwarz, *Noncommutative geometry and matrix theory: Compactification on tori*, *JHEP* **02** (1998) 003 [hep-th/9711162].

[10] H. Aoki, N. Ishibashi, S. Iso, H. Kawai, Y. Kitazawa and T. Tada, *Noncommutative Yang-Mills in IIB matrix model*, *Nucl. Phys.* **B565** (2000) 176 [hep-th/9908141].

[11] M.R. Douglas and N.A. Nekrasov, *Noncommutative field theory*, *Rev. Mod. Phys.* **73** (2001) 977 [hep-th/0106048].

[12] S. Minwalla, M. Van Raamsdonk and N. Seiberg, *Noncommutative perturbative dynamics*, *JHEP* **02** (2000) 020 [hep-th/9912072].

[13] C.S. Chu, J. Madore and H. Steinacker, *Scaling limits of the fuzzy sphere at one loop*, *JHEP* **08** (2001) 038 [hep-th/0106205].

[14] H.C. Steinacker, *String states, loops and effective actions in noncommutative field theory and matrix models*, *Nucl. Phys.* **B910** (2016) 346 [arXiv:1606.00646].

[15] X. Martin, *A Matrix phase for the ϕ^4 scalar field on the fuzzy sphere*, *JHEP* **04** (2004) 077 [hep-th/0402230].

[16] M. Panero, *Numerical simulations of a non-commutative theory: The Scalar model on the fuzzy sphere*, *JHEP* **05** (2007) 082 [hep-th/0608202].

[17] M. Panero, *Quantum field theory in a non-commutative space: Theoretical predictions and numerical results on the fuzzy sphere*, *SIGMA* **2** (2006) 081 [hep-th/0609205].

[18] C.R. Das, S. Digal and T.R. Govindarajan, *Finite temperature phase transition of a single scalar field on a fuzzy sphere*, *Mod. Phys. Lett.* **A23** (2008) 1781 [arXiv:0706.0695].

[19] F. García Flores, X. Martin and D. O'Connor, *Simulation of a scalar field on a fuzzy sphere*, *Int. J. Mod. Phys.* **A24** (2009) 3917 [arXiv:0903.1986].

[20] K. Hatakeyama and A. Tsuchiya, *Correlation functions and renormalization in a scalar field theory on the fuzzy sphere*, *PTEP* **2017** (2017) 063B01 [arXiv:1704.01698].

[21] K. Hatakeyama, A. Tsuchiya and K. Yamashiro, *Renormalization on the fuzzy sphere*, *PTEP* **2018** (2018) 063B05 [arXiv:1805.03975].

[22] K. Hatakeyama, A. Tsuchiya and K. Yamashiro, *Renormalization on the fuzzy sphere*, *PoS* **LATTICE2018** (2019) 045 [arXiv:1811.10806].

[23] S. Vaidya and B. Ydri, *On the origin of the UV-IR mixing in noncommutative matrix geometry*, *Nucl. Phys.* **B671** (2003) 401 [hep-th/0305201].

[24] D. O'Connor and C. Sämann, *Fuzzy Scalar Field Theory as a Multitrace Matrix Model*, *JHEP* **08** (2007) 066 [arXiv:0706.2493].

[25] V.P. Nair, A.P. Polychronakos and J. Tekel, *Fuzzy spaces and new random matrix ensembles*, *Phys. Rev.* **D85** (2012) 045021 [arXiv:1109.3349].

[26] J. Tekel, *Random matrix approach to scalar fields on fuzzy spaces*, *Phys. Rev.* **D87** (2013) 085015 [arXiv:1301.2154].

[27] A.P. Polychronakos, *Effective action and phase transitions of scalar field on the fuzzy sphere*, *Phys. Rev.* **D88** (2013) 065010 [arXiv:1306.6645].

[28] J. Tekel, *Uniform order phase and phase diagram of scalar field theory on fuzzy $\mathbb{C}P^n$*, *JHEP* **10** (2014) 144 [arXiv:1407.4061].

[29] C. Sämann, *Bootstrapping Fuzzy Scalar Field Theory*, *JHEP* **04** (2015) 044 [arXiv:1412.6255].

[30] S. Kawamoto and T. Kuroki, *Existence of new nonlocal field theory on noncommutative space and spiral flow in renormalization group analysis of matrix models*, *JHEP* **06** (2015) 062 [arXiv:1503.08411].

[31] J. Tekel, *Matrix model approximations of fuzzy scalar field theories and their phase diagrams*, *JHEP* **12** (2015) 176 [arXiv:1510.07496].

[32] W. Bietenholz, F. Hofheinz and J. Nishimura, *Phase diagram and dispersion relation of the noncommutative $\lambda\phi^4$ model in $d = 3$*, *JHEP* **06** (2004) 042 [hep-th/0404020].

[33] H. Mejía-Díaz, W. Bietenholz and M. Panero, *The continuum phase diagram of the 2d non-commutative $\lambda\phi^4$ model*, *JHEP* **10** (2014) 056 [arXiv:1403.3318].

[34] T. Eguchi and H. Kawai, *Reduction of Dynamical Degrees of Freedom in the Large N Gauge Theory*, *Phys. Rev. Lett.* **48** (1982) 1063.

[35] H. Kawai, S. Shimasaki and A. Tsuchiya, *Large N reduction on group manifolds*, *Int. J. Mod. Phys.* **A25** (2010) 3389 [arXiv:0912.1456].

[36] H. Kawai, S. Shimasaki and A. Tsuchiya, *Large N reduction on coset spaces*, *Phys. Rev.* **D81** (2010) 085019 [arXiv:1002.2308].

[37] T. Ishii, G. Ishiki, S. Shimasaki and A. Tsuchiya, *N=4 Super Yang-Mills from the Plane Wave Matrix Model*, *Phys. Rev.* **D78** (2008) 106001 [arXiv:0807.2352].

[38] D.J. Gross, R.D. Pisarski and L.G. Yaffe, *QCD and Instantons at Finite Temperature*, *Rev. Mod. Phys.* **53** (1981) 43.

[39] G. Bhanot, U.M. Heller and H. Neuberger, *The Quenched Eguchi-Kawai Model*, *Phys. Lett.* **113B** (1982) 47.

[40] G. Parisi, *A Simple Expression for Planar Field Theories*, *Phys. Lett.* **112B** (1982) 463.

[41] D.J. Gross and Y. Kitazawa, *A Quenched Momentum Prescription for Large N Theories*, *Nucl. Phys.* **B206** (1982) 440.

[42] S.R. Das and S.R. Wadia, *Translation Invariance and a Reduced Model for Summing Planar Diagrams in QCD*, *Phys. Lett.* **117B** (1982) 228. [Erratum: *Phys. Lett.* **121B** (1983) 456].

[43] A. González-Arroyo and M. Okawa, *The Twisted Eguchi-Kawai Model: A Reduced Model for Large N Lattice Gauge Theory*, *Phys. Rev.* **D27** (1983) 2397.

[44] T. Eguchi and R. Nakayama, *Simplification of Quenching Procedure for Large N Spin Models*, *Phys. Lett.* **122B** (1983) 59.

[45] A. González-Arroyo and C.P. Korthals Altes, *Reduced Model for Large N Continuum Field Theories*, *Phys. Lett.* **131B** (1983) 396.

[46] R. Narayanan and H. Neuberger, *Large N reduction in continuum*, *Phys. Rev. Lett.* **91** (2003) 081601 [hep-lat/0303023].

[47] W. Bietenholz, J. Nishimura, Y. Susaki and J. Volkholz, *A Non-perturbative study of 4-D U(1) non-commutative gauge theory: The Fate of one-loop instability*, *JHEP* **10** (2006) 042 [hep-th/0608072].

[48] M. Teper and H. Vairinhos, *Symmetry breaking in twisted Eguchi-Kawai models*, *Phys. Lett.* **B652** (2007) 359 [hep-th/0612097].

[49] P. Kovtun, M. Ünsal and L.G. Yaffe, *Volume independence in large N(c) QCD-like gauge theories*, *JHEP* **06** (2007) 019 [hep-th/0702021].

[50] T. Azeyanagi, M. Hanada, T. Hirata and T. Ishikawa, *Phase structure of twisted Eguchi-Kawai model*, *JHEP* **01** (2008) 025 [arXiv:0711.1925].

[51] M. Ünsal and L.G. Yaffe, *Center-stabilized Yang-Mills theory: Confinement and large N volume independence*, *Phys. Rev.* **D78** (2008) 065035 [arXiv:0803.0344].

[52] B. Bringoltz and S.R. Sharpe, *Breakdown of large-N quenched reduction in SU(N) lattice gauge theories*, *Phys. Rev.* **D78** (2008) 034507 [arXiv:0805.2146].

[53] B. Bringoltz and S.R. Sharpe, *Non-perturbative volume-reduction of large-N QCD with adjoint fermions*, *Phys. Rev.* **D80** (2009) 065031 [arXiv:0906.3538].

[54] A. González-Arroyo and M. Okawa, *Large N reduction with the Twisted Eguchi-Kawai model*, *JHEP* **07** (2010) 043 [arXiv:1005.1981].

[55] B. Lucini and M. Panero, *SU(N) gauge theories at large N*, *Phys. Rept.* **526** (2013) 93 [arXiv:1210.4997].

[56] S.W. Kim, J. Nishimura and A. Tsuchiya, *Expanding (3+1)-dimensional universe from a Lorentzian matrix model for superstring theory in (9+1)-dimensions*, *Phys. Rev. Lett.* **108** (2012) 011601 [arXiv:1108.1540].

[57] Y. Ito, S.W. Kim, Y. Koizuka, J. Nishimura and A. Tsuchiya, *A renormalization group method for studying the early universe in the Lorentzian IIB matrix model*, *PTEP* **2014** (2014) 083B01 [arXiv:1312.5415].

[58] Y. Ito, J. Nishimura and A. Tsuchiya, *Power-law expansion of the Universe from the bosonic Lorentzian type IIB matrix model*, *JHEP* **11** (2015) 070 [arXiv:1506.04795].

[59] Y. Ito, J. Nishimura and A. Tsuchiya, *Universality and the dynamical space-time dimensionality in the Lorentzian type IIB matrix model*, *JHEP* **03** (2017) 143 [arXiv:1701.07783].

[60] T. Azuma, Y. Ito, J. Nishimura and A. Tsuchiya, *A new method for probing the late-time dynamics in the Lorentzian type IIB matrix model*, *PTEP* **2017** (2017) 083B03 [arXiv:1705.07812].

[61] T. Aoki, M. Hirasawa, Y. Ito, J. Nishimura and A. Tsuchiya, *On the structure of the emergent 3d expanding space in the Lorentzian type IIB matrix model*, *PTEP* **2019** (2019) 093B03 [arXiv:1904.05914].

[62] J. Nishimura and A. Tsuchiya, *Complex Langevin analysis of the space-time structure in the Lorentzian type IIB matrix model*, *JHEP* **06** (2019) 077 [arXiv:1904.05919].

[63] K.N. Anagnostopoulos, T. Azuma and J. Nishimura, *Monte Carlo studies of the spontaneous rotational symmetry breaking in dimensionally reduced super Yang-Mills models*, *JHEP* **11** (2013) 009 [arXiv:1306.6135].

[64] K.N. Anagnostopoulos, T. Azuma, Y. Ito, J. Nishimura and S.K. Papadoudis, *Complex Langevin analysis of the spontaneous symmetry breaking in dimensionally reduced super Yang-Mills models*, *JHEP* **02** (2018) 151 [arXiv:1712.07562].

[65] S.W. Kim, J. Nishimura and A. Tsuchiya, *Expanding universe as a classical solution in the Lorentzian matrix model for nonperturbative superstring theory*, *Phys. Rev.* **D86** (2012) 027901 [arXiv:1110.4803].

[66] S.W. Kim, J. Nishimura and A. Tsuchiya, *Late time behaviors of the expanding universe in the IIB matrix model*, *JHEP* **10** (2012) 147 [arXiv:1208.0711].

[67] A. Chaney, L. Lu and A. Stern, *Matrix Model Approach to Cosmology*, *Phys. Rev.* **D93** (2016) 064074 [arXiv:1511.06816].

[68] H.C. Steinacker, *Cosmological space-times with resolved Big Bang in Yang-Mills matrix models*, *JHEP* **02** (2018) 033 [arXiv:1709.10480].

[69] A. Chatzistavrakidis, H. Steinacker and G. Zoupanos, *Intersecting branes and a standard model realization in matrix models*, *JHEP* **09** (2011) 115 [arXiv:1107.0265].

[70] H.C. Steinacker and J. Zahn, *An extended standard model and its Higgs geometry from the matrix model*, *PTEP* **2014** (2014) 083B03 [arXiv:1401.2020].

[71] H. Aoki, J. Nishimura and A. Tsuchiya, *Realizing three generations of the Standard Model fermions in the type IIB matrix model*, *JHEP* **05** (2014) 131 [arXiv:1401.7848].

[72] H. Aoki, J. Nishimura and Y. Susaki, *Finite-matrix formulation of gauge theories on a non-commutative torus with twisted boundary conditions*, *JHEP* **04** (2009) 055 [arXiv:0810.5234].

[73] H. Aoki, *Chiral fermions and the standard model from the matrix model compactified on a torus*, *Prog. Theor. Phys.* **125** (2011) 521 [arXiv:1011.1015].

[74] M. Honda, *Matrix model and Yukawa couplings on the noncommutative torus*, *JHEP* **04** (2019) 079 [arXiv:1901.00095].

[75] F.A. Berezin, *General Concept of Quantization*, *Commun. Math. Phys.* **40** (1975) 153.

[76] J.P. Gazeau, *Coherent states in quantum physics*, Wiley-VCH, Weinheim, Germany (2009).

[77] K. Hatakeyama and A. Tsuchiya, *Equivalence of large-N gauge theories on a group manifold and its coset space*, *Phys. Lett.* **B782** (2018) 503 [arXiv:1805.10743].

[78] K. Hatakeyama, A. Matsumoto, J. Nishimura, A. Tsuchiya and A. Yosprakob, *The emergence of expanding space-time and intersecting D-branes from classical solutions in the Lorentzian type IIB matrix model*, arXiv:1911.08132.

[79] J. Nishimura and A. Tsuchiya, *Realizing chiral fermions in the type IIB matrix model at finite N*, *JHEP* **12** (2013) 002 [arXiv:1305.5547].

[80] T. Ishii, G. Ishiki, S. Shimasaki and A. Tsuchiya, *Fiber Bundles and Matrix Models*, *Phys. Rev.* **D77** (2008) 126015 [arXiv:0802.2782].

[81] T. Ishii, G. Ishiki, K. Ohta, S. Shimasaki and A. Tsuchiya, *On relationships among Chern-Simons theory, BF theory and matrix model*, *Prog. Theor. Phys.* **119** (2008) 863 [arXiv:0711.4235].

[82] S.S. Gubser and S.L. Sondhi, *Phase structure of noncommutative scalar field theories*, *Nucl. Phys.* **B605** (2001) 395 [hep-th/0006119].

[83] J. Ambjørn and S. Catterall, *Stripes from (noncommutative) stars*, *Phys. Lett.* **B549** (2002) 253 [hep-lat/0209106].

[84] G. Ishiki, S. Shimasaki, Y. Takayama and A. Tsuchiya, *Embedding of theories with SU(2|4) symmetry into the plane wave matrix model*, *JHEP* **11** (2006) 089 [hep-th/0610038].

[85] K. Furuuchi, *From free fields to AdS: Thermal case*, *Phys. Rev.* **D72** (2005) 066009 [hep-th/0505148].

[86] K. Furuuchi, *Large N reductions and holography*, *Phys. Rev.* **D74** (2006) 045027 [hep-th/0506183].

[87] E. Poppitz and M. Ünsal, *AdS/CFT and large-N volume independence*, *Phys. Rev.* **D82** (2010) 066002 [arXiv:1005.3519].

[88] D. Young and K. Zarembo, *Holographic Dual of the Eguchi-Kawai Mechanism*, *JHEP* **06** (2014) 030 [arXiv:1404.0225].

[89] E. Shaghoulian, *Emergent gravity from Eguchi-Kawai reduction*, *JHEP* **03** (2017) 011 [arXiv:1611.04189].

[90] F.R. Klinkhamer, *On the emergence of an expanding universe from a Lorentzian matrix model*, arXiv:1912.12229.

[91] D.A. Varshalovich, A.N. Moskalev and V.K. Khersonsky, *Quantum Theory of Angular Momentum: Irreducible Tensors, Spherical Harmonics, Vector Coupling Coefficients, 3nj Symbols*, World Scientific, Singapore (1988).

[92] S. Duane, A.D. Kennedy, B.J. Pendleton and D. Roweth, *Hybrid Monte Carlo*, *Phys. Lett.* **B195** (1987) 216.

[93] N. Metropolis, A.W. Rosenbluth, M.N. Rosenbluth, A.H. Teller and E. Teller, *Equation of state calculations by fast computing machines*, *J. Chem. Phys.* **21** (1953) 1087.